DECENTRALIZED, COOPERATIVE CONTROL OF MULTIVEHICLE SYSTEMS: DESIGN AND STABILITY ANALYSIS

A Dissertation

by

LESLEY ANNE WEITZ

Submitted to the Office of Graduate Studies of
Texas A&M University
in partial fulfillment of the requirements for the degree of

DOCTOR OF PHILOSOPHY

May 2009

Major Subject: Aerospace Engineering

DECENTRALIZED, COOPERATIVE CONTROL OF MULTIVEHICLE SYSTEMS: DESIGN AND STABILITY ANALYSIS

A Dissertation

by

LESLEY ANNE WEITZ

Submitted to the Office of Graduate Studies of
Texas A&M University
in partial fulfillment of the requirements for the degree of

DOCTOR OF PHILOSOPHY

Approved by:

Chair of Committee,	John E. Hurtado
Committee Members,	John L. Junkins
	Raktim Bhattacharya
	Darbha Swaroop
Head of Department,	Dimitris Lagoudas

May 2009

Major Subject: Aerospace Engineering

ABSTRACT

Decentralized, Cooperative Control of Multivehicle Systems:
Design and Stability Analysis. (May 2009)
Lesley Anne Weitz, B.S., The State University of New York at Buffalo;
M.S., Texas A&M University
Chair of Advisory Committee: John E. Hurtado

This dissertation addresses the design and stability analysis of decentralized, cooperative control laws for multivehicle systems. Advances in communication, navigation, and surveillance systems have enabled greater autonomy in multivehicle systems, and there is a shift toward decentralized, cooperative systems for computational efficiency and robustness. In a decentralized control scheme, control inputs are determined onboard each vehicle; therefore, decentralized controllers are more efficient for large numbers of vehicles, and the system is more robust to communication failures and reconfiguration.

The design of decentralized, cooperative control laws is explored for a nonlinear vehicle model that can be represented in a double-integrator form. Cooperative controllers are functions of spacing errors with respect to other vehicles in the system, where the communication structure defines the information that is available to each vehicle. Control inputs are selected to achieve internal stability, or zero steady-state spacing errors, between vehicles in the system.

Closed-loop equations of motion for the cooperative system can be written in a structural form, where damping and stiffness matrices contain control gains acting on the velocity and positions of the vehicles, respectively. The form of the stiffness matrix is determined by the communication structure, where different communication struc-

tures yield different control forms. Communication structures are compared using two structural analysis tools: modal cost and frequency-response functions, which evaluate the response of the multivehicle systems to disturbances. The frequency-response information is shown to reveal the string stability of different cooperative control forms.

The effects of time delays in the feedback states of the cooperative control laws on system stability are also investigated. Closed-loop equations of motion are modeled as delay differential equations, and two stability notions are presented: delay-independent and delay-dependent stability.

Lastly, two additional cooperative control forms are investigated. The first control form spaces vehicles along an arbitrary path, where distances between vehicles are constant for a given spacing parameter. This control form shows advantages over spacing vehicles using control laws designed in an inertial frame. The second control form employs a time-based spacing scheme, which spaces vehicles at constant-time intervals at a desired endpoint. The stability of these control forms is presented.

To my parents, William and Debra, and my brother, Jeffrey.

ACKNOWLEDGMENTS

First and foremost, I would like to thank my graduate advisor, Dr. John E. Hurtado. His support and encouragement throughout my graduate career are appreciated beyond words. I am grateful for the innumerable discussions from research to career options to balancing work and family that have made my graduate experience both fulfilling and enjoyable. I look forward to our continued research collaboration.

I would also like to acknowledge my committee members, Dr. John Junkins, Dr. Raktim Bhattacharya, and Dr. Darbha Swaroop. I have benefited immensely from taking your classes and your research suggestions and discussions. Magda Lagoudas has also been a great mentor and friend, and I will always be very grateful for my involvement in the Space Engineering Institute. Drs. Valasek and Lagoudas have also served as mentors to me, and I have enjoyed my conversations and jokes with them (even the jokes about my weight, Dr. Lagoudas). Thank you to Lisa Willingham for all of her help over the years in organizing travel plans and keeping me up-to-date on department gossip. Thanks to Dr. Haisler and Karen Knabe for the continued assistance in navigating through the paperwork and requirements of grad school.

I wish to acknowledge the external financial support that I have received over the last four years including the National Science Foundation Graduate Research Fellowship, the Amelia Earhart Fellowship from Zonta International, the Lindbergh Grant from the Charles A. and Anne Morrow Lindbergh Foundation, the AIAA Guidance, Navigation, and Control Graduate Award, and the NASA Graduate Student Research Program Fellowship. I am very grateful for the support that I have received from Dr. Bryan Barmore, Terry Abbott, Mark Ballin, Brian Baxley, Mike Palmer, Lisa Rippy, and David Wing at the NASA Langley Research Center and from Dr. Robert Lindberg at the National Institute of Aerospace.

Over the six years that I have spent at Texas A&M University, I feel that I have grown significantly (both professionally and personally) due in great part to the friendships of many people including, but not limited to, Xiaoli Bai, Roshawn Bowers, Jeremy Davis, Nick Denissen, James Doebbler, Thomas Elsom, Kristen Holmstrom, Heather Jones, Morgan Medina, Aditya Murthi, Josh and Marie O'Neil, Joe O'Neil, Julie and Allen Parish, Carolina Restrepo, Dasia Reyes, Theresa Spaeth, and Drew Woodbury.

I have dedicated my dissertation to my parents, William and Debra Weitz, and my brother, Jeffrey Weitz. At the risk of being called a "suck-up" by my brother, I want to acknowledge my parents for the support that they have given me throughout this long process. My parents have supported and trusted my decisions without interfering, have laughed and cried with me through the emotional highs and lows that graduate school induces, and have respected my long hours and stressful lifestyle. I could not have asked for better parents.

I would like to leave the reader of this dissertation with a short dialogue from "Tommy Boy," a movie that cemented my friendship early on with Josh, Joe, and Thomas.

Tommy: Did you hear I finally graduated?

Richard: Yeah, and just a shade under a decade too, all right.

Tommy: You know a lot of people go to college for seven years.

Richard: I know, they're called doctors.

Well, I have been going to college for eleven years, and as some may say, I am not even the kind of doctor that helps people.

TABLE OF CONTENTS

CHAPTER Page

CHAPTER Page

Page

LIST OF TABLES

LIST OF FIGURES

FIGURE Page

FIGURE Page

FIGURE Page

CHAPTER I

INTRODUCTION

This dissertation investigates the design and analysis of decentralized, cooperative control laws for multivehicle systems. Advances in communication, navigation, and computational systems have enabled greater autonomy in multivehicle systems, and there has been a shift toward decentralized, cooperative systems where decision-making occurs at the individual vehicle level. Applications include decentralized, cooperative control of robotic vehicles, unmanned or micro air vehicles (UAVs/MAVs), automated highway systems, and next-generation air traffic systems.

Cooperative control involves the control of a group of dynamic vehicles that are working collectively to meet a common objective by using state and environmental information to influence control decisions [1]. The basis of a cooperative control scheme lies within the ability to use state information from other vehicles and the environment to determine appropriate control inputs to each vehicle in the system. Understanding the dynamic behavior that governs these multivehicle systems is key to designing cooperative control laws that will influence how vehicles interact to achieve a desired goal. Decentralized cooperative control, sometimes referred to as distributed control, is a subset of cooperative control where vehicles use the state information of other vehicles to autonomously determine their own control inputs that achieve the group objective. A decentralized control regime is typically considered superior to more traditional centralized controllers. A central control authority uses state and environmental information to determine the control inputs for all vehicles in the system. This is an effective method for controlling a small number of vehicles,

---

Thé journal model is *IEEE Transactions on Automatic Control*.

but centralized control becomes computationally inefficient as the number of vehicles increases. Moreover, decentralization is more robust to communication failures and structural reconfigurations [2].

The design of decentralized, cooperative control laws is largely based upon the communication structure of the multivehicle system. The communication structure defines the information available to each vehicle in the system, which may be constrained by sensing, communication, or computational limitations. For example, in many applications, vehicles only communicate with their "nearest neighbors" rather than all vehicles in the system. Past research has shown that control laws that achieve the desired objective in the absence of disturbances may not reject some disturbances, thus driving the system unstable. Additionally, decentralized control schemes are subject to time delays in feedback control due to delays in measurement and communication. Therefore, the design of communication structures and decentralized, cooperative control laws must investigate internal stability to ensure that the desired system objective is met, as well as disturbance rejection and time-delay effects on system stability.

The development of decentralized, cooperative control theories has been investigated for ground-based robotic applications in homeland security, search-and-rescue missions, and extra-terrestrial exploration. The distribution of tasks amongst many smaller, expendable vehicles ensures that the loss of a single vehicle will not compromise mission success when compared to the loss of a single, expensive vehicle. Formation control for robotic vehicles has been investigated by Feddema, et al., where the system of robotic vehicles is modeled as a large-dimensional interconnected system derived from a distributed communication structure that couples the individual vehicles [3]. Robinett and Hurtado have investigated decentralized localization of unknown sources using a gradient-based feedback control approach [4, 5].

The work in decentralized formation control of UAVs and MAVs has been extensive and varied. Stipanovíc, et al. investigated control of UAVs by modeling the formation as interconnected and overlapping subsystems that can be expanded into a higher-dimensional space where the subsystems appear decoupled [6–8]. Caicedo, et al. investigated formation control using a structurally-analogous dynamic inversion control law where the formation tracks the mass center of the vehicle system [9]. Graph theory has also been applied to the formation-control problem in order to investigate the effects of information flow on system stability [10, 11]. Fax and Murray show that the eigenvalues of the graph Laplacian, derived from the desired communication structure, can be used to determine stability of the formation using the Nyquist-stability criterion [11]. This graph-theory approach was extended to evaluate the stability of interconnected systems subject to disturbances and time delays [12].

Automated highway systems have been examined as a means to improve the capacity and efficiency of highways, and several references explore different control-law forms to achieve desired spacing characteristics in a platoon of vehicles. Research in control-law development for automated highways addresses the concept of string stability, which is a measure of how spacing errors between adjacent vehicles propagate through a string, or sequence, of vehicles. Whereas a string-stable control form attenuates disturbances and spacing errors decrease along the string, inter-vehicle spacing errors increase along the string when a string-unstable control form is used. Researchers have investigated string stability for a variety of communication structures, or control forms, and spacing policies [13–17]. Many of these approaches use a frequency-domain analysis to investigate spacing-error transfer functions that determine how spacing errors propagate through a vehicle string.

The increased demand for air travel is stressing the current, mostly human-

operated, air traffic management system. Several research institutions are investigating next-generation air traffic systems for the development of a decentralized system with some autonomous operations. Researchers at NASA Langley Research Center (LaRC) have developed an aircraft-centric spacing algorithm for autonomous terminal-area merging and spacing operations. This tool has been tested in several simulation environments including flight and fast-time experiments [18–20]. Whereas system stability has been demonstrated using Monte-Carlo analysis, formal theoretical analysis has not been used to prove internal stability between aircraft pairs and string stability of a sequence of aircraft.

This research seeks to address some of the challenges in the control-law design for and stability analysis of multivehicle systems. In the aforementioned multivehicle-control applications, several design challenges are encountered when analyzing the stability and performance of a decentralized, cooperative system. Different control forms, which are defined based upon the information that is available to each vehicle, can lead to very different stability and performance. This dissertation research will specifically focus on addressing some of the challenges in the development and stability analysis of decentralized, cooperative control laws using a mechanics-based approach. The new contributions of this dissertation include:

1. a unifying approach to the design of decentralized, cooperative control laws as motivated by a differentially-flat nonlinear vehicle model;

2. the analogy of cooperative control laws to structural systems, and subsequently, the analysis and design of cooperative control laws using the structural form to express the closed-loop equations of motion;

3. the investigation of time-delay effects on the stability of decentralized, cooperative vehicle systems by exploiting the structural form; and

4. the design of decentralized, cooperative control laws using non-inertial spacing parameters.

The four research contributions are briefly described here.

A. Design of Decentralized, Cooperative Control Laws

The design of decentralized, cooperative control laws is investigated for a formation-control problem using a planar, nonlinear vehicle model that represents vehicles with negligible sideslip. This vehicle model represents a wide range of vehicles including differentially-driven robotic vehicles and planar UAV flight with regulated sideslip. The nonlinear model is differentially flat, which allows the model to be represented by a linear form that is decoupled in the x and y directions.

The design objective is the development of cooperative control laws to maintain the internal stability of the formation, i.e., drive errors between vehicle pairs to zero [21]. Error variables are defined using a double-integrator model for the vehicles, which is an exact linear representation of the nonlinear model. Closed-loop error dynamics are written, and a form for the control laws is chosen to drive the error variables to zero in order to achieve the desired formation. A leader-follower communication structure is assumed, where each vehicle receives state information from its immediately preceding vehicle only. In addition, the lead vehicle in the formation tracks a reference trajectory.

Different control forms can be achieved by setting certain control gains equal to zero. If each vehicle tracks both its immediately preceding vehicle and the reference trajectory, the cooperative control law is string stable. Tracking the immediately preceding vehicle only leads to a string-unstable control form for certain reference trajectories. In addition, rate-estimation and rate-free control forms are investigated,

which reveal challenges in assuming the linear vehicle representation when all vehicle states are not measured or known.

The primary contribution of this research thrust is the decentralized, cooperative control design, which is motivated by the nonlinear vehicle model. This design approach can be extended to any vehicle model or system that can be expressed as decoupled double integrators. Therefore, a multivehicle system can achieve a desired formation or spacing by selecting control laws based upon a desired communication structure that drive inter-vehicle spacing errors to zero.

B. Structural Analogies in the Design and Analysis of Cooperative Control Laws

The cooperative control laws developed in this dissertation are shown to be analogous to structural systems where the multivehicle systems are coupled through shared state information. Error terms in the control laws mimic physical connections between vehicles, and the equations of motion can be written in a structural form.

$$M\ddot{\boldsymbol{x}} + C\dot{\boldsymbol{x}} + K\boldsymbol{x} = D\boldsymbol{u}$$

Here, $\boldsymbol{x}$ is a vector of vehicle positions, and the C and K matrices are referred to as the damping and stiffness matrices, respectively. The form of the stiffness and damping matrices is determined by the assumed communication structure, which defines the information that is shared between vehicles. The system's natural frequencies and mode shapes are in turn determined by the form of the stiffness matrix. Thus, it is intuitive that multivehicle systems can respond very differently to disturbances based upon the assumed communication structure.

There are several structural analysis tools available in the literature to evaluate the disturbance response of structural systems. This research thrust explores the

application of these structural-analysis tools to the multivehicle control application to both evaluate and compare communication structures. In addition, these tools can be used to determine appropriate control gains to achieve a desired response. Two analysis tools are investigated: modal cost and frequency-response functions. Modal cost compares the communication structures based upon system response to impulsive disturbances, and frequency-response functions are used to evaluate system response to periodic excitation. The traditional structural-analysis tools do not directly apply to the cooperative control of multivehicle systems, and thus, the tools have been interpreted and modified for the multivehicle-control application. Frequency-response information is shown to reveal the string stability of a cooperative control form, which indicates that disturbance effects are mitigated along a string of vehicles.

The primary contributions of this research thrust are the analogy of the closed-loop control laws to structural systems and the application of structural-analysis tools to evaluate disturbance rejection and string stability of the different control forms. Whereas other researchers have explored the structural analogy of cooperative control laws, the structural analogy has been treated literally in that only communication structures that are representative of physical systems were considered. Here, the structural form for the equations of motion is exploited, but the theory includes systems that are not able to be represented by physical systems. Additionally, the modal-cost and frequency-response analysis tools have not previously been applied to evaluate disturbance response. The structural form enables control-gain design to achieve desired system performance and string stability.

C. Investigation of Time-Delay Effects on Formation Stability

Time-delay effects due to measurement, actuation, communication, or operator delays are introduced as system complexity increases, and these delays can affect system stability and performance. Delay differential equations (DDEs) have been used to determine stability bounds on time delays [22,23]; however, the determination of delay bounds may require the solution to linear matrix inequalities [24, 25], the selection of a Lyapunov-Krasovskiĭ function [23], or expensive, problem-specific computation [26]. The structural form of the closed-loop equations of motion is exploited to investigate delay-independent and delay-dependent stability for the multivehicle system. The innovation of this research is the development of a straightforward method to quantify stable time delays in the feedback states of decentralized, cooperative control laws [27].

The method to determine maximum allowable delays is motivated by the ability to write the closed-loop equations of motion in a structural form. The coupled equations of motion are decoupled using a modal-coordinate transformation, and results for a first-order scalar DDE are applied to determine the maximum allowable delay. The estimation of the maximum delay requires only the solution to an eigenvalue problem in order to decouple the equations of motion. Simulation results are used to support the theoretical developments; however, some challenges are encountered in a key assumption in the theory to determine the maximum delay.

The primary contribution of this research thrust is using the structural form of the closed-loop equations of motion in order to investigate the effects of feedback delays on system stability. Decoupling the equations of motion has not previously been explored to determine maximum allowable time delays for a coupled system.

D. Control Law Design using Non-Inertial Spacing Parameters

In the previous research thrusts, cooperative control laws are designed and stability is analyzed for spacing vehicles in an inertial reference frame with constant desired distances between vehicles. The double-integrator representation allows the model to be decoupled in the x and y directions; therefore, spacing errors are defined in the x and y directions, and control laws can be chosen such that the errors in the x and y directions go to zero. This approach can be extended to spacing vehicles with non-constant distances; however, in some cases, it may be difficult to determine how desired inter-vehicle distances change as a function of time, which motivates a different approach to designing spacing control laws. This research thrust investigates the development of control laws where vehicles are spaced using a non-inertial spacing parameter. Two applications are investigated: spacing vehicles along an arbitrary path and time-based spacing to a desired endpoint.

In the first application, an arbitrary reference path is parameterized using an arclength parameter. Along-path and perpendicular-to-path spacing errors are defined between adjacent vehicles. From the spacing-error definitions, a reference position, velocity, and acceleration are determined relative to the immediately preceding vehicle's arclength and perpendicular distance from the path. Control laws are designed to track the reference position, velocity, and acceleration, which are nonlinear, implicit functions of the preceding vehicle's states. In this implementation, all vehicles require knowledge of the reference path.

A time-based spacing control law is designed to space vehicles with constant-time intervals at a desired endpoint. Constant-time spacing is more ideal for some multivehicle applications, such as airport terminal-area spacing operations where the vehicles in a string are decelerating. A time-based spacing scheme will also allow

vehicle spacing on dissimilar trajectories, where the relative time between vehicles can be determined with respect to a desired endpoint. Inter-vehicle spacing errors use the time-to-go as the spacing parameter, which is the time it will take to reach the desired endpoint from the current position. Similarly to the control development for spacing along an arbitrary path, a reference position, velocity, and acceleration are determined from the preceding vehicle's time-to-go. Each vehicle tracks the generated reference to achieve the desired time-based spacing at the endpoint.

A common control strategy is used for the two applications explored here. Internal stability is proved using a cascade approach; however, string stability is more difficult to investigate for this control form due to the generated reference trajectory that each vehicle tracks.

The primary contribution of this research thrust is the approach to develop cooperative spacing control laws using non-inertial spacing parameters. This control-design framework follows from the previous research thrusts and provides a theoretical development for real-world spacing applications.

E. Dissertation Organization

The dissertation is organized as follows. The assumed vehicle model and linear representation that have motivated the decentralized, cooperative control design approach are presented in Chapter II. The decentralized, cooperative control design development and simulation examples are shown in Chapter III, and background on string stability is reviewed in Chapter IV. In Chapter V, the analogy of cooperative control laws to structural systems is presented, including some of the mathematical preliminaries necessary for the analysis of structural systems. The use of structural analysis methods to analyze the disturbance-rejection properties of cooperative control laws

is described in Chapter VI. Time-delay effects on multivehicle formation stability are presented in Chapter VII. In Chapter VIII, deviations from the cooperative control development in the inertial frame are explored for two applications: spacing vehicles along an arbitrary path and time-based spacing. The research is summarized in Chapter IX. The included appendices provide further background on various topics throughout the dissertation as noted.

CHAPTER II

VEHICLE MODEL

The theoretical developments presented in this dissertation are based upon a commonly-used nonlinear vehicle model. The derivation of the vehicle model is presented here, and the model is shown to be differentially flat. The differential-flatness property allows the nonlinear model to be represented in a linear form.

A. Nonlinear Vehicle Model

The nonholonomically-constrained vehicle model shown in Figure 1 represents a wide variety of vehicle types, where the nonholonomic nature of the vehicle prevents motion perpendicular to the heading direction. For example, planar motion of a UAV with negligible sideslip has been described using this model, as well as differentially-driven robotic platforms where the wheel friction prevents motion perpendicular to the wheel direction. Figure 1 shows a top view of the vehicle with a body-fixed reference frame aligned with the vehicle's heading. Inputs to the vehicle are a force $\boldsymbol{F}$ aligned with the vehicle heading, and a torque $\boldsymbol{T}$ in the $\hat{\boldsymbol{b}}_3$ direction.

The vehicle configuration is uniquely described by the generalized coordinates, $\boldsymbol{q} = [x, y, \theta]^T$. Kinematic equations for the inertial position and velocity of the center of the vehicle can be derived.

$$\boldsymbol{r} = x\hat{\boldsymbol{n}}_1 + y\hat{\boldsymbol{n}}_2 \tag{2.1}$$

$$\dot{\boldsymbol{r}} = \dot{x}\hat{\boldsymbol{n}}_1 + \dot{y}\hat{\boldsymbol{n}}_2 \tag{2.2}$$

Coordinatizing the inertial velocity vector in the body-fixed frame yields the following expression from which the nonholonomic constraint is determined by setting the $\hat{\boldsymbol{b}}_2$

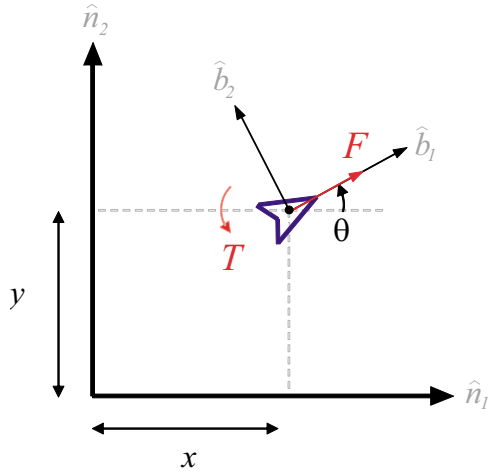

Fig. 1.: Nonholonomically-constrained vehicle model.

component equal to zero.

$$\dot{\boldsymbol{r}} = (\dot{x}\cos\theta + \dot{y}\sin\theta)\hat{\boldsymbol{b}}_1 + (-\dot{x}\sin\theta + \dot{y}\cos\theta)\hat{\boldsymbol{b}}_2 \tag{2.3}$$

Therefore, the constraint can be written in the following matrix form.

$$\phi(\boldsymbol{q}, \dot{\boldsymbol{q}}, t) = \begin{bmatrix} -\sin\theta & \cos\theta & 0 \end{bmatrix} \begin{bmatrix} \dot{x} \\ \dot{y} \\ \dot{\theta} \end{bmatrix} = C\dot{\boldsymbol{q}} = 0 \tag{2.4}$$

The equations of motion can be determined using Lagrange's equations subject to nonholonomic constraints [28].

$$\frac{d}{dt}\left(\frac{\partial L}{\partial \dot{q}_j}\right) - \frac{\partial L}{\partial q_j} = Q_j - C_{ji}^T \lambda_i, \qquad j = 1, ..., n, i = 1, ..., l \tag{2.5}$$

Here, n is the number of generalized coordinates, and l is the number of nonholonomic constraints. For this system, $n = 3$ and $l = 1$. The Langrangian function, L, is equal

to the kinetic energy of the vehicle in the absence of conservative forces.

$$L = T = \frac{1}{2}m\left(\dot{x}^2 + \dot{y}^2\right) + \frac{1}{2}I\dot{\theta}^2 \tag{2.6}$$

Generalized forces, Q_j, can be found using the *work/energy rate principle* as described by Junkins and Kim [29] and restated below.

$$\frac{dE_j}{dt} = \frac{d}{dt}\left(T_j + V_j\right) = Q_j^T\dot{\boldsymbol{q}} = \dot{W}_{trans} + \dot{W}_{rot} \tag{2.7}$$

Therefore, the generalized forces are the terms acting on the time derivatives of the generalized coordinates found from the expression for the work rate. The work rate for this problem is shown.

$$\begin{aligned}\dot{W} &= \dot{W}_{trans} + \dot{W}_{rot} \\ &= \boldsymbol{F}\cdot\dot{\boldsymbol{r}} + \boldsymbol{T}\cdot\boldsymbol{\omega} \\ &= F\hat{\boldsymbol{b}}_1\cdot\left[(\dot{x}\cos\theta + \dot{y}\sin\theta)\hat{\boldsymbol{b}}_1 + (-\dot{x}\sin\theta + \dot{y}\cos\theta)\hat{\boldsymbol{b}}_2\right] + T\hat{\boldsymbol{b}}_3\cdot\dot{\theta}\hat{\boldsymbol{b}}_3\end{aligned} \tag{2.8}$$

The generalized forces are determined directly from Equation (2.8).

$$Q_x = F\cos\theta; \quad Q_y = F\sin\theta; \quad Q_\theta = T \tag{2.9}$$

The seventh-order differential-algebraic equations of motion can then be derived.

$$m\ddot{x} = F\cos\theta - \lambda\sin\theta \tag{2.10}$$

$$m\ddot{y} = F\sin\theta + \lambda\cos\theta \tag{2.11}$$

$$I\ddot{\theta} = T \tag{2.12}$$

$$\text{Subject to: } -\dot{x}\sin\theta + \dot{y}\cos\theta = 0 \tag{2.13}$$

Suppose that new velocity quantities called generalized speeds are defined. The generalized speeds are linearly related to the true velocities, or time rates of change

of the generalized coordinates, and the linear relationship is invertible.

$$\begin{bmatrix} v_1 \\ v_2 \\ v_3 \end{bmatrix} = \begin{bmatrix} \cos\theta & \sin\theta & 0 \\ -\sin\theta & \cos\theta & 0 \\ 0 & 0 & 1 \end{bmatrix} \begin{bmatrix} \dot{x} \\ \dot{y} \\ \dot{\theta} \end{bmatrix} \Leftrightarrow \begin{bmatrix} \dot{x} \\ \dot{y} \\ \dot{\theta} \end{bmatrix} = \begin{bmatrix} \cos\theta & -\sin\theta & 0 \\ \sin\theta & \cos\theta & 0 \\ 0 & 0 & 1 \end{bmatrix} \begin{bmatrix} v_1 \\ v_2 \\ v_3 \end{bmatrix} \tag{2.14}$$

Note that v_1 is the inertial velocity in the $\hat{\boldsymbol{b}}_1$ direction; v_2 is the inertial velocity in the $\hat{\boldsymbol{b}}_2$ direction, or the constraint equation, and is therefore equal to zero; and, v_3 is the angular velocity. The kinematic equations can thus be simplified as shown.

$$\dot{x} = v_1 \cos\theta; \quad \dot{y} = v_1 \sin\theta; \quad \dot{\theta} = v_3 \tag{2.15}$$

To determine the dynamical equations, Equations (2.10) and (2.11) are multiplied by $\cos\theta$ and $\sin\theta$, respectively, and added together.

$$m\ddot{x}\cos\theta + m\ddot{y}\sin\theta = F \tag{2.16}$$

Expressions for $\ddot{x}$ and $\ddot{y}$ are determined from the kinematic relationships and substituted into Equation (2.16).

$$m(\dot{v}_1\cos\theta - v_1 v_3 \sin\theta)\cos\theta + m(\dot{v}_1\sin\theta + v_1 v_3\cos\theta)\sin\theta = F \tag{2.17}$$

Equation (2.17) can be simplified to $m\dot{v}_1 = F$. Redefining $v = v_1$ and $\omega = v_3$, the fifth-order system of ordinary differential equations can be written.

$$\dot{x} = v\cos\theta \tag{2.18}$$

$$\dot{y} = v\sin\theta \tag{2.19}$$

$$\dot{\theta} = \omega \tag{2.20}$$

$$m\dot{v} = F \tag{2.21}$$

$$I\dot{\omega} = T \tag{2.22}$$

If the inputs to the vehicle are the velocity, v, and angular turn rate, ω, the vehicle motion can be described by the kinematic equations alone: Equations (2.18) - (2.20). The full set of equations is used if the vehicle inputs are the force and torque.

B. Linear Representation of the Nonlinear Vehicle Model

The development and design of the decentralized, cooperative control laws presented in this dissertation are based upon a vehicle model described by the kinematic equations of motion in Equations (2.18), (2.19), and (2.20). Therefore, the vehicle states are the inertial position of the vehicle, x and y, and the heading angle, θ, and the control inputs are the velocity, v, and angular turn rate, ω.

The nonlinear, kinematic vehicle model is affine in control with codimension one (3 states and 2 controls); and thus, the model is differentially flat with flat outputs x and y [30, 31]. Differential flatness is further explained in Appendix A. Because the model is differentially flat, the state θ and the two control inputs can be written as functions of the flat outputs and their derivatives as shown below.

$$\theta = \tan^{-1}\left(\frac{\dot{y}}{\dot{x}}\right); \quad v = \sqrt{\dot{x}^2 + \dot{y}^2}; \quad \omega = \frac{\ddot{y}\dot{x} - \dot{y}\ddot{x}}{v^2} \tag{2.23}$$

The second derivatives of the flat outputs are the highest derivatives that appear in the control ω. A derivative of the vehicle velocity reveals the second derivatives of the flat outputs.

$$\dot{v} = \frac{\dot{x}\ddot{x} + \dot{y}\ddot{y}}{v} \tag{2.24}$$

Therefore, new control inputs can be defined as $(\ddot{x}, \ddot{y}) = (u, w)$. This transformation enables the nonlinear system in Equations (2.18)-(2.20) to be represented as

uncoupled double integrators.

$$\begin{bmatrix} \dot{x} \\ \dot{y} \\ \ddot{x} \\ \ddot{y} \end{bmatrix} = \begin{bmatrix} 0 & 0 & 1 & 0 \\ 0 & 0 & 0 & 1 \\ 0 & 0 & 0 & 0 \\ 0 & 0 & 0 & 0 \end{bmatrix} \begin{bmatrix} x \\ y \\ \dot{x} \\ \dot{y} \end{bmatrix} + \begin{bmatrix} 0 & 0 \\ 0 & 0 \\ 1 & 0 \\ 0 & 1 \end{bmatrix} \begin{bmatrix} u \\ w \end{bmatrix} \tag{2.25}$$

Thus, the control-law design is made easier by the transformation to the linear representation. It should be noted that Equation (2.25) is not a linear approximation of the nonlinear vehicle model, but an exact linear representation. The behavior of the differentially-flat system enables the design of arbitrary trajectories in the flat-output (x, y) space, which can then be mapped to the appropriate inputs using a linear transformation.

$$\begin{bmatrix} \dot{v} \\ \omega \end{bmatrix} = \frac{1}{v} \begin{bmatrix} \dot{x} & \dot{y} \\ -\frac{\dot{y}}{v} & \frac{\dot{x}}{v} \end{bmatrix} \begin{bmatrix} u \\ w \end{bmatrix} = T\left(\dot{x}, \dot{y}\right) \begin{bmatrix} u \\ w \end{bmatrix}; \quad v = \sqrt{\dot{x}^2 + \dot{y}^2} \tag{2.26}$$

Here, the velocity v is a state, and the control inputs to the vehicle are $\dot{v}$ and ω.

$$\dot{x} = v\cos\theta; \quad \dot{y} = v\sin\theta; \quad \dot{\theta} = \frac{\dot{x}w - \dot{y}u}{v^2}; \quad \dot{v} = \frac{\dot{x}u + \dot{y}w}{v} \tag{2.27}$$

These equations completely characterize the nonlinear vehicle model for the control inputs designed using the decoupled, double-integrator representation.

Whereas the kinematics vehicle model presented here is for planar vehicle motion, a guidance model for vehicle motion in three dimensions is also shown to be differentially flat. Therefore, the nonlinear vehicle model can also be represented as uncoupled double integrators: $(\ddot{x}, \ddot{y}, \ddot{z}) = (u_x, u_y, u_z)$, and the theory presented in this dissertation in two dimensions also holds for three-dimensional vehicle motion. The derivation of the three-dimensional guidance model and control transformations are presented in Appendix B.

CHAPTER III

DECENTRALIZED, COOPERATIVE CONTROL DESIGN

In this chapter, control-law design and the internal stability of multivehicle formations are explored. The differential-flatness property of the nonlinear vehicle model is exploited, which allows the vehicle motion to be described using the linear form [32–34]. The control-law design is then approached from an error-dynamics perspective where the form of the vehicle model is used to formulate error variables between neighboring vehicles in the formation. In addition to the control-law design, two rate-estimation techniques are explored. Using rate estimates complicates the nonlinear-to-linear model transformation, and stability is difficult to analyze. To deal with this problem, rate-estimation equations are designed using the linear model representation and formation stability is explored using simulation results. Last, a rate-free control law is designed, which does not require state information from other vehicles in the formation to implement.

The major contributions of this chapter are the straightforward formation-control design for an accelerating formation using the linear form of the vehicle model, the exploration of rate-estimation techniques and associated challenges related to the nonlinear model, the rate-free control-law development including an asymptotic stability proof of the rate-free control law using Lyapunov theory, and finally, the comparison of these control techniques for a multivehicle formation.

The development of the cooperative control laws, as well as the form of the system error dynamics are presented in Section A, and rate-estimation techniques are presented in Section B. The development of the rate-free controller is in Section C. Simulation results using both the simple, nonlinear model and a six degree-of-freedom UAV model are presented in Section D.

A. Control-Law Development

A leader-follower communication structure is assumed for the decentralized formation-control problem. Figure 2 shows a five-vehicle formation where each leader-follower vehicle pair is denoted by the dashed lines, and communication flow is shown by the arrows between vehicles [6]. For example, V_2 receives state information from its lead V_1, and V_3 receives information from V_2. V_1 will be referred to as the formation lead. Figure 2 shows two vehicle platoons; the formation control laws for each platoon can be implemented independently. The vehicle indices in the development below are consistent with platoon 1; however, all development is also applicable to platoon 2.

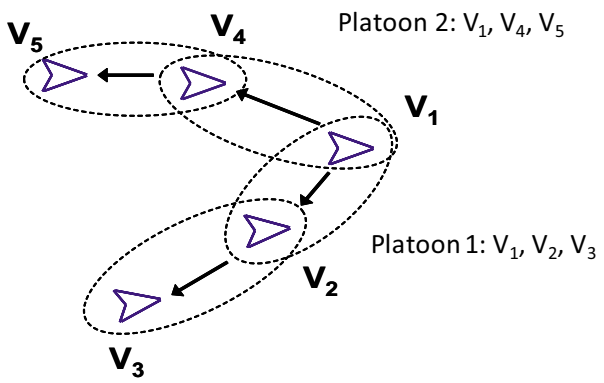

Fig. 2.: Leader-follower communication structure for a multivehicle formation.

The design focus is on the internal stability of the formation, i.e., the ability to achieve the desired formation in the steady state. The control laws are developed by defining error variables between the leader-follower vehicle pairs as shown below. The defined errors are in the x-direction only. Due to the uncoupled nature of the

equations of motion, the development is identical in the y-direction.

$$\begin{aligned} e_1 &= x_r - x_1 - d_1; \quad \dot{e}_1 = \dot{x}_r - \dot{x}_1; \quad \ddot{e}_1 = \ddot{x}_r - \ddot{x}_1 = \ddot{x}_r - u_1 \\ e_2 &= x_1 - x_2 - d_2; \quad \dot{e}_2 = \dot{x}_1 - \dot{x}_2; \quad \ddot{e}_2 = \ddot{x}_1 - \ddot{x}_2 = u_1 - u_2 \\ &\vdots \qquad\qquad \vdots \qquad\qquad \vdots \\ e_i &= x_{i-1} - x_i - d_i; \quad \dot{e}_i = \dot{x}_{i-1} - \dot{x}_i; \quad \ddot{e}_i = \ddot{x}_{i-1} - \ddot{x}_i = u_{i-1} - u_i \end{aligned} \tag{3.1}$$

The formation lead tracks a reference trajectory, x_r, at some constant distance, d_1, as denoted by the e_1 equation; e_2 is the relative error between vehicles 1 and 2 separated by some constant distance d_2; and, the error equation of the ith vehicle with respect to the $(i-1)$th vehicle can be generalized as shown above.

The control objective is to design control inputs, u_i, that stabilize the error dynamics for a system of n vehicles described by the differential equation $\dot{\boldsymbol{e}} = A\boldsymbol{e} + B\boldsymbol{U}$.

$$\boldsymbol{e} = \begin{bmatrix} e_1 & \dot{e}_1 & e_2 & \dot{e}_2 & \dots & e_n & \dot{e}_n \end{bmatrix}^T \tag{3.2}$$

$$\boldsymbol{U} = \begin{bmatrix} \ddot{x}_r & u_1 & u_2 & \dots & u_n \end{bmatrix}^T = \begin{bmatrix} \ddot{x}_r & \boldsymbol{u} \end{bmatrix}^T \tag{3.3}$$

$$A = \begin{bmatrix} 0 & 1 & 0 & 0 & \dots & 0 & 0 \\ 0 & 0 & 0 & 0 & \dots & 0 & 0 \\ 0 & 0 & 0 & 1 & \dots & 0 & 0 \\ 0 & 0 & 0 & 0 & \dots & 0 & 0 \\ \vdots & \vdots & \vdots & \vdots & \ddots & \vdots & \vdots \\ 0 & 0 & 0 & 0 & \dots & 0 & 1 \\ 0 & 0 & 0 & 0 & \dots & 0 & 0 \end{bmatrix}; \quad B = \begin{bmatrix} 0 & 0 & 0 & \dots & 0 & 0 \\ 1 & -1 & 0 & \dots & 0 & 0 \\ 0 & 0 & 0 & \dots & 0 & 0 \\ 0 & 1 & -1 & \dots & 0 & 0 \\ \vdots & \vdots & \vdots & \ddots & \vdots & \vdots \\ 0 & 0 & 0 & \dots & 0 & 0 \\ 0 & 0 & 0 & \dots & 1 & -1 \end{bmatrix} \tag{3.4}$$

Here, A is a $2n \times 2n$ matrix, and B is a $2n \times (n+1)$ matrix. The following form is

assumed for the control inputs u_i.

$$\boldsymbol{u} = \begin{bmatrix} k_{p_1} & k_{v_1} & 0 & 0 & \dots & 0 & 0 \\ 0 & 0 & k_{p_2} & k_{v_2} & \dots & 0 & 0 \\ \vdots & \vdots & \vdots & \vdots & \ddots & \vdots & \vdots \\ 0 & 0 & 0 & 0 & \dots & k_{p_n} & k_{v_n} \end{bmatrix} \boldsymbol{e} + \begin{bmatrix} c_{p_1} & c_{v_1} & 0 & 0 & \dots & 0 & 0 \\ c_{p_2} & c_{v_2} & c_{p_2} & c_{v_2} & \dots & 0 & 0 \\ \vdots & \vdots & \vdots & \vdots & \ddots & \vdots & \vdots \\ c_{p_n} & c_{v_n} & c_{p_n} & c_{v_n} & \dots & c_{p_n} & c_{v_n} \end{bmatrix} \boldsymbol{e} + \ddot{x}_r \tag{3.5}$$

The ith control law can be generalized, and the terms are expanded using the definitions for the error terms in Equation (3.1).

$$\begin{aligned} u_i &= k_{p_i} e_i + k_{v_i} \dot{e}_i + c_{p_i}(e_1 + e_2 + \cdots + e_i) + c_{v_i}(\dot{e}_1 + \dot{e}_2 + \cdots + \dot{e}_i) + \ddot{x}_r \\ &= k_{p_i}(x_{i-1} - x_i - d_i) + k_{v_i}(\dot{x}_{i-1} - \dot{x}_i) + \\ &\qquad + c_{p_i}(x_r - x_i - \sum_{j=1}^{i} d_j) + c_{v_i}(\dot{x}_r - \dot{x}_i) + \ddot{x}_r \end{aligned} \tag{3.6}$$

This choice of $\boldsymbol{u}$ yields homogeneous error dynamics of the form $\dot{\boldsymbol{e}} = A_{cl}\boldsymbol{e}$ such that there are no steady-state spacing errors.

Due to the selected leader-follower communication structure, the homogeneous error dynamics always have a lower-diagonal block form. The closed-loop characteristic polynomial can then be determined from the diagonal blocks. Therefore, the characteristic polynomial of the closed-loop error dynamics has the following form, and the equivalent eigenvalues are easily found.

$$\begin{aligned} &\prod_{i=1}^{n} \left[s^2 + (k_{v_i} + c_{v_i})s + (k_{p_i} + c_{p_i}) \right] = 0 \Rightarrow \\ &\qquad \Rightarrow \lambda_{i_{1,2}} = -\frac{(k_{v_i} + c_{v_i})}{2} \pm \frac{\sqrt{(k_{v_i} + c_{v_i})^2 - 4(k_{p_i} + c_{p_i})}}{2} \end{aligned} \tag{3.7}$$

Based upon the form of the general control law in Equation (3.6), some specific control-gain choices are presented here.

- **Case 1:** $k_p, k_v \neq 0$, $c_p, c_v = 0$. For this choice of gains each vehicle tracks its lead vehicle's position and velocity.

- **Case 2:** $k_p, k_v = 0$, $c_p, c_v \neq 0$. In this case, each vehicle tracks the reference trajectory rather than its assigned lead vehicle's position and velocity. Therefore, it would be assumed in this case that each vehicle knows the reference trajectory of the formation lead, as well as its desired separation from the reference trajectory.

- **Case 3:** $k_p, k_v, c_v \neq 0$, $c_p = 0$. Case 3 combines some of the behaviors in the previous two cases: the ith vehicle tracks its lead's position and velocity and the reference velocity.

- **Case 4:** $k_p, k_v, c_p, c_v \neq 0$. In this case, the control law combines both reference-trajectory and lead-vehicle tracking schemes.

Case 4 leads to both lead-vehicle and reference-trajectory tracking strategies where the gains are chosen based upon the desired weighting of each strategy. Case 1 may be utilized if the reference trajectory is not known by all vehicles in the formation, whereas Case 2 may be chosen if lead-vehicle information is unavailable.

B. Rate-Estimation Control

In the previous control-law developments, the control input to the ith vehicle requires knowledge of its own position and rates: x_i, y_i, $\dot{x}_i$, and $\dot{y}_i$. To implement the control law in Case 4, position and rate information from the assigned lead vehicle (x_{i-1}, y_{i-1}, $\dot{x}_{i-1}$, and $\dot{y}_{i-1}$) and reference-trajectory position and rate information (x_r, y_r, $\dot{x}_r$, and $\dot{y}_r$) are required. In this section, control-law implementation without direct measurement of vehicle velocity, v, from which the rates $\dot{x}$ and $\dot{y}$ can be determined is

explored. In many aerospace applications, full-state measurement eliminates the need for rate estimation, but interest in this development stems from vehicle applications with limited sensor packages, such as small robotic vehicles or cheap, easily deployable UAVs.

When rates are known, the computation of the control inputs in the nonlinear form is straightforward using u and w from the linear control design. However, this relationship is complicated if rates are unknown. When rate estimates for $\dot{x}$ and $\dot{y}$, denoted as $\dot{\hat{x}}$ and $\dot{\hat{y}}$, are used to compute the original controls, "estimation dynamics" are added to the system response as shown below.

$$\begin{bmatrix} \dot{v} \\ \omega \end{bmatrix} = \frac{1}{\hat{v}} \begin{bmatrix} \dot{\hat{x}} & \dot{\hat{y}} \\ -\frac{\dot{\hat{y}}}{\hat{v}} & \frac{\dot{\hat{x}}}{\hat{v}} \end{bmatrix} \begin{bmatrix} u \\ w \end{bmatrix} = T\left(\dot{\hat{x}}, \dot{\hat{y}}\right) \begin{bmatrix} u \\ w \end{bmatrix}; \quad \hat{v} = \sqrt{\dot{\hat{x}}^2 + \dot{\hat{y}}^2} \tag{3.8}$$

From a first-order linearization of $T\left(\dot{\hat{x}}, \dot{\hat{y}}\right)$ about $\dot{x}$ and $\dot{y}$, it can be seen that a rate-estimation scheme adds error terms to the control transformation. These errors terms are related to the errors between the actual and estimated rates.

$$\begin{aligned} T\left(\dot{\hat{x}}, \dot{\hat{y}}\right) &\approx T\left(\dot{x}, \dot{y}\right) + \frac{\partial T}{\partial \dot{\hat{x}}}\Big|_{\dot{x}} \left(\dot{\hat{x}} - \dot{x}\right) + \frac{\partial T}{\partial \dot{\hat{y}}}\Big|_{\dot{y}} \left(\dot{\hat{y}} - \dot{y}\right) \\ &\approx T\left(\dot{x}, \dot{y}\right) + \begin{bmatrix} \frac{1}{v} - \frac{\dot{x}^2}{v^3} & -\frac{\dot{y}\dot{x}}{v^3} \\ \frac{2\dot{y}\dot{x}}{v^4} & \frac{1}{v^2} - \frac{2\dot{x}^2}{v^4} \end{bmatrix} \left(\dot{\hat{x}} - \dot{x}\right) + \begin{bmatrix} -\frac{\dot{x}\dot{y}}{v^3} & \frac{1}{v} - \frac{\dot{y}^2}{v^3} \\ -\frac{1}{v^2} + \frac{2\dot{y}^2}{v^4} & -\frac{2\dot{x}\dot{y}}{v^4} \end{bmatrix} \left(\dot{\hat{y}} - \dot{y}\right) \end{aligned} \tag{3.9}$$

These rate-estimation errors are amplified through the Jacobian of the transformation evaluated at the true rates. Because the stability of the above transformation is difficult to determine analytically, rate-estimation schemes are designed using the double-integrator model in Equation (2.25). System stability is then evaluated using simulation results for the nonlinear system using the control transformation with rate estimates in Equation (3.8).

Vehicle rate estimation is explored in two ways. First, a Luenberger-observer method is presented, which is a straightforward derivation given the linear vehicle model and the control-law form described in Equation (3.6). Second, a first-order passive filter of the position states is explored.

1. Luenberger Observer

Rate estimation using a Luenberger observer [35] is an alternative to measuring all required states using onboard sensing. The general control law for the ith vehicle in Equation (3.6) requires the following state information: $(x_i, \dot{x}_i, x_{i-1}, \dot{x}_{i-1}, x_r, \dot{x}_r)$. The objective is to estimate the vehicle rates, $\dot{x}_i$ and $\dot{x}_{i-1}$; the estimated states are denoted as $\dot{\hat{x}}_i$ and $\dot{\hat{x}}_{i-1}$, respectively. In addition, it is assumed that the (i-1)th vehicle communicates its own rate estimate to the ith vehicle. Note that estimating the rate of the (i-1)th vehicle onboard the ith vehicle would not meet the leader-follower communication structure that was previously defined because the ith vehicle would then need state information from all of the preceding vehicles to implement the observer.

The closed-loop equations of motion for the ith vehicle are expressed in the matrix form below assuming full-state knowledge.

$$\begin{bmatrix} \dot{x}_i \\ \ddot{x}_i \end{bmatrix} = \left(\begin{bmatrix} 0 & 1 \\ -(k_{p_i} + c_{p_i}) & 0 \end{bmatrix} + \begin{bmatrix} 0 & 0 \\ 0 & -(k_{v_i} + c_{v_i}) \end{bmatrix} \right) \begin{bmatrix} x_i \\ \dot{x}_i \end{bmatrix} + \begin{bmatrix} 0 & 0 \\ k_{p_i} & k_{v_i} \end{bmatrix} \begin{bmatrix} x_{i-1} \\ \dot{\hat{x}}_{i-1} \end{bmatrix} + \\ + \begin{bmatrix} 0 & 0 & 0 \\ c_{p_i} & c_{v_i} & 1 \end{bmatrix} \begin{bmatrix} x_r \\ \dot{x}_r \\ \ddot{x}_r \end{bmatrix} + \begin{bmatrix} 0 \\ -k_{p_i} d_i - c_{p_i} \sum_{j=1}^{i} d_j \end{bmatrix} \quad (3.10)$$

Equation (3.10) is rewritten in the following matrix notation.

$$\dot{\boldsymbol{x}}_i = (A_1 + A_2)\boldsymbol{x}_i + B_1\boldsymbol{x}_{i-1} + B_2\boldsymbol{x}_r + B_3 \tag{3.11}$$

Here, the A_1 matrix represents the kinematics and contains the position gains from the control law, and A_2 contains the velocity gains. The A_1 and A_2 matrices are divided into terms that will act on known states and terms that will act on estimated states. The B_1 matrix is the input matrix from the (i-1)th vehicle, the B_2 matrix is the input matrix for the reference trajectory states, and the B_3 matrix is the input matrix for the desired spacing of the ith vehicle with respect to its lead vehicle and the reference trajectory. The vectors in this matrix representation are defined as $\boldsymbol{x}_i = [x_i,\, \dot{x}_i]^T$, $\boldsymbol{x}_{i-1} = [x_{i-1},\, \dot{\hat{x}}_{i-1}]^T$, and $\boldsymbol{x}_r = [x_r,\, \dot{x}_r,\, \ddot{x}_r]^T$.

In developing the state estimator for the ith vehicle, it is assumed that the vehicle position is known and the measured position, x_{i_m}, can be represented by a linear equation.

$$x_{i_m} = C\boldsymbol{x}_i, \qquad C = \begin{bmatrix} 1 & 0 \end{bmatrix} \tag{3.12}$$

The closed-loop estimator can be written by replacing $\boldsymbol{x}_i$ with $\hat{\boldsymbol{x}}_i$ and by adding an error term between the estimated and the measured quantities. The estimation-gain matrix, L_i, is selected to drive the estimated states to the actual states.

$$\begin{aligned} \dot{\hat{\boldsymbol{x}}}_i &= (A_1 + A_2)\hat{\boldsymbol{x}}_i + B_1\boldsymbol{x}_{i-1} + B_2\boldsymbol{x}_r + B_3 + L_i(x_{i_m} - C\hat{\boldsymbol{x}}_i) \\ &= (A_1 + A_2 - L_iC)\hat{\boldsymbol{x}}_i + B_1\boldsymbol{x}_{i-1} + B_2\boldsymbol{x}_r + B_3 + L_iC\boldsymbol{x}_i \end{aligned} \tag{3.13}$$

From Equations (3.11) and (3.13), the equations for the feedback system to estimate both x_i and $\dot{x}_i$ can be determined; the rate estimate $\dot{\hat{x}}_i$ is used in place of $\dot{x}_i$ in the feedback control law. The overall system of equations for the ith vehicle has the

following form.

$$\begin{bmatrix} \dot{\boldsymbol{x}}_i \\ \dot{\hat{\boldsymbol{x}}}_i \end{bmatrix} = \left[\begin{array}{c|c} A_1 & A_2 \\ \hline L_i C & A_1 + A_2 - L_i C \end{array}\right] \begin{bmatrix} \boldsymbol{x}_i \\ \hat{\boldsymbol{x}}_i \end{bmatrix} + \begin{bmatrix} B_1 \\ B_1 \end{bmatrix} \boldsymbol{x}_{i-1} + \begin{bmatrix} B_2 \\ B_2 \end{bmatrix} \boldsymbol{x}_r + \begin{bmatrix} B_3 \\ B_3 \end{bmatrix} \tag{3.14}$$

Note that only the kinematics term in the matrix A_1 acts on $\dot{x}_i$, and the position-gain term acts on x_i, which is known. The matrix A_2 only acts on the rate term in $\hat{\boldsymbol{x}}_i$, which is an estimated quantity. The top row of Equation (3.14) represents the vehicle dynamics responding to the control input with estimated rates, and the bottom row is the onboard filter that determines the estimated states.

The stability of the closed-loop control law with the filter in Equation (3.14) can be evaluated using the eigenvalues of the matrix that acts on $[\boldsymbol{x}_i \ \hat{\boldsymbol{x}}_i]^T$. Stability is achieved if the estimation-gain matrix, L_i, is chosen such that the estimation filter is faster than the closed-loop dynamics. The eigenvalues for the overall system of n vehicles are equal to the union of the eigenvalues of each individual vehicle; therefore, the state-estimation filters can be designed for each individual vehicle independently. The system eigenvalues are shown below.

$$\begin{aligned} \lambda_{i_{1,2}} &= \frac{-(k_{v_i} + c_{v_i})}{2} \pm \frac{\sqrt{(k_{v_i} + c_{v_i})^2 - 4(k_{p_i} + c_{p_i})}}{2} \\ \lambda_{i_{3,4}} &= \frac{-L_{i_1}}{2} \pm \frac{\sqrt{L_{i_1}^2 - 4(k_{p_i} + c_{p_i} + L_{i_2})}}{2}; \qquad L_i = [L_{i_1} \ \ L_{i_2}]^T \end{aligned} \tag{3.15}$$

Thus, the rate-estimation scheme leads to the following general control form.

$$u_i = k_{p_i}(x_{i-1} - x_i - d_i) + k_{v_i}(\dot{\hat{x}}_{i-1} - \dot{\hat{x}}_i) + c_{p_i}(x_r - x_i - \sum_{j=1}^{i} d_j) + c_{v_i}(\dot{x}_r - \dot{\hat{x}}_i) \tag{3.16}$$

When there is no error in the initial rate estimates, i.e., the estimated and true rates are equal at time zero, the formation behavior is identical to the behavior with known states because the Luenberger observer is an exact estimate of the closed-loop vehicle

response.

2. Passivity Filter

Using a passivity filter is another method for estimating rate information. There are several examples in the literature of using passive filters to estimate rate information for control of robotic manipulators and attitude stabilization [36–38]. These concepts are utilized here to develop an expression to estimate vehicle rates. The passive filter has the form shown below, where the vehicle position is filtered using a fictitious state, ϕ_i.

$$\dot{\phi}_i = -\tau_i \phi_i + k_i x_i \tag{3.17}$$

The position, x_i, in the filter equation is equivalent to a function of the reference trajectory and position errors.

$$x_i = x_r - e_1 - e_2 - \ldots - e_i - \sum_{j=1}^{i} d_j \tag{3.18}$$

When the n-vehicle formation has reached its desired formation, all of the spacing errors, e_i, are zero, and $x_i = x_r - \sum_{j=1}^{i} d_j$. Assuming that x_r has a constant acceleration, we can substitute $x_i = \frac{1}{2}\ddot{x}_r t^2 + \dot{x}_r(0)t - \sum_{j=1}^{i} d_j$, and a solution for $\phi_i(t)$ can be found.

$$\begin{aligned}
\phi_i(t) &= Ce^{-\tau_i t} + \frac{k_i}{2\tau_i}\ddot{x}_r t^2 + \left(\frac{k_i \dot{x}_r(0)}{\tau_i} - \frac{k_i}{\tau_i^2}\ddot{x}_r\right) t + \left(-\frac{k_i \sum_{j=1}^{i} d_j}{\tau_i} - \frac{k_i \dot{x}_r(0)}{\tau_i^2} + \frac{k_i}{\tau_i^3}\ddot{x}_r\right) \\
&= Ce^{-\tau_i t} + \frac{k_i}{\tau_i}\left(\frac{1}{2}\ddot{x}_r t^2 + \dot{x}_r(0)t - \sum_{j=1}^{i} d_j\right) - \frac{k_i}{\tau_i^2}\left(\ddot{x}_r t + \dot{x}_r(0)\right) + \frac{k_i}{\tau_i^3}\ddot{x}_r \\
&= Ce^{-\tau_i t} + \frac{k_i}{\tau_i}x_i - \frac{k_i}{\tau_i^2}\dot{x}_r + \frac{k_i}{\tau_i^3}\ddot{x}_r
\end{aligned} \tag{3.19}$$

As t becomes large, $Ce^{-\tau_i t}$ becomes small; thus, this term can be neglected. The reference velocity, $\dot{x}_r$, is equal to $\dot{x}_i$ when the position errors have gone to zero, and

because ϕ_i lags x_i, the equation below is an estimate of $\dot{x}_i$.

$$\dot{\hat{x}}_i \approx \dot{x}_r = \tau_i x_i - \frac{\tau_i^2}{k_i}\phi_i + \frac{1}{\tau_i}\ddot{x}_r \tag{3.20}$$

As was the case in the Luenberger-observer design, the passivity filters can be designed for the individual vehicles, and the overall system stability is guaranteed given individual vehicle stability. The following equation shows the closed-loop state and passivity-filter equations for the ith vehicle, where $\dot{x}_i$ has been replaced with equation (3.20).

$$\begin{bmatrix} \dot{x}_i \\ \ddot{x}_i \\ \dot{\phi}_i \end{bmatrix} = \begin{bmatrix} 0 & 1 & 0 \\ -(k_{p_i}+c_{p_i}) - \tau_i(k_{v_i}+c_{v_i}) & 0 & \frac{\tau_i^2}{k_i}(k_{v_i}+c_{v_i}) \\ k_i & 0 & -\tau_i \end{bmatrix} \begin{bmatrix} x_i \\ \dot{x}_i \\ \phi_i \end{bmatrix} + \begin{bmatrix} 0 & 0 \\ k_{p_i} & k_{v_i} \\ 0 & 0 \end{bmatrix} \begin{bmatrix} x_{i_1} \\ \dot{\hat{x}}_{i-1} \end{bmatrix} + \\ + \begin{bmatrix} 0 & 0 & 0 \\ c_{p_i} & c_{v_i} & 1 - \frac{(k_{v_i}+c_{v_i})}{\tau_i} \\ 0 & 0 & 0 \end{bmatrix} \begin{bmatrix} x_r \\ \dot{x}_r \\ \ddot{x}_r \end{bmatrix} + \begin{bmatrix} 0 \\ -k_{p_i}d_i - c_{p_i}\sum_{j=1}^{i} d_j \\ 0 \end{bmatrix} \tag{3.21}$$

The eigenvalues of Equation (3.21) do not have a concise analytical form; however, the characteristic equation is $s^3+\tau_i s^2+[(k_{p_i}+c_{p_i})+\tau_i(k_{v_i}+c_{v_i})]\,s+(k_{p_i}+c_{p_i})\,\tau_i = 0$. Routh-Hurwitz analysis indicates that for stability $\tau_i > 0$, and k_i has no bounds as it does not appear in the characteristic equation.

C. Rate-Free Control

Passive filtering can also be used to implement rate-free control laws that do not require rate information for implementation [36, 39]. In this case, the elimination of rate information leads to a self-contained control law, which does not require state information from other vehicles. The derivation begins by redefining the position

error of the ith vehicle relative to the reference trajectory.

$$\epsilon_i = x_r - x_i - \sum_{j=1}^{i} d_j; \quad \dot{\epsilon}_i = \dot{x}_r - \dot{x}_i; \quad \ddot{\epsilon}_i = \ddot{x}_r - \ddot{x}_i = \ddot{x}_r - u_i \tag{3.22}$$

In addition, the error equations are augmented with a first-order filter of the position error, ϵ_i.

$$\dot{\beta}_i = -\tau_i \beta_i + k_i \epsilon_i \tag{3.23}$$

Lyapunov stability theory [29] is used to determine an appropriate controller to drive the system to its equilibrium state where error, ϵ_i, is zero.

$$V(\epsilon_i, \dot{\epsilon}_i, \beta_i) = \frac{\gamma_i}{2}\epsilon_i^2 + \frac{1}{2}\dot{\epsilon}_i^2 + \frac{1}{2}\left(-\tau_i \beta_i + k_i \epsilon_i\right)^2 \tag{3.24}$$

It is easily verified that $V = 0$ at $\epsilon_i = \dot{\epsilon}_i = -\tau_i \beta_i + k_i \epsilon_i = 0$. The design parameter γ_i was added to influence system performance. A time derivative of Equation (3.24) introduces the control input, u_i.

$$\begin{aligned} \dot{V}(\epsilon_i, \dot{\epsilon}_i, \beta_i, \dot{\beta}_i) &= \gamma_i \epsilon_i \dot{\epsilon}_i + \dot{\epsilon}_i \ddot{\epsilon}_i + \left(-\tau_i \beta_i + k_i \epsilon_i\right)\left(-\tau_i \dot{\beta}_i + k_i \dot{\epsilon}_i\right) \\ &= \dot{\epsilon}_i\left(\gamma_i \epsilon_i + \ddot{x}_r - u_i - k_i \tau_i \beta_i + k_i^2 \epsilon_i\right) - \tau_i\left(-\tau_i \beta_i + k_i \epsilon_i\right)^2 \end{aligned} \tag{3.25}$$

Stability requires that $\dot{V} \leq 0$, and a control is selected to achieve this result.

$$\begin{aligned} u_i &= \left(\gamma_i + k_i^2\right)\epsilon_i - k_i \tau_i \beta_i + \ddot{x}_r \\ &= \left(\gamma_i + k_i^2\right)\left(x_r - x_i - \sum_{j=1}^{i} d_j\right) - k_i \tau_i \beta_i + \ddot{x}_r \end{aligned} \tag{3.26}$$

The control u_i requires position, x_i, reference information, x_r, and filter-state information, β_i, only. This controller development has eliminated the need for rate information in the control input.

For this choice of u_i, the first term in Equation (3.25) is equal to zero, which leaves $\dot{V} = -\tau_i\left(-\tau_i \beta_i + k_i \epsilon_i\right)^2 \leq 0$. The condition $\dot{V} \leq 0$ indicates local stability

around the equilibrium states of ϵ_i, $\dot{\epsilon}_i$, and β_i; however, by taking higher derivatives of V we are able to determine that ϵ_i, $\dot{\epsilon}_i$, and β_i, go to zero asymptotically (see Appendix C). This proof of asymptotic stability is an alternative to checking the closed-loop eigenvalues of the state and filter equations.

Whereas the control input does not require rate information, the rates $\dot{x}_i$ still must be estimated to compute the original controls v and ω in Equation (2.23). The first-order filter of position used to determine $\dot{\hat{x}}_i$ in the previous section can be implemented here to estimate the rates. The closed-loop rate-free control law augmented with the two first-order filters is shown below. Here, the gains on the position-error filter shown in Equation (3.23) are denoted by subscript 1, and the gains on the position filter in Equation (3.17) are denoted by subscript 2.

$$\begin{bmatrix} \dot{x}_i \\ \ddot{x}_i \\ \dot{\beta}_i \\ \dot{\phi}_i \end{bmatrix} = \begin{bmatrix} 0 & 1 & 0 & 0 \\ -(\gamma_i + k_{i_1}^2) & 0 & -k_{i_1}\tau_{i_1} & 0 \\ -k_{i_1} & 0 & -\tau_{i_1} & 0 \\ k_{i_2} & 0 & 0 & -\tau_{i_2} \end{bmatrix} \begin{bmatrix} x_i \\ \dot{x}_i \\ \beta_i \\ \phi_i \end{bmatrix} + \\ + \begin{bmatrix} 0 & 0 & 0 \\ (\gamma_i + k_{i_1}^2) & 0 & 1 \\ k_{i_1} & 0 & 0 \\ 0 & 0 & 0 \end{bmatrix} \begin{bmatrix} x_r \\ \dot{x}_r \\ \ddot{x}_r \end{bmatrix} + \begin{bmatrix} 0 \\ -(\gamma_i + k_{i_1}^2) \sum_{j=1}^{i} d_j \\ -k_{i_1} \sum_{j=1}^{i} d_j \\ 0 \end{bmatrix} \tag{3.27}$$

Again, the eigenvalues do not have a concise, analytical form. Routh-Hurwitz analysis of the characteristic equation:

$$s^4 + (\tau_{i_1} + \tau_{i_2})s^3 + (\tau_{i_1}\tau_{i_2} + \gamma_i + k_{i_1}^2)s^2 + \left[(\tau_{i_1} + \tau_{i_2})\gamma_i + \tau_{i_2}k_{i_1}^2)\right] s + \tau_{i_1}\tau_{i_2}\gamma_i = 0$$

becomes quite complicated; however, design parameters may be chosen to satisfy the necessary condition for stability where all of the coefficients in the characteristic

equation must be positive.

D. Simulation Results

Simulation results are presented here to illustrate control-law performance. Firstly, a non-dimensional example is presented using the full-state-measurement, rate-estimation, and rate-free control laws presented in Sections A through C. Secondly, simulation results are presented for a formation of UAVs using the full-state measurement control law in order to demonstrate the applicability of the decentralized formation controller to a realistic UAV application.

1. Non-Dimensional Simulation Results

The simulation results presented here are intended to demonstrate the performance characteristics of the different formation control schemes; therefore, the user must appropriately design the control gains and reference trajectory of the formation for a specific vehicle application. All units will be in terms of distance units (DU) and time units (TU) to eliminate any relation to a specific application.

In all simulations in this section, the reference trajectory of the formation from the origin is $x_r = \frac{1}{2}\ddot{x}_r t^2 + \dot{x}_r(0)t$, where $\ddot{x}_r = 1$ and $\dot{x}_r(0) = 0.5$. These values were chosen such that the formation-lead vehicle travels one DU in one TU. The desired separation between vehicles in the x and y directions is 0.1 DU.

a. Full-State-Measurement Control

A five-vehicle formation is simulated for the four gain cases described in Section A. Figure 3 shows the (x, y) positions of the vehicles over one time unit (TU). Note that the vehicles are traveling from left to right in the figure, and each vehicle has

initial position and velocity errors. The eigenvalues of the characteristic equation are chosen to be equal in all control-gain cases. Although it is difficult to detect in the figure, there are some slight differences in the performance of each control law. These differences are expected due to the different forms of the closed-loop error dynamics for each gain case. Whereas identical eigenvalues provide the same decay rates for each solution, each gain case has a unique closed-loop form with unique eigenvectors, which leads to variations in the performance of each controller.

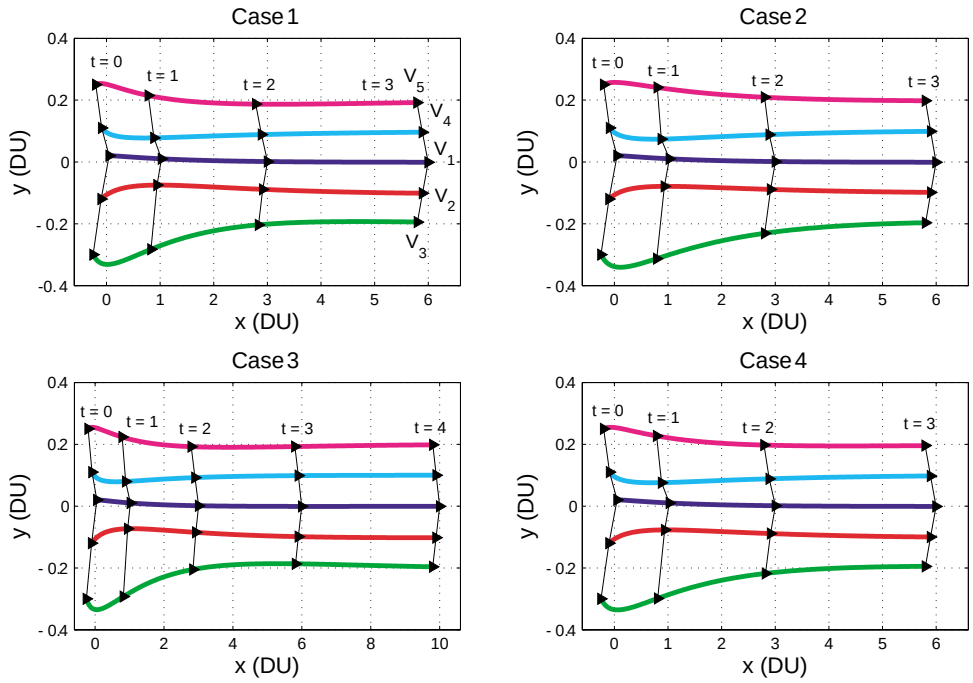

Fig. 3.: Simulation results for the general formation control laws with different gain choices.

Table I shows the convergence times for each control law and the minimum separation between vehicle pairs in the formation, where the desired separation is $\sqrt{2(0.1)^2} = 0.1414$ DU. The convergence time is defined as the time when the four

Table I.: Control-Law Convergence and Minimum-Separation Results.

Case #	Gains	Convergence Time (TU)	Min Separation (DU)
1	$k_p, k_v \neq 0, c_p, c_v = 0$	1.99	0.1165
2	$k_p, k_v = 0, c_p, c_v \neq 0$	2.40	0.1247
3	$k_p, k_v, c_v \neq 0, c_p = 0$	3.40	0.1097
4	$k_p, k_v, c_p, c_v \neq 0$	2.08	0.1208

trailing vehicles are within 10% of their desired separation from their leads. For these gain choices, Case 1 provides the fastest convergence and Case 3 is the slowest to converge; however, the differences in the table are quite small, and changes to the gains may not result in the same performance trends as shown here. Further gain tuning could provide desired performance for any of these control choices. Whereas active collision avoidance has not been investigated in the control-law design, gain selection and initial vehicle conditions directly affect the aggressiveness of the formation convergence. The gains chosen in this example have been selected to provide reasonable separation between the vehicles during convergence. However, in a case of poor initial conditions, the gains could be chosen to make the lead vehicle quickly converge to the reference trajectory, vehicles 2 and 4 less aggressive than the lead, and vehicles 3 and 5 less aggressive than vehicles 2 and 4.

Additionally, the gains used here are selected to limit vehicle accelerations to 1.2 DU/TU^2 (20% greater than the desired accleration) and angular turn rates to 90 deg/TU. These were arbitrarily chosen limits; however, the gains can be adjusted to achieve any desired acceleration and turn-rate constraints.

b. Rate-Estimation Control

Luenberger-Observer Estimation Method

Simulation results are used to evaluate the rate-estimation scheme for initial filter errors in the vehicle rates. The estimation-gain matrices, L_i, are identical for each vehicle and are chosen such that the state estimators are at least ten times faster than the closed-loop dynamics. Figure 4 shows one example of the formation convergence (for Case 4) with initial-rate inputs to the estimation filter randomly perturbed using a normal distribution with a variance of 1.00 DU/TU. The top plot in Figure 4 shows (x, y) positions over 5 TU. Formation convergence is achieved in 2.55 TU with a minimum separation of 0.1081 DU.

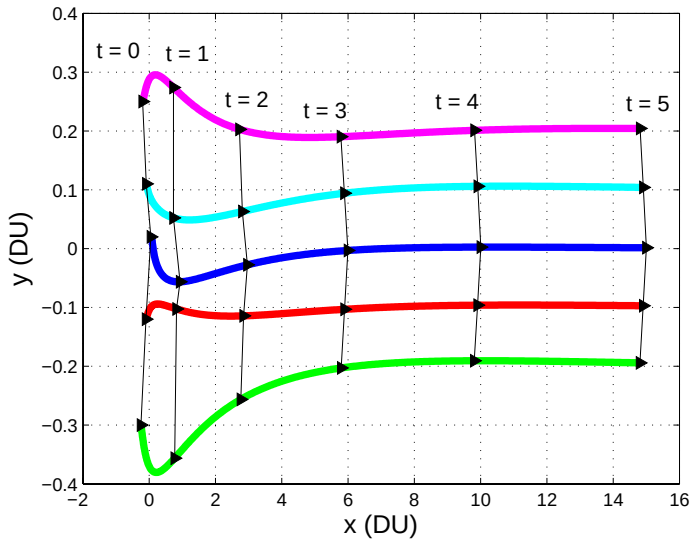

Fig. 4.: Simulation results for the Luenberger-observer estimation scheme (Case 4).

One hundred simulations were run for perturbed initial rate estimates with a variance of 1.00 DU/TU. The simulations converged in an average of 2.45 TU, which indicates that on average the formation converges more slowly for estimated rates

than when the actual rates are used in the control law. In addition, some of the cases violated the acceleration and turn-rate limits, which indicates that the control gains would need to be less aggressive in the rate-estimate case.

Passive-Filtering Estimation Method

In the nonlinear-model implementation of the passive filter, the formation stability is sensitive to the initial guesses for ϕ_i. The desired value of $\phi_i(0)$ can be calculated from Equation (3.20) and then perturbed by a random error with some variance to investigate the formation stability around the initial condition for ϕ_i. For a variance of 0.10 DU/TU and $k_i = 5$, the formation does converge to the desired formation; however, there are large oscillations in the vehicle positions causing the vehicle paths to cross. Improved performance is achieved by increasing k_i to 50. An example of this result is shown in Figure 5, where the formation converges to the desired formation in 1.60 TU with a minimum separation of 0.1396 DU. Over 100 simulations, the average convergence time is 1.50 TU, which means that the passive-filtering technique provides faster convergence for this set of gains than when true rates are known.

In the case that there are no errors on the initial filter states, the value of k_i does not influence the results. However, this gain directly affects the stability and performance of the passive-filter system when there are initial errors in ϕ_i. This result is obvious from Equation (3.20), where larger values of k_i decrease the contribution of ϕ_i in the calculation of $\dot{\hat{x}}_i$.

c. Rate-Free Control

The rate-free controller performance is demonstrated in Figure 6 for 5 TU. Here, the gains τ_{i_1} and k_{i_1} remain the same as in the passive-filter implementation, and the gains τ_{i_2}, k_{i_2}, and γ_i are tuned to limit the acceleration and turn rates to the

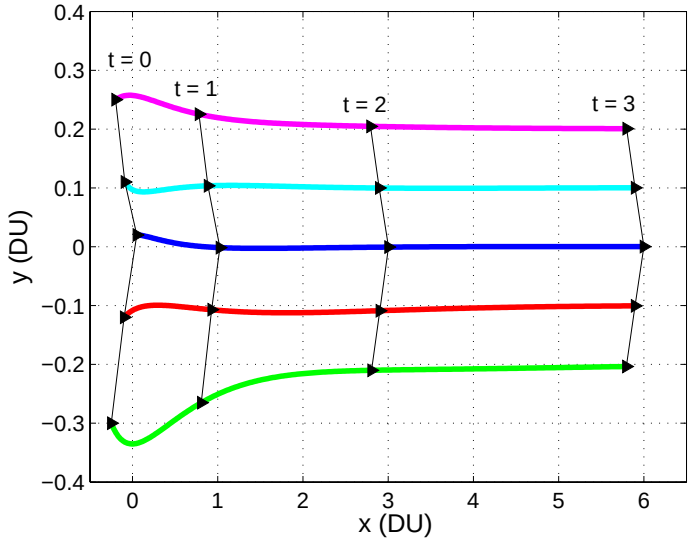

Fig. 5.: Simulation results for the passive-filtering estimation scheme (Case 4).

previously specified conditions. In this case, the initial conditions for β_i are set to zero, and the initial conditions for ϕ_i are perturbed from the desired values using a random error. Due to the more sluggish behavior of the rate-free controller, the variance on the errors in $\phi_i(0)$ is increased to 0.50 DU/TU from 0.10 DU/TU in the previous section. For these conditions, the formation converged in 10.79 TU with a minimum separation of 0.0862 DU.

Out of 100 simulations, all of the initial conditions yielded stable formations with an average convergence time of 11.41 TU. Vehicle separation is more of a concern with the rate-free controller due to the lack of state information from other vehicles; therefore, gains must be carefully selected based upon the initial formation in order to provide adequate separation.

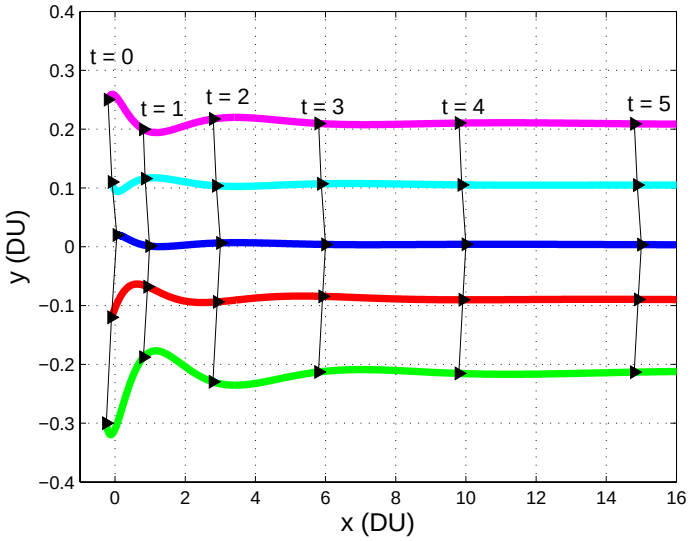

Fig. 6.: Simulation results for the rate-free controller (Case 4).

2. UAV Simulation Results

The UCAV6 aircraft model, which is roughly a 60% scale version of the AV-8B Harrier Aircraft [40,41], is used to simulate a formation of five UAVs. A six degree-of-freedom state-space aircraft model was obtained by linearizing a nonlinear simulation model about a steady, level, trimmed flight condition (the trim angle of attack is $\alpha_1 = 4.35$ deg, the trim velocity is $V_1 = 128.7$ m/s, the trim elevator deflection is $\delta_{e_1} = 7.5$ deg, and the trim engine thrust is 55%). The vectors of aircraft states and inputs are shown below.

$$\boldsymbol{x} = [\delta X \quad \delta Y \quad \delta Z \quad u \quad v \quad w \quad p \quad q \quad r \quad \phi \quad \theta \quad \psi]^T$$

$$\boldsymbol{u} = [\delta_e \quad \delta_T \quad \delta_a \quad \delta_r]^T$$

The states, δX, δY, and δZ are perturbations in the aircraft position, u, v, and w are perturbations in the body-fixed velocities, p, q, and r are perturbations in the body-fixed angular velocities, and ϕ, θ, and ψ are Euler angles. The aircraft controls are the elevator, aileron, rudder deflections from trim, δ_e, δ_a and δ_r, respectively, and the thrust perturbation from trim, δ_T. The A and B matrices are also shown.

$$A = \begin{bmatrix} 0_{12\times 3} & \bar{A}_{12\times 9} \end{bmatrix}; \quad B = \begin{bmatrix} 0_{3\times 4} & \bar{B}_{6\times 4} & 0_{3\times 4} \end{bmatrix}^T \tag{3.28}$$

$$\bar{A} = \begin{bmatrix} 0.99 & 0 & 0.0759 & 0 & 0 & 0 & 0 & -32.06 & 0 \\ 0 & 1 & 0 & 0 & 0 & 0 & -32.06 & 0 & 422.2 \\ -0.07 & 0 & 0.99 & 0 & 0 & 0 & 0 & -417.4 & 0 \\ -0.03 & 0 & 0.16 & 0 & -31.99 & 00 & -32.02 & 0 & \\ 0 & -0.33 & 0 & 31.9 & 0 & -418 & 32.02 & 0 & 0 \\ -0.06 & 0 & -1.34 & 0 & 409.5 & 0 & 0 & -2.43 & 0 \\ 0 & -0.02 & 0 & -3.64 & 0 & 1.72 & 0 & 0 & 0 \\ 0 & 0 & -0.02 & 0 & -0.77 & 0 & 0 & 0 & 0 \\ 0 & 0.02 & 0 & -0.21 & 0 & -1.19 & 0 & 0 & 0 \\ 0 & 0 & 0 & 1 & 0 & 0.07 & 0 & 0 & 0 \\ 0 & 0 & 0 & 0 & 1 & 0 & 0 & 0 & 0 \\ 0 & 0 & 0 & 0 & 0 & 1.003 & 0 & 0 & 0 \end{bmatrix} \tag{3.29}$$

$$\bar{B} = \begin{bmatrix} 0.0081 & 0.2559 & 0 & 0 \\ 0 & 0 & -0.2945 & 0.4481 \\ 0.2772 & 0.2286 & 0 & 0 \\ 0 & 0 & 0.5171 & 0.0704 \\ 0.1164 & 0.0143 & 0 & 0 \\ 0 & 0 & 0.0239 & -0.0895 \end{bmatrix} \tag{3.30}$$

Velocity and heading-angle commands come from the integration of the $\dot{v}$ and ω control inputs, described in Equation (2.26), that are determined using the full-state-measurement control law (Case 4). An optimal non-zero set point (NZSP) controller is then used to control the aircraft states along desired trajectories in order to track the commanded velocity and heading-angle commands from the formation controller [40,41]. The velocity in the body-fixed y axis is regulated to zero in order to meet the negligible sideslip assumption from the nonlinear vehicle model in Equations (2.18)-(2.20). Details on the optimal NZSP controller are included in Appendix D.

The output matrix, H, is chosen to track the velocity projected on the $x-y$ plane, the heading angle, ψ, the altitude, z, and the velocity in the body-fixed y axis.

$$H = \begin{bmatrix} 0\ 0\ 0 & \cos(\theta+\alpha) & 0 & \sin(\theta+\alpha) & 0\ 0\ 0\ 0\ 0\ 0 \\ 0\ 0\ 0 & 0 & 0 & 0 & 0\ 0\ 0\ 0\ 0\ 1 \\ 0\ 0\ 1 & 0 & 0 & 0 & 0\ 0\ 0\ 0\ 0\ 0 \\ 0\ 0\ 0 & 0 & 1 & 0 & 0\ 0\ 0\ 0\ 0\ 0 \end{bmatrix} \tag{3.31}$$

Because the A and H matrices do not have any nonzero entries for δx and δy, these columns are removed, and similarly, the top two rows of the A and B matrices are removed. The submatrices, $\bar{A}$, $\bar{B}$, and $\bar{H}$, and the matrix $D = 0_{4\times4}$ make up a non-singular Quad-Partition matrix, from which the trim states and controls can be determined for y^* (see Appendix D). The optimal NZSP controller has the form below, where $\boldsymbol{x}^*$ and $\boldsymbol{u}^*$ are the trim states and controls, and the gain K is found by solving the LQR problem with $\bar{A}$, $\bar{B}$, and weighting matrices Q and R.

$$\boldsymbol{u} = (\boldsymbol{u}^* + K\boldsymbol{x}^*) - K\boldsymbol{x} \tag{3.32}$$

The selected state and control weighting matrices for the LQR problem are shown.

$$Q = \text{diag}(10,\ 100,\ 10,\ 100,\ 1,\ 1,\ 10,\ 0.1,\ 0.1,\ 10 \times 10^4)$$

$$R = \text{diag}(100,\ 0.1,\ 10,\ 1)$$

The outer-loop control gains are: $k_p, c_p = 0.001$ and $k_v, c_v = 0.04$. This combination of gains limits control-surface deflections to within appropriate bounds.

The first vehicle in the formation follows a constant-velocity reference trajectory in the x-direction from $(x, y) = (0, 0)$ with $\dot{x}_r = V_1 t$, and the desired separation between vehicles is 100 meters in both the x and y directions. Formation results are presented in Figure 7. The formation converges in 93 seconds with a minimum vehicle separation of 137 meters. The distances between the vehicle pairs are shown in Figure 8, where the vehicles converge to the desired formation from a more-widespread initial configuration. Results indicate little overshoot of the desired separation, and thus vehicle collisions are not a concern.

Other state histories are shown in Figures 9 through 11. Altitude perturbations are not presented, but deviations were limited to ± 0.2 m from the trim altitude. All perturbed states went to zero as expected. Formation-control and NZSP gains were selected to limit control surface deflections as shown in Figure 12. All control-surface deflections are reasonable for UAV performance.

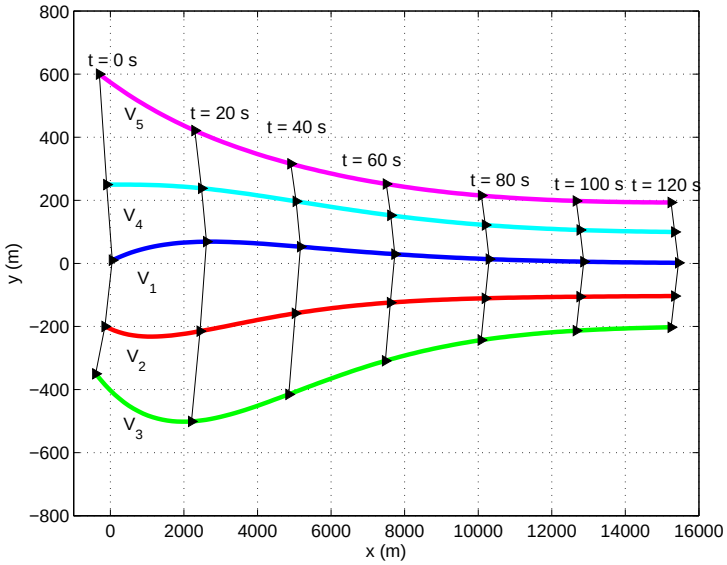

Fig. 7.: Simulation results for the UAV formation.

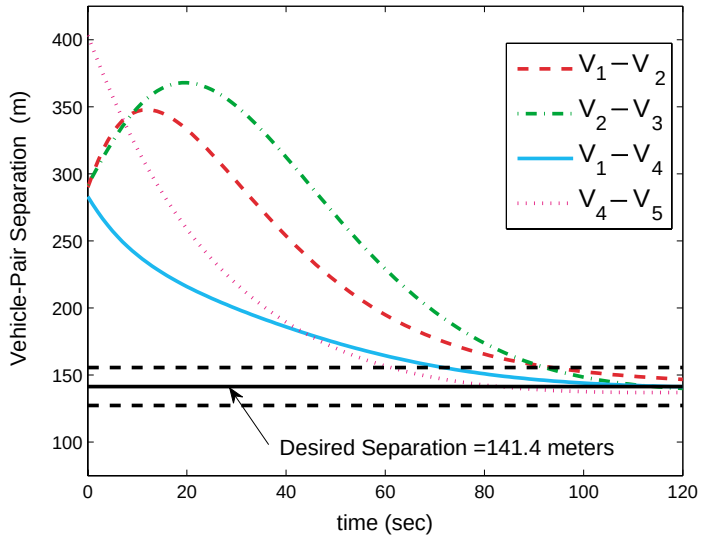

Fig. 8.: Separation between vehicle pairs for the UAV simulation.

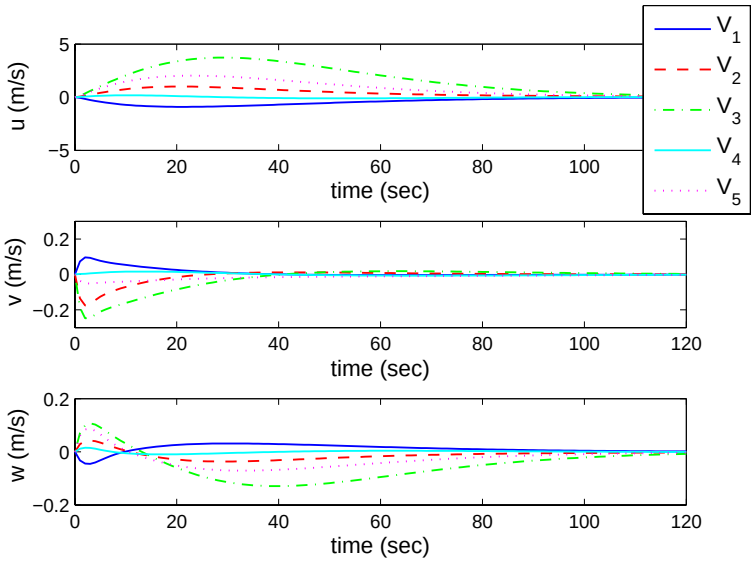

Fig. 9.: UAV states: body-fixed velocity perturbations.

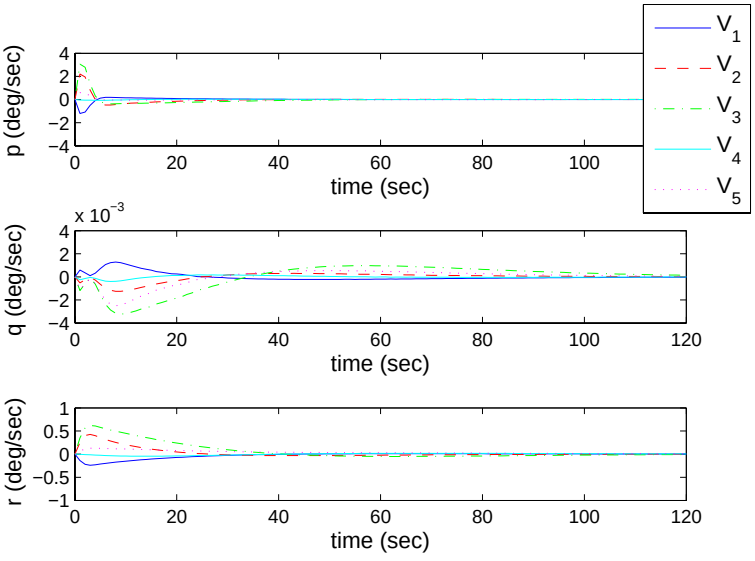

Fig. 10.: UAV states: body-fixed angular-velocity perturbations.

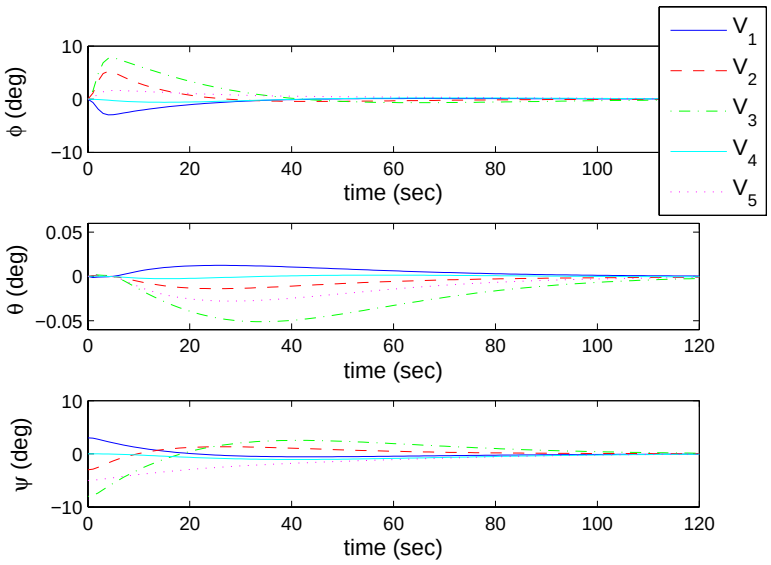

Fig. 11.: UAV states: Euler angles.

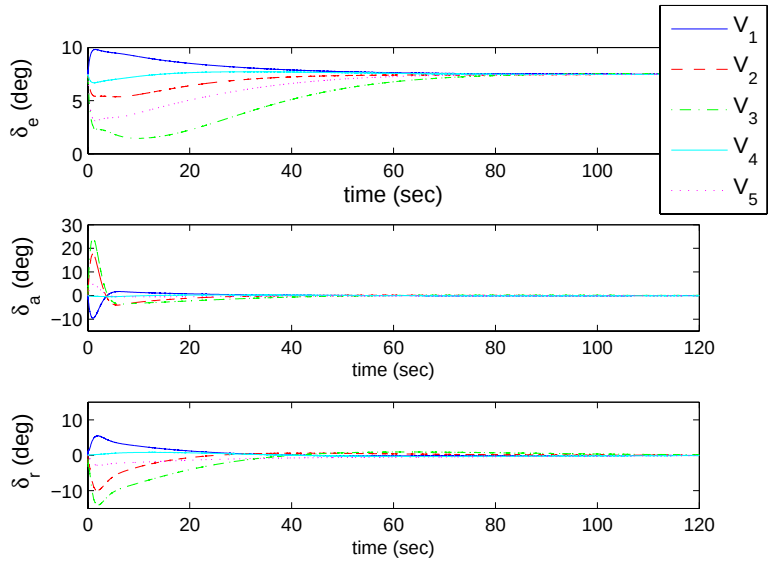

Fig. 12.: UAV control inputs: control-surface deflections.

E. Chapter Summary

This chapter focused on decentralized, cooperative control design for a multivehicle formation problem where the vehicles were modeled using a nonlinear, differentially-flat form. Exploiting the differential-flatness properties of the model led to a linear representation of the vehicle model from which position and velocity errors were defined using a leader-follower communication structure. A general control form for an accelerating formation was derived, which contains terms to track both the reference trajectory and the assigned lead-vehicle states. Control gains can be selected to implement a desired tracking strategy and bound control inputs to desired limits.

In addition, two rate-estimation techniques were examined, Luenberger observer and passive filtering, for the case when rate information was not known. Rate-estimation provided a challenge in the transformation of the controls in the linear representation to the controls in the nonlinear form. "Estimation dynamics" influenced the system behavior and were related to the errors between the estimated and actual states. In the rate-estimation case, stability was difficult to quantify. To deal with this challenge, the rate-estimation schemes were designed using the linear representation, and simulation results were used to examine stability results. In the rate-estimation case, the passive filter is superior to the Luenberger observer in both convergence performance and efficiency.

Lastly, a rate-free controller was developed, which does not include rate information in the control form. Coupled with the passive-filter to estimate vehicle rates, the formation convergence was more sluggish than when rates were included in the control law. However, the sluggish behavior permits greater errors in the initial filter states, thus providing a more robust solution than the Luenberger-observer and passive-filtering schemes when subjected to initial rate-estimation errors. The rate-

free control law does not require information from other vehicles in the formation, which can cause concern in vehicle separation; however, gains can be chosen to limit control inputs in order to provide adequate separation throughout convergence.

Simulation results were presented to demonstrate formation convergence for a non-dimensional example using the simple, nonlinear model. In addition, simulation results were presented to demonstrate the applicability of the decentralized, formation control laws to a higher-fidelity, six-degree-of-freedom UAV model.

The rate-estimation and rate-free controller developments in this chapter were used to illustrate some of the challenges in assuming the linear vehicle representation for control-law design. In the remaining developments in this dissertation, it is assumed that vehicle velocities are measured, and therefore, $\dot{x}$ and $\dot{y}$ are known.

CHAPTER IV

STRING STABILITY: DEFINITIONS AND EXAMPLES

Two stability concepts arise in the design of decentralized, cooperative control laws for vehicle spacing: 1.) internal stability and 2.) string stability. Internal stability, as defined in Chapter III, means that spacing errors between vehicle pairs go to zero in the steady-state and the multivehicle system reaches the desired formation. String stability deals with how errors are propagated through the vehicle string due to disturbances or the reference trajectory of the formation lead. A string-stable control form means that spacing errors between adjacent vehicles do not grow or amplify along the vehicle string. The form, or communication structure, of the cooperative control law determines whether certain disturbances or reference trajectories will lead to instabilities along a sequence or string of vehicles.

The concept of string stability has been extensively studied for automated highway systems where vehicle strings of infinite length are considered [14, 15, 17, 42–44]. Swaroop and Hedrick investigated constant-spacing control strategies, where the control objective is to maintain a constant distance between adjacent vehicles in a string [14]. Some of these results are presented here to illustrate string-stability concepts and the analysis approaches used in some of the literature.

In this chapter, the string-stability concept is further defined including the mathematical definition of string stability, and several examples from the literature are presented to illustrate the analysis. The general form of the cooperative control law developed in the previous chapter, Equation (3.6), is analyzed and the string stability of that control form is discussed.

A. Mathematical Definitions of String Stability

The theory presented here is a summary of the string-stability results presented by Swaroop and Hedrick [14]. Consider a string of identical vehicles that are interconnected by a cooperative control law. The input to the ith vehicle is a function of the spacing error between the ith and $(i-1)$th vehicles, e_i, as shown in Figure 13.

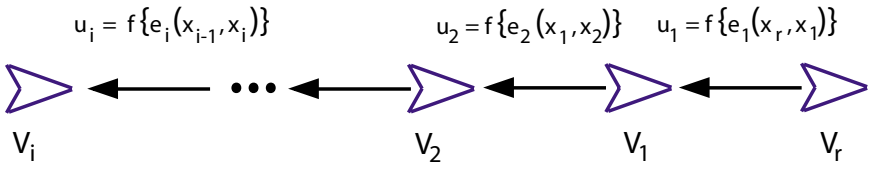

Fig. 13.: Example vehicle string where control inputs are functions of spacing errors between vehicles.

If the maximum gain of every system is α, then the error of the ith vehicle is bounded by the following inequality.

$$||e_i||_\infty \leq \alpha||e_{i-1}||_\infty \leq \alpha^{i-1}||e_1||_\infty \tag{4.1}$$

If $\alpha \geq 1$ the spacing errors will be amplified along the vehicle string. For $\alpha < 1$, string stability is achieved, and weak string stability is achieved for $\alpha = 1$.

The gain α is the maximum gain of the error propagation transfer function, $\hat{H}(s)$, which relates the errors of the ith and jth vehicles with respect to their immediately preceding vehicles. For example, assume that the error of the ith vehicle depends on the spacing errors of the two preceding vehicles. The error e_i can then be expressed in the frequency domain as shown.

$$E_i(s) = \hat{H}_1(s)E_{i-1}(s) + \hat{H}_2(s)E_{i-2}(s); \quad \hat{H}_1(s) = \frac{E_i(s)}{E_{i-1}(s)}, \quad \hat{H}_2(s) = \frac{E_i(s)}{E_{i-2}(s)} \tag{4.2}$$

The ith error can then be bounded by the inequality.

$$||e_i||_\infty \leq \alpha_1||e_{i-1}||_\infty + \alpha_2||e_{i-2}||_\infty \tag{4.3}$$

The worst-case difference equation from Equation (4.3) is: $z^2 - \alpha_1 z - \alpha_2 = 0$, and the spacing control law is string stable if the roots of the characteristic equations are within the unit circle. This can be generalized for control laws that use information from r preceding vehicles. The spacing error dynamics have the following form.

$$E_i(s) = \sum_{j=1}^{r} \hat{H}_j(s)E_{i-j}(s) + \hat{M}(s, e_i(0), e_{i-1}(0), ..., e_{i-r}(0)) \tag{4.4}$$

Here, $\hat{H}_j(s)$ is the transfer function between the ith and jth spacing errors, and $\hat{M}$ is related to the initial conditions. Following the development above, the maximum gain of each transfer function is $\alpha_j = ||\mathcal{L}^{-1}\left(\hat{H}_j(s)\right)||_1$, and the characteristic polynomial, $P_r(z)$, is the worst-case difference equation.

$$P_r(z) = z^r - \sum_{j=1}^{r} \alpha_j z^{r-j} \tag{4.5}$$

Swaroop and Hedrick define the spectral radius of $P_r(z)$ as a performance metric to both determine string stability and compare control-law spacing performance between control forms.

$$\rho = \max\{|z| : P_r(z) = 0\} \tag{4.6}$$

The performance metric, ρ, represents the maximum rate of error attenuation along the vehicle string. The control law is string stable for $\rho < 1$, which occurs when $\sum_{j=1}^{r} |\alpha_j| < 1$; the control law is string stable in the weak sense for $\rho = 1$, which occurs when $\sum_{j=1}^{r} |\alpha_j| = 1$; and, the control law is unstable for $\rho > 1$. The paper by Swaroop and Hedrick includes the proofs of the above statements.

B. Spacing Control Law Examples

Four spacing control law examples from the literature are presented in this section. These examples are relevant to the cooperative control laws presented in the previous chapter. The spacing errors are defined between adjacent vehicles as was done previously.

$$e_1 = x_r - x_1 - d_1; \quad e_2 = x_1 - x_2 - d_2; \quad \ldots \quad e_i = x_{i-1} - x_i - d_i \tag{4.7}$$

The double-integrator model is again assumed: $\ddot{x}_i = u_i$.

1. Reference-Trajectory Tracking Only

For this control scheme each vehicle tracks the reference trajectory only. Therefore, each vehicle in the formation must know the position and velocity of the reference trajectory and its desired distance from the reference. The control input to the ith vehicle has the following form.

$$u_i = c_p \left(x_r - x_i - \sum_{j=1}^{i} d_j \right) + c_v \left(\dot{x}_r - \dot{x}_i \right) + \ddot{x}_r \tag{4.8}$$

The second derivative of the error terms yields the difference in control effort between two adjacent vehicles: $\ddot{e}_i = \ddot{x}_{i-1} - \ddot{x}_i = u_{i-1} - u_i$. Using this relationship, the error dynamics can be shown to have the form: $\ddot{e}_i + c_v \dot{e}_i + c_p e_i = 0$. Here, the characteristic polynomial is $z = 0$, and the performance metric $\rho = 0$. Whereas this is the best achievable performance, the ith vehicle's control law does not include information about the position and velocity of its preceding vehicle, and thus this control scheme is considered unsafe. This result is applicable to the control form in Equation (3.6): Case 2.

2. Lead-Vehicle Tracking Only

The control law for the lead-vehicle tracking scheme takes into account the position and velocity of the immediately preceding vehicle only.

$$u_i = k_p e_i + k_v \dot{e}_i \tag{4.9}$$

In the literature, this control scheme has been termed "autonomous" because it requires state information that can be obtained from onboard sensors only. This control form leads to the error dynamics below.

$$\ddot{e}_i + k_v \dot{e}_i + k_p e_i = k_v \dot{e}_{i-1} + k_p e_{i-1} \tag{4.10}$$

The error dynamics can be written in the frequency domain.

$$E_1(s) = \hat{G}(s) V_r(s), \quad \hat{G}(s) = \frac{-s}{s^2 + k_v s + k_p} \tag{4.11}$$

$$E_i(s) = \hat{H}(s) E_{i-1}(s), \quad \hat{H}(s) = \frac{k_v s + k_p}{s^2 + k_v s + k_p}, \quad i \geq 2 \tag{4.12}$$

The term $V_r(s)$ is the Laplace transform of the reference vehicle's velocity. To determine the error propagation properties of this control scheme, the magnitude of $\hat{H}(s)$ is found by substituting $s = j\omega$ into the transfer function and then taking the square root of the squares of the real and imaginary parts.

$$|\hat{H}(j\omega)| = \left[\frac{k_p^2 + k_v^2 \omega^2}{(k_p - \omega^2)^2 + k_v^2 \omega^2} \right]^{1/2} \tag{4.13}$$

For values of $k_p, k_v > 0$, there is a range of excitation frequencies where the magnitude is greater than one (as shown in Figure 14 for $k_p = k_v = 1$). The excitation frequencies are a result of a sinusoidal velocity profile from the reference vehicle. Therefore, for sufficiently small input frequencies, this control form is not string stable, and spacing errors would grow along the vehicle string. This control form is equivalent to Equation

(3.6): Case 1.

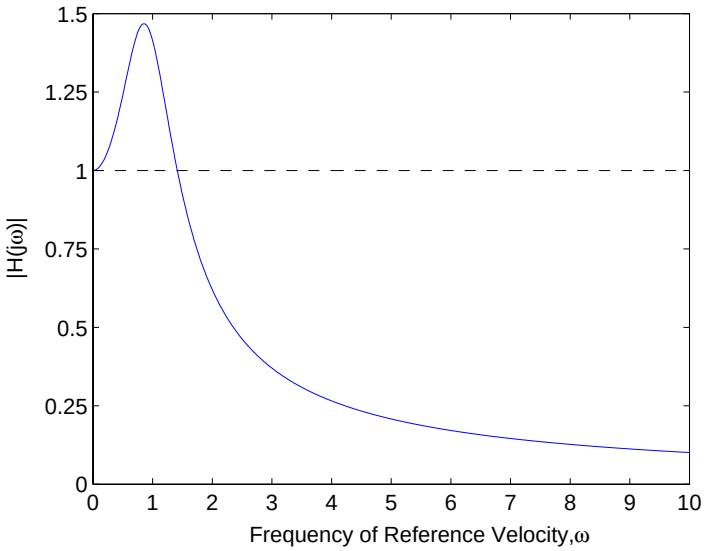

Fig. 14.: Magnitude of the error-propagation transfer function for the lead-vehicle tracking control scheme.

3. Lead-Vehicle Tracking with Acceleration Information

The control law for this scheme has a similar form to the previous control law, but it includes the acceleration information from the preceding vehicle.

$$u_i = k_p e_i + k_v \dot{e}_i + k_a \ddot{x}_{i-1} \tag{4.14}$$

The spacing error dynamics in the frequency domain now have the form shown below.

$$E_1(s) = \hat{G}(s) V_r(s), \quad \hat{G}(s) = \frac{(k_a - 1)s}{s^2 + k_v s + k_p} \tag{4.15}$$

$$E_i(s) = \hat{H}(s) E_{i-1}(s), \quad \hat{H}(s) = \frac{k_a s^2 + k_v s + k_p}{s^2 + k_v s + k_p}, \quad i \geq 2 \tag{4.16}$$

The magnitude plot for $\hat{H}(s)$ in Figure 15 shows that for $k_a > 1$ (for $k_p = k_v = 1$), the magnitude is greater than one for sufficiently high input frequencies, which results in string instabilities for those frequencies. When $k_a = 1$, the magnitude is equal to one and weak string stability is achieved. For $k_a < 1$, the magnitude is greater than one for sufficiently low input frequencies resulting in string instabilities for this choice of gain.

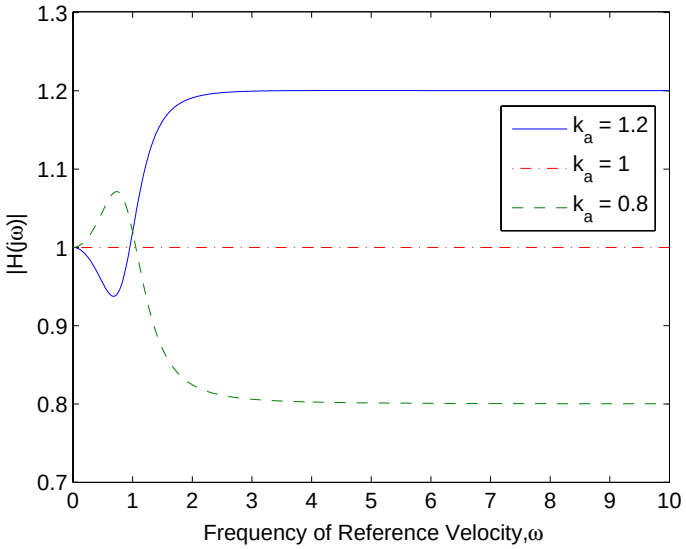

Fig. 15.: Magnitude of the error-propagation transfer function for the lead-vehicle tracking with acceleration control scheme.

4. Reference-Trajectory and Lead-Vehicle Tracking Control (Form 1)

Hedrick et al. designed a sliding-mode control law that combines both reference-trajectory and lead-vehicle information [42]. The sliding surface, S_i, is selected such that the spacing error dynamics on the surface are string stable and S_i goes to zero

with sliding-mode dynamics $\dot{S}_i + \lambda S_i = 0$.

$$S_i = -\dot{e}_i - q_1 e_i + q_3 \left(\dot{x}_i - \dot{x}_r\right) + q_4 \left(x_i - x_r + \sum_{j=1}^{i} d_j\right) \tag{4.17}$$

The control law is determined by substituting Equation (4.17) into the sliding-mode dynamics.

$$u_i = \frac{1}{1+q_3} \times \left[\ddot{x}_{i-1} + q_3 \ddot{x}_r + (q_1 + \lambda)\dot{e}_i - (q_4 + \lambda q_3)(\dot{x}_i - \dot{x}_r) + q_1 \lambda e_i - \lambda q_4 \left(x_i - x_r + \sum_{j=1}^{i} d_j\right)\right] \tag{4.18}$$

Note that the control input is a function of the preceding vehicle's position, velocity, and acceleration and the reference-trajectory position and velocity. The spacing error dynamics can be found by setting the sliding surface $S_i = S_{i-1} = 0$.

$$\begin{aligned} S_i + \dot{e}_i + q_1 e_i - q_3 \left(\dot{x}_i - \dot{x}_r\right) - q_4 \left(x_i - x_r + \sum_{j=1}^{i} d_j\right) = \\ = S_{i-1} + \dot{e}_{i-1} + q_1 e_{i-1} - q_3 \left(\dot{x}_{i-1} - \dot{x}_r\right) - q_4 \left(x_{i-1} - x_r + \sum_{j=1}^{i-1} d_j\right) \end{aligned} \tag{4.19}$$

Rearranging Equation (4.19) yields the following equation expressed in the time domain.

$$(1 + q_3)\dot{e}_i + (q_1 + q_4) e_i = S_{i-1} - S_i + \dot{e}_{i-1} + q_1 e_{i-1} \tag{4.20}$$

Equation (4.20) can be expressed in the frequency-domain and rearranged to yield the error-propagation transfer function, $\hat{H}(s)$, and the initial-condition term, $\hat{M}(s)$.

$$E_i(s) = \hat{H}(s) E_{i-1}(s) + \hat{M}\left(s, e_i(0), e_{i-1}(0)\right) \tag{4.21}$$

$$\hat{H}(s) = \frac{s + q_1}{(1+q_3)s + (q_1 + q_4)}; \quad \hat{M}(s) = \frac{(S_{i-1} - S_i) + [(1+q_3)e_i(0) - e_{i-1}(0)]}{(1+q_3)s + (q_1 + q_4)} \tag{4.22}$$

The magnitude of the error-propagation transfer function is shown in Figure 16 for a choice of three different sets of gains, which shows that the magnitude is less than one for all excitation frequencies. Therefore, this control scheme is string stable for these gains. Swaroop and Hedrick state that this control scheme has an upper bound on the error-propagation magnitude, and thus, is string stable for all choices of gains.

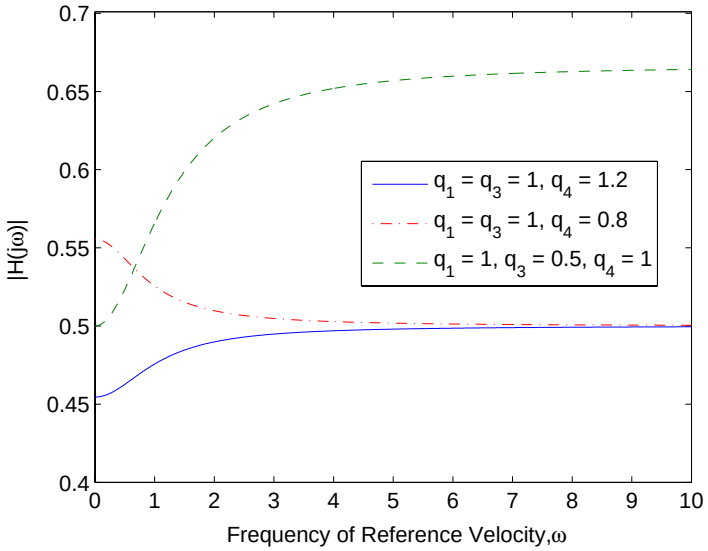

Fig. 16.: Magnitude of the error-propagation transfer function for the reference-trajectory and lead-vehicle tracking control law (form 1).

5. Reference-Trajectory and Lead-Vehicle Tracking Control (Form 2)

The cooperative control law in Equation (3.6): Case 4 also combines reference-trajectory and lead-vehicle tracking. The control law is restated below.

$$u_i = k_p e_i + k_v \dot{e}_i + c_p \left(e_1 + e_2 + ... + e_i\right) + c_v \left(\dot{e}_1 + \dot{e}_2 + ... + \dot{e}_i\right) + \ddot{x}_r \qquad (4.23)$$

Spacing error dynamics are determined by substituting the control law in Equation (4.23) into the equation for the second derivative of the error, $\ddot{e}_i$.

$$\begin{aligned}\ddot{e}_i &= \ddot{x}_{i-1} - \ddot{x}_i = u_{i-1} - u_i \\ &= [k_p e_{i-1} + k_v \dot{e}_{i-1} + c_p (e_1 + e_2 + ... + e_{i-1}) + c_v (\dot{e}_1 + \dot{e}_2 + ... + \dot{e}_{i-1}) + \ddot{x}_r] - \\ &\quad - [k_p e_i + k_v \dot{e}_i + c_p (e_1 + e_2 + ... + e_i) + c_v (\dot{e}_1 + \dot{e}_2 + ... + \dot{e}_i) + \ddot{x}_r] \\ &= k_p (e_{i-1} - e_i) + k_v (\dot{e}_{i-1} - \dot{e}_i) - c_p e_i - c_v \dot{e}_i \end{aligned} \tag{4.24}$$

Recall that the terms with the k control gains are errors with respect to an assigned lead vehicle, and the terms with the c control gains are errors with respect to the reference trajectory. The error-propagation transfer function can be determined from Equation (4.24).

$$\hat{H}(s) = \frac{E_i(s)}{E_{i-1}(s)} = \frac{k_v s + k_p}{s^2 + (k_v + c_v)s + (k_p + c_p)} \tag{4.25}$$

The magnitude of $\hat{H}(s)$ is shown in Figure 17 for four sets of gains as denoted in the legend. This figure shows that gains can be chosen such that the magnitude is less than one for all frequencies and the control law is string stable. In the case that the gains $k_p = k_v = 0$, the control law uses reference-vehicle (trajectory) tracking only, and as shown previously, this control form is considered unsafe. When $c_p = c_v = 0$, the control law uses lead-vehicle tracking only, and this control form is string unstable for all $k_p, k_v > 0$. The combination of the reference-trajectory and lead-vehicle tracking terms yields a string stable control law for certain choices of gains.

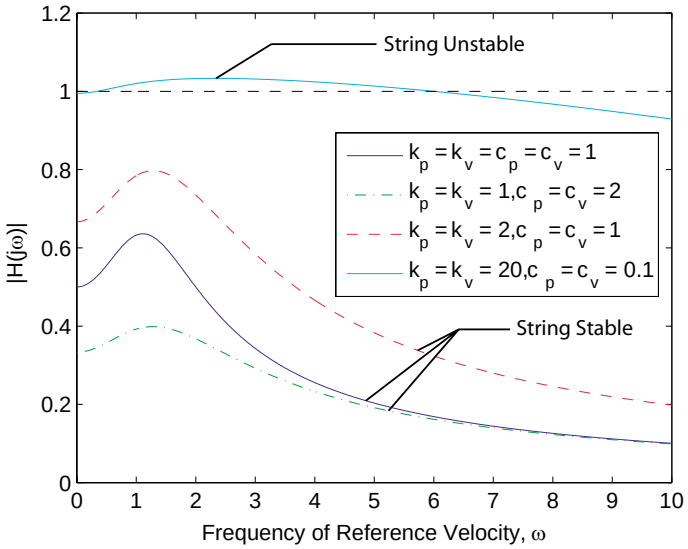

Fig. 17.: Magnitude of the error-propagation transfer function for the reference-trajectory and lead-vehicle tracking control law (form 2).

C. Chapter Summary

This chapter presented the concept of string stability with some mathematical preliminaries. Examples from the literature were used to illustrate the analysis of cooperative control forms to determine how spacing errors are propagated through a vehicle string. The cooperative control form developed in the previous chapter was analyzed using this method and was shown to be string stable when reference-trajectory and lead-vehicle tracking are combined.

The concept of string stability will be revisited in Chapter VI. Frequency-response analysis, motivated by the structural analogies presented in Chapter V, reveals the string-stability characteristics of a given cooperative control form.

CHAPTER V

STRUCTURAL ANALOGIES TO COOPERATIVE CONTROL LAWS

Cooperative control laws couple multivehicle systems through the state information that is shared in order to achieve a common group objective. Cooperative multivehicle systems are analogous to structural systems where terms in the equations of motion can be grouped into mass, stiffness, and damping matrices. The stiffness and damping matrices are determined by the assumed communication structure, which defines how the vehicles in the formation communicate. The structural form allows many of the tools developed for the analysis of structural systems to be applied to the multivehicle-control application. This chapter presents the structural analogy and some preliminaries that will be used in the development of the analysis tools presented in Chapter VI.

In Section A, the structural form of the closed-loop equations of motion for an n-vehicle formation is presented. The modal-coordinate transformation, used to decouple the equations of motion into n second-order equations, is discussed in Section B. The sensitivity of the system's eigenvalues and eigenvectors to changes in the stiffness matrix is presented in Section C. In Section D, the form of the damping matrix and its relation to the modal-coordinate transformation is discussed.

A. Equations of Motion in the Structural Form

Cooperative control laws, written in physical coordinates, are analogous to physically connecting the individual vehicles with springs and dampers. For example, consider a two degree-of-freedom system with two masses connected by a spring and damper as shown in Figure 18. The second-order equations of motion can be written in a

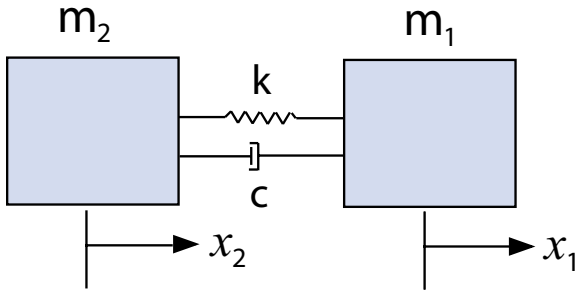

Fig. 18.: Two-mass system.

matrix form: $M\ddot{\boldsymbol{x}} + C\dot{\boldsymbol{x}} + K\boldsymbol{x} = 0$.

$$\begin{bmatrix} m_1 & 0 \\ 0 & m_2 \end{bmatrix} \begin{bmatrix} \ddot{x}_1 \\ \ddot{x}_2 \end{bmatrix} + \begin{bmatrix} c & -c \\ -c & c \end{bmatrix} \begin{bmatrix} \dot{x}_1 \\ \dot{x}_2 \end{bmatrix} + \begin{bmatrix} k & -k \\ -k & k \end{bmatrix} \begin{bmatrix} x_1 \\ x_2 \end{bmatrix} = \begin{bmatrix} 0 \\ 0 \end{bmatrix} \tag{5.1}$$

The M, C, and K matrices are referred to as the mass, damping, and stiffness matrices, respectively, and $\boldsymbol{x} = [x_1 \;\; x_2]^T$.

Using the general form of the cooperative control law in Equation 3.6, the closed-loop, coupled equations of motion can be arranged in the structural form. For example, assume a three-vehicle formation. The control inputs for the first three vehicles are shown, and recall that $\ddot{x}_i = u_i$.

$$\begin{aligned}
u_1 &= k_{p_1}(x_r - x_1 - d_1) + k_{v_1}(\dot{x}_r - \dot{x}_1) + c_{p_1}(x_r - x_1 - d_1) + c_{v_1}(\dot{x}_r - \dot{x}_1) + \ddot{x}_r \\
u_2 &= k_{p_2}(x_1 - x_2 - d_2) + k_{v_2}(\dot{x}_1 - \dot{x}_2) + \\
&\qquad + c_{p_2}\left(x_r - x_2 - (d_1 + d_2)\right) + c_{v_2}(\dot{x}_r - \dot{x}_2) + \ddot{x}_r \\
u_3 &= k_{p_3}(x_2 - x_3 - d_3) + k_{v_3}(\dot{x}_2 - \dot{x}_3) + \\
&\qquad + c_{p_3}\left(x_r - x_3 - (d_1 + d_2 + d_3)\right) + c_{v_3}(\dot{x}_r - \dot{x}_3) + \ddot{x}_r
\end{aligned}$$

The equations of motion have the form $M\ddot{\boldsymbol{x}} + C\dot{\boldsymbol{x}} + K\boldsymbol{x} = D\boldsymbol{u}_r$, where the mass matrix

is the identity matrix, and the damping and stiffness matrices have the following forms.

$$C = \begin{bmatrix} k_{v_1} + c_{v_1} & 0 & 0 \\ -k_{v_2} & k_{v_2} + c_{v_2} & 0 \\ 0 & -k_{v_3} & k_{v_3} + c_{v_3} \end{bmatrix} \tag{5.2}$$

$$K = \begin{bmatrix} k_{p_1} + c_{p_1} & 0 & 0 \\ -k_{p_2} & k_{p_2} + c_{p_2} & 0 \\ 0 & -k_{p_3} & k_{p_3} + c_{p_3} \end{bmatrix} \tag{5.3}$$

The term on the right-hand side of the structural form, $D\boldsymbol{u}_r$, is a forcing term that includes the reference trajectory and constant desired distances between vehicles: d_1, d_2, and d_3. The vector $\boldsymbol{u}_r = [x_r(t),\ \dot{x}_r(t),\ \ddot{x}_r(t),\ d_1,\ d_2,\ d_3]^T$.

$$D = \begin{bmatrix} k_{p_1} + c_{p_1} & k_{v_1} + c_{v_1} & 1 & -(k_{p_1} + c_{p_1}) & 0 & 0 \\ c_{p_2} & c_{v_2} & 1 & -c_{p_2} & -(k_{p_2} + c_{p_2}) & 0 \\ c_{p_3} & c_{v_3} & 1 & -c_{p_3} & -c_{p_3} & -(k_{p_3} + c_{p_3}) \end{bmatrix} \tag{5.4}$$

The chosen communication structure, which defines the information that is available to each vehicle in the system, determines the form of the damping and stiffness matrices. In this case, each vehicle has the state information of its immediately preceding, or lead vehicle, as well as information about the reference trajectory including its desired spacing relative to the reference trajectory. This particular communication structure constrains certain elements of the stiffness and damping matrices to equal zero. Constraints on the elements of these matrices are termed *communicability constraints*, which will be discussed in greater detail in the next chapter.

Note that this communication structure yields stiffness and damping matrices that cannot be represented by a true physical system; i.e., the closed-loop equations of motion cannot be represented by a mass-spring system (vehicle 2 is connected to

vehicle 1, but vehicle 1 is not connected to vehicle 2). Here, the structural analogy refers to the ability to write the closed-loop equations of motion in the linear structural form, rather than an analogy to true physical systems.

B. Modal Coordinates

Second-order, coupled equations of motion in the general structural form can be decoupled using a modal-coordinate transformation to yield n second-order, scalar equations. The physical coordinates are transformed to the decoupled modal coordinates using a matrix of eigenvectors or mode shapes. The modal-coordinate form can be used to design controllers for a true structural system, where the control design is made easier by the decoupled, scalar equations. In the multivehicle application, the control laws couple the system to create a structurally-analogous form, and the modal-coordinate transformation reveals information about the natural frequencies and mode shapes of the system. In the next chapter, the modal-coordinate transformation is used to decouple the closed-loop equations of motion in order to analyze the disturbance-rejection properties of different cooperative control forms derived from their communication structures.

In this section, the modal-coordinate transformation for a general undamped and unforced system of equations is presented. Some specific modifications for the multivehicle control problem are discussed, and an example is shown to illustrate the physical meaning of the modes.

1. Modal-Coordinate Transformation for the General Case

An undamped, unforced system of equations is assumed, where the stiffness matrix K can be asymmetric.

$$M\ddot{\boldsymbol{x}} + K\boldsymbol{x} = 0 \tag{5.5}$$

Solutions to this undamped system are referred to as the free vibration response. Substituting a solution of the form $\boldsymbol{x} = \boldsymbol{\phi}e^{st}$ into Equation (5.5) yields the following expression.

$$\left(Ms^2 + K\right)\boldsymbol{\phi} = 0 \tag{5.6}$$

If $s^2 = -\lambda$, the above equation becomes an eigenvalue problem with unknowns λ and $\boldsymbol{\phi}$.

$$K\boldsymbol{\phi}_i = \lambda_i M\boldsymbol{\phi}_i; \quad i = 1, 2, ..., n \tag{5.7}$$

Here, $\boldsymbol{\phi}_i$ is the eigenvector associated with the ith eigenvalue, λ_i.

The equations of motion can be decoupled using the transformation $\boldsymbol{x} = \Phi\boldsymbol{\eta}$, where the matrix $\Phi = [\boldsymbol{\phi}_1, \boldsymbol{\phi}_2, ..., \boldsymbol{\phi}_n]^T$ is an $n \times n$ matrix of the eigenvectors found by solving the right eigenvalue problem in Equation (5.7), and $\boldsymbol{\eta}$ is an $n \times 1$ vector of modal positions. The eigenvectors from the solution to the left eigenvalue problem are also found.

$$K^T\boldsymbol{\psi}_i = \lambda_i M^T\boldsymbol{\psi}_i; \quad i = 1, 2, ..., n \tag{5.8}$$

The left and right eigenvectors are normalized by the biorthogonality conditions such that the following statements are true [29].

$$\begin{aligned} \boldsymbol{\phi}_i^T M\boldsymbol{\phi}_i &= 1, \quad i = 1, 2, ..., n \\ \boldsymbol{\psi}_j^T M\boldsymbol{\phi}_i &= \delta_{ij}, \quad i, j = 1, 2, ..., n \\ \boldsymbol{\psi}_j^T K\boldsymbol{\phi}_i &= \lambda_i\delta_{ij}, \quad i, j = 1, 2, ..., n \end{aligned} \tag{5.9}$$

The n decoupled equations are found by substituting for $\boldsymbol{x}$ in Equation (5.5), pre-multiplying the expression by $\Psi^T = [\boldsymbol{\psi}_1, \boldsymbol{\psi}_2, ..., \boldsymbol{\psi}_n]^T$, and applying the conditions in Equation (5.9).

$$\ddot{\eta}_i + \lambda_i \eta_i = 0; \quad i = 1, 2, ..., n \tag{5.10}$$

The eigenvalues are equal to the squares of the natural frequencies, thus Equation (5.10) is more commonly written as shown.

$$\ddot{\eta}_i + \omega_i^2 \eta_i = 0; \quad i = 1, 2, ..., n \tag{5.11}$$

In the case that the stiffness matrix, K, is symmetric, the left and right eigenvectors are equal: $\Psi_j = \Phi_j$. Thus, the biorthogonality conditions are modified to reflect this special case.

$$\begin{aligned} \boldsymbol{\phi}_i^T M \boldsymbol{\phi}_i &= 1, \quad i = 1, 2, ..., n \\ \boldsymbol{\phi}_j^T M \boldsymbol{\phi}_i &= \delta_{ij}, \quad i, j = 1, 2, ..., n \\ \boldsymbol{\phi}_j^T K \boldsymbol{\phi}_i &= \lambda_i \delta_{ij}, \quad i, j = 1, 2, ..., n \end{aligned} \tag{5.12}$$

The equations are then decoupled by substituting for $\boldsymbol{x}$ and pre-multiplying by Φ^T.

The eigenvectors, $\boldsymbol{\phi}_i$, that comprise the matrix Φ are known as mode shapes. Mode shapes describe the relative movement of the physical coordinates that oscillate at the same frequency, or the natural frequencies of the system. The solution to the coupled equations of motion, Equation (5.5), is the linear combination of the mode shapes and the solutions to the decoupled equations of motion in modal coordinates [45].

$$\boldsymbol{x}(t) = \eta_1(t)[\boldsymbol{\phi}_1] + \eta_2(t)[\boldsymbol{\phi}_2] + ... + \eta_n(t)[\boldsymbol{\phi}_n] \tag{5.13}$$

2. Modal-Coordinate Transformation for Multivehicle Control

In the previous section, an underlying assumption of the development is that the left and right eigenvector matrices are full rank, and in true structural systems, this assumption holds. However, in the multivehicle control application, the stiffness matrix may not yield full-rank eigenvector matrices. To deal with this challenge, the stiffness matrix is diagonalized using the right-eigenvector matrix, Φ, only; therefore, the diagonal matrix of eigenvalues $\Lambda = \text{diag}\,(\omega_1^2, \omega_2^2, ..., \omega_n^2) = \Phi^{-1}K\Phi$. If the stiffness matrix is symmetric, by the finite-dimensional spectral theorem, there is an orthonormal basis formed by the eigenvectors; thus, Φ is invertible [46]. In the case of an asymmetric stiffness matrix, two scenarios are possible. If the $n \times n$ stiffness matrix has n distinct eigenvalues, then the set of eigenvectors is linearly independent and Φ is invertible. However, if the eigenvalues are not distinct, then the eigenvector matrix may or may not be full rank [35]. To permit invertibility of Φ for the asymmetric case with a rank-deficient eigenvector matrix, the control gains can be perturbed to yield n distinct eigenvalues and equivalently a full-rank eigenvector matrix.

The mass matrix in the multivehicle control application is identity. Therefore, the modal coordinate transformation can be determined using the right eigenvectors only and no normalization is required.

$$\Phi^{-1}M\Phi\ddot{\boldsymbol{\eta}} + \Phi^{-1}K\Phi\boldsymbol{\eta} = I\ddot{\boldsymbol{\eta}} + \Lambda\boldsymbol{\eta} = 0 \tag{5.14}$$

In the multivehicle control problem, the physical coordinates represent the positions of the vehicles. Therefore, the mode shapes indicate how the vehicles move with respect to one another when the modes are excited. To illustrate this, the eigenvector matrix, or mode shapes, for the stiffness matrix in Equation (5.3) with gains $k_{p_1} = c_{p_1} = 1$, $k_{p_2} = c_{p_2} = 1.2$, and $k_{p_3} = c_{p_3} = 1.4$ is shown below. The gains have

been perturbed to yield an invertible Φ matrix.

$$\Phi = \begin{bmatrix} 0.1632 & 0 & 0 \\ 0.4895 & 0.2747 & 0 \\ 0.8566 & 0.9615 & 1.0000 \end{bmatrix} \tag{5.15}$$

The columns of Φ are associated with the modes, where the columns are ordered from the lowest to highest natural frequencies. If the first mode is excited, vehicles 1, 2, and 3 move in the same direction, with vehicles 2 and 3 moving with amplitudes that are 3.00 and 5.25 times greater than the amplitude of vehicle 1, respectively. In the second mode, vehicles 2 and 3 move in the same direction with different amplitudes, and only vehicle 3 is excited in the third mode. Values with opposite signs in the ith eigenvector indicate that vehicles move in opposing directions when the ith mode is excited.

C. Eigenvalue and Eigenvector Sensitivities

Perturbing the control gains in the stiffness matrix perturbs the eigenvalues and eigenvectors, which leads to different natural frequencies and mode shapes than the unperturbed case. Eigenvalue and eigenvector sensitivities can indicate how gain perturbations will change the behavior of a structural system. The sensitivities for the general case are presented, followed by the assumptions for the multivehicle control application. An example is presented for the stiffness matrix in Equation (5.3) to show how perturbations to the control gains affect the natural frequencies and mode shapes.

1. Sensitivities for the General Case

Junkins and Kim derive partial derivatives of eigenvalues and eigenvectors with respect to some perturbing parameter, ρ, for the general system $B\dot{\boldsymbol{x}} = A\boldsymbol{x}$ (with associated eigenvalue problem $A\boldsymbol{\phi} = \lambda_i B\boldsymbol{\phi}_i$ and biorthogonality conditions), where $A = A(\rho)$ and $B = B(\rho)$ [29]. Those results are presented here without derivation.

$$\frac{\partial \lambda_i}{\partial \rho} = \boldsymbol{\psi}_i^T \left(\frac{\partial A}{\partial \rho} - \lambda_i \frac{\partial B}{\partial \rho} \right) \boldsymbol{\phi}_i, \quad i = 1, ..., n \tag{5.16}$$

$$\begin{aligned}
\tfrac{\partial \boldsymbol{\phi}_i}{\partial \rho} = \sum_{j=1}^{n} a_{ji}\boldsymbol{\phi}_j; \quad a_{ji} &= \tfrac{1}{\lambda_i - \lambda_j} \boldsymbol{\psi}_j^T \left(\tfrac{\partial A}{\partial \rho} - \lambda_i \tfrac{\partial B}{\partial \rho} \right) \boldsymbol{\phi}_i, && j \neq i \\
&= -\tfrac{1}{2} \left[\boldsymbol{\phi}_i^T \tfrac{\partial B}{\partial \rho} \boldsymbol{\phi}_i + \sum_{\substack{k=1 \\ k \neq i}}^{n} a_{ki} \boldsymbol{\phi}_k^T (B + B^T) \boldsymbol{\phi}_i \right], && j = i \\
\tfrac{\partial \boldsymbol{\psi}_i}{\partial \rho} = \sum_{j=1}^{n} b_{ji}\boldsymbol{\psi}_j; \quad b_{ji} &= \tfrac{1}{\lambda_i - \lambda_j} \boldsymbol{\psi}_i^T \left(\tfrac{\partial A}{\partial \rho} - \lambda_i \tfrac{\partial B}{\partial \rho} \right) \boldsymbol{\phi}_j, && j \neq i \\
&= -\boldsymbol{\psi}_i^T \tfrac{\partial B}{\partial \rho} \boldsymbol{\phi}_i - a_{ii}, && j = i
\end{aligned} \tag{5.17}$$

2. Sensitivities for Multivehicle Control

In the multivehicle case, $B = I$ and $A = K$; therefore B is not a function of the parameter, ρ. Equations (5.16) and (5.17) are thus simplified to the following expressions.

$$\frac{\partial \lambda_i}{\partial \rho} = \boldsymbol{\psi}_i^T \frac{\partial K}{\partial \rho} \boldsymbol{\phi}_i, \quad i = 1, ..., n \tag{5.18}$$

$$\begin{aligned}
\frac{\partial \boldsymbol{\phi}_i}{\partial \rho} = \sum_{j=1}^{n} a_{ji}\boldsymbol{\phi}_j; \quad a_{ji} &= \tfrac{1}{\lambda_i - \lambda_j}\boldsymbol{\psi}_j^T \tfrac{\partial K}{\partial \rho}\boldsymbol{\phi}_i, \quad j \neq i \\
&= -\sum_{\substack{k=1 \\ k\neq i}}^{n} a_{ki}\boldsymbol{\phi}_k^T\boldsymbol{\phi}_i, \quad j = i \\
\frac{\partial \boldsymbol{\psi}_i}{\partial \rho} = \sum_{j=1}^{n} b_{ji}\boldsymbol{\psi}_j; \quad b_{ji} &= \tfrac{1}{\lambda_i - \lambda_j}\boldsymbol{\psi}_i^T \tfrac{\partial K}{\partial \rho}\boldsymbol{\phi}_j, \quad j \neq i \\
&= -a_{ii}, \qquad\qquad j = i
\end{aligned} \tag{5.19}$$

Equations (5.18) and (5.19) can be used to indicate which natural frequencies and mode shapes are affected by perturbations to certain gains. The eigenvalue and eigenvector sensitivities can be used as a design tool to select control gains.

To demonstrate the effects of control gain perturbations on natural frequencies and mode shapes, consider the stiffness matrix shown in Equation (5.3). This communication structure yields a stiffness matrix with a lower-diagonal form; therefore, the eigenvalues are determined directly from the diagonal elements of K. For this set of gains, the first vehicle is associated with the first mode or the smallest natural frequency, the second vehicle is associated with the second mode, and similarly, the third vehicle is associated with the third mode. Thus, perturbing the control gains for any one of the vehicles has a direct effect on the natural frequency associated with that vehicle. If the control gains for either the first or second vehicle are perturbed, then the first and second modes are affected. For all control-gain perturbations, the third mode remains unchanged because it only includes motion of one vehicle.

The most significant information that the eigenvalue and eigenvector sensitivities can provide is which natural frequencies and mode shapes are unaffected by perturbations to the control gains. More complex stiffness matrices will not have the decoupled nature that is inherent to the form of the stiffness matrix in Equation (5.3). The coupled nature between gains in the stiffness matrix and the sensitivities of the

natural frequencies and mode shapes will be illustrated in the next chapter.

D. Proportional Damping

To this point, the modal-coordinate transformation has only been discussed for the undamped, unforced equations of motion. The modal coordinate transformation is performed using the eigenvector matrix found from the stiffness matrix, K. Adding damping to the equations of motion ($M\ddot{\boldsymbol{x}}+C\dot{\boldsymbol{x}}+K\boldsymbol{x}=0$) does not change the process of decoupling or diagonalizing the stiffness matrix if the system has proportional damping. The system is proportionally damped if the damping matrix, C, is a linear combination of the mass and stiffness matrices, where the weighting terms are scalar constants [45].

$$C = \alpha M + \beta K \tag{5.20}$$

The decoupled, second-order equations of motion now include the damping term.

$$\ddot{\eta}_i + 2\zeta_i\omega_i\dot{\eta}_i + \omega_i^2\eta_i = 0, \quad i = 1, .., n \tag{5.21}$$

Here, ζ_i is the damping ratio of the ith mode. This term can be found directly from the constants α and β in Equation (5.20).

$$\zeta_i = \frac{\alpha}{2\omega_i} + \frac{\beta\omega_i}{2} \tag{5.22}$$

In designing cooperative control laws, the form of the damping matrix is such that the error dynamics are stable and homogeneous. However, it must be verified that non-zero values of α yield the proper form of the damping matrix to maintain homogeneous error dynamics, which ensure non-zero steady-state spacing errors. For example, assuming proportional damping with non-zero α and β and the stiffness

matrix in Equation (5.3), the damping matrix has the form below.

$$C = \begin{bmatrix} \beta(k_{p_1} + c_{p_1}) + \alpha & 0 & 0 \\ -\beta k_{p_2} & \beta(k_{p_2} + c_{p_2}) + \alpha & 0 \\ 0 & -\beta k_{p_3} & \beta(k_{p_3} + c_{p_3}) + \alpha \end{bmatrix} \tag{5.23}$$

Comparing Equation (5.2) and Equation (5.23), it can be seen that non-zero values of α will still yield homogeneous error dynamics if the velocity gains are chosen as: $k_{v_i} = \beta k_{p_i}$ and $c_{v_i} = \beta c_{p_i} + \alpha$.

For a desired set of damping ratios, $\zeta_d = [\zeta_1, \zeta_2, ..., \zeta_n]^T$, one could use Equation (5.22) and a minimum-norm solution to find the values of α and β that minimize the error between the desired and resulting damping ratios [29].

$$\boldsymbol{X} = A^T \left(AA^T\right)^{-1} B; \quad \text{where } \boldsymbol{X} = \begin{bmatrix} \alpha \\ \beta \end{bmatrix}, \quad A = \begin{bmatrix} \frac{1}{2\omega_1} & \frac{\omega_1}{2} \\ \frac{1}{2\omega_2} & \frac{\omega_2}{2} \\ \vdots & \vdots \\ \frac{1}{2\omega_n} & \frac{\omega_n}{2} \end{bmatrix}, \quad B = \begin{bmatrix} \zeta_1 \\ \zeta_2 \\ \vdots \\ \zeta_n \end{bmatrix} \tag{5.24}$$

E. Chapter Summary

The analogy of cooperative multivehicle systems to structural systems was shown, where the closed-loop equations of motion for the multivehicle systems can be written using mass, damping, and stiffness matrices. The modal-coordinate transformation was described, and this transformation decouples the equations of motions into n second-order, scalar equations. For the multivehicle-control application, the form of the stiffness matrix may not lead to a full-rank matrix of eigenvectors. The control gains in the stiffness matrix can be perturbed in order to yield a full-rank eigenvector matrix, which enables the system to be decoupled. Eigenvalue and eigenvector sensitivities to perturbations in the stiffness matrix and proportional damping were also

discussed.

The structural analogy presented in this chapter will be used in the next chapter to investigate the effects of disturbances on cooperative multivehicle systems. To this end, two analysis tools will be presented to evaluate disturbance rejection, and these tools enable comparison between different control forms. More specifically, the concept of communication structures, which determine the form of the stiffness and damping matrices, will be further explored, and the analysis tools will be used to evaluate the behavior and stability of different communication structures.

CHAPTER VI

EVALUATING COMMUNICATION STRUCTURES USING STRUCTURAL ANALYSIS AND DESIGN METHODOLOGIES

The previous chapter showed that cooperative control laws are analogous to structural systems where the multivehicle systems are coupled through shared state information. Error terms in the control laws mimic physical connections between vehicles, and the equations of motion can be written in a structural form. It was shown that the form of the stiffness and damping matrices is determined by the assumed communication structure, which defines the information that is shared between vehicles. The system's natural frequencies and mode shapes are determined by the form of the stiffness matrix. Thus, it is intuitive that multivehicle systems can respond very differently to disturbances based upon the assumed communication structure. Whereas the work presented in previous chapters assumed a leader-follower communication structure and knowledge of a reference trajectory, other communication structures may be more ideal based upon system constraints and disturbance-rejection behavior.

There are several structural analysis tools available in the literature to evaluate the disturbance response of structural systems. The application of these structural-analysis tools to the multivehicle control application is explored to both evaluate and compare communication structures. In addition, these tools can be used to determine appropriate control gains to achieve a desired response. Two analysis tools are investigated: modal cost and frequency-response functions. Modal cost compares the communication structures based upon system response to impulsive disturbances, and frequency-response functions are used to evaluate system response to periodic excitation. The traditional structural-analysis tools presented here do not directly apply to the cooperative control of multivehicle systems, and thus, the tools

have been interpreted and modified for the multivehicle control application. The frequency-response analysis, in particular, reveals the string stability of the different control forms.

The chapter is organized as follows. First, the disturbed vehicle model is presented in Section A to show how the disturbances affect the transformation to the double-integrator design space that was first described in Chapter II. The structural-analysis tools are then presented in Section B. Seven communication structures are described in Section C, and in Section D, the analysis tools are used to compare the seven communication structures. In Section E, the analysis and control design of a ten-vehicle formation illustrates the use of the analysis tools in the design process. Lastly, a nonlinear programming problem is presented in Section F to aid in the design of control gains for a given communication structure.

A. Vehicle Model with Disturbances

The analysis of disturbance effects on system performance will be used to compare communication structures that couple multivehicle systems. Disturbances in the original nonlinear vehicle model are first related to the transformation that allows the vehicle model to be represented by the double-integrator form that has motivated the research to this point. If the disturbances are known, then the transformation essentially cancels the effects of the disturbances. However, the disturbance-rejection properties of the system are important in the case when the disturbances are unknown and cannot be canceled.

The nonlinear vehicle model used throughout this research represents vehicles with no sideslip, and the transformation to the double-integrator representation enforces the nonholonomic or kinematic constraint. Disturbances to the nonlinear

model, of the form shown, can be considered disturbances to the kinematic constraint.

$$\begin{aligned} \dot{x} &= v\cos\theta + d_x \\ \dot{y} &= v\sin\theta + d_y \\ \dot{\theta} &= \omega \end{aligned} \tag{6.1}$$

The disturbed vehicle model requires some definition of terms. The velocity v is the ideal velocity, or the commanded velocity of the vehicle, which can be measured using onboard sensors, and the angle θ is the true heading angle of the vehicle. The $v\cos\theta$ and $v\sin\theta$ terms are the projections of the ideal velocities in the x and y directions and are denoted as v_x and v_y, respectively. The sum of the projections of the ideal velocities and the disturbance terms, $\dot{x}$ and $\dot{y}$, are the true velocities in the x and y directions, respectively. These relationships are illustrated in Figure 19.

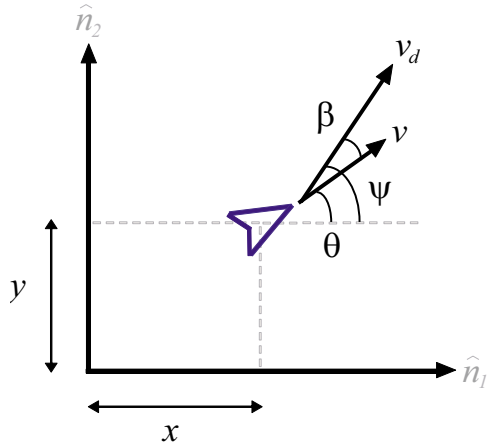

Fig. 19.: Disturbed vehicle model.

The disturbance velocity has magnitude v_d and angle ψ with respect to the horizontal axis.

$$v_d = \sqrt{\dot{x}^2 + \dot{y}^2} = \sqrt{(v_x + d_x)^2 + (v_y + d_y)^2} \tag{6.2}$$

$$\psi = \tan^{-1}\left(\frac{\dot{y}}{\dot{x}}\right) = \tan^{-1}\left(\frac{v_y + d_y}{v_x + d_x}\right) \tag{6.3}$$

The sideslip angle is the difference between the angle of the disturbance velocity and the true vehicle heading: $\beta = \psi - \theta$.

The ideal velocity and the true heading angle can also be written as a function of the true velocities and the disturbances.

$$v = \sqrt{(\dot{x} - d_x)^2 + (\dot{y} - d_y)^2}; \quad \theta = \tan^{-1}\left(\frac{\dot{y} - d_y}{\dot{x} - d_x}\right) \tag{6.4}$$

Vehicle controls, $\dot{v}$ and ω, are found by taking derivatives of the above expressions.

$$\dot{v} = \frac{(\dot{x} - d_x)(\ddot{x} - \dot{d}_x) + (\dot{y} - d_y)(\ddot{y} - \dot{d}_y)}{v} \tag{6.5}$$

$$\omega = \frac{(\dot{x} - d_x)(\ddot{y} - \dot{d}_y) - (\dot{y} - d_y)(\ddot{x} - \dot{d}_x)}{v^2} \tag{6.6}$$

If the disturbances, d_x, $\dot{d}_x$, d_y, and $\dot{d}_y$, are known, then the controls are chosen as $\ddot{x} = u(x, \dot{x})$ and $\ddot{y} = w(y, \dot{y})$. In other words, if one can determine the true velocities from knowledge of d_x and d_y, then the controls are functions of positions and true velocities. The transformation to $\dot{v}$ and ω becomes a function of disturbance rates.

$$\begin{bmatrix} \dot{v} \\ \omega \end{bmatrix} = \frac{1}{v} \begin{bmatrix} v_x & v_y \\ -\frac{v_y}{v} & \frac{v_x}{v} \end{bmatrix} \begin{bmatrix} u - \dot{d}_x \\ w - \dot{d}_y \end{bmatrix} \tag{6.7}$$

This transformation essentially cancels the effects of the disturbances by controlling the true accelerations of the vehicle and subtracting the disturbance rates.

If the disturbances are unknown, then the controls are chosen as $\dot{v}_x = u(x, v_x)$ and $\dot{v}_y = w(y, v_y)$. Therefore, the controls are calculated using knowledge of the ideal velocity and true heading angle only. In this case, the controls and transformation are not functions of the disturbances, and the transformation looks the same as when

no disturbances are present.

$$\begin{bmatrix} \dot{v} \\ \omega \end{bmatrix} = \frac{1}{v} \begin{bmatrix} v_x & v_y \\ -\frac{v_y}{v} & \frac{v_x}{v} \end{bmatrix} \begin{bmatrix} u \\ w \end{bmatrix} \tag{6.8}$$

The disturbed vehicle model in Equation (6.1) can be expressed as double integrators that are decoupled in the x and y directions. The disturbances act at the kinematics level in the double-integrator form.

Known Disturbance:	$\dot{x} = v_x + d_x$	$\dot{y} = v_y + d_y$
	$\ddot{x} = u(x, \dot{x})$	$\ddot{y} = w(y, \dot{y})$
Unknown Disturbance:	$\dot{x} = v_x + d_x$	$\dot{y} = v_y + d_y$
	$\dot{v}_x = u(x, v_x)$	$\dot{v}_y = w(y, v_y)$

As in Chapter II, the double-integrator form serves as a design space, and control inputs designed in this space are transformed to the vehicle controls using the appropriate transformation.

It is likely that in many cases, the disturbance is unknown; therefore, the disturbance-rejection properties of the control laws must be investigated. Some communication structures may demonstrate better disturbance rejection than others. Two approaches to evaluate disturbance effects are described: modal cost and frequency-response functions. These analysis tools, developed to analyze structural systems, serve as both a means to compare different communication structures and as a design tool to evaluate control gains.

B. Cooperative-Control-Law Analysis Tools

1. Modal Cost

Modal cost fits within a broader topic: component cost analysis [29]. A system can be divided into components that represent physical subsystems, such as actuators or sensors, or mathematical subsystems like modal coordinates. The component cost is the contribution of a specific component to an overall performance index or cost function. A quadratic performance index is developed as the cost function, and the performance index is decomposed into the contributions from each component of interest [29]. Modal coordinates are in many ways ideal for component-cost analysis. As will be shown in the development presented here, when modal coordinates are used as the system states, the component cost is each mode's contribution to the system performance index.

In the past, modal-cost analysis has been used for model reduction or actuator placement in structural systems. In the case of model reduction, the system is disturbed and the modal cost reveals which modes contribute the least to the overall system cost. Therefore, the modes with small contributions to the cost are eliminated, and the system is modeled with fewer modes [47, 48]. Whereas the number of modal coordinates is reduced, the number of physical coordinates does not change. In the case of actuator placement, different configurations with actuators placed in varying locations can be compared using the modal cost as an indicator of controllability. For a given configuration of actuators, the system is disturbed, and the modal cost indicates how well the actuator configuration is able to control the modes [49, 50].

Modal cost for the multivehicle system is used to evaluate modal disturbability, which describes the excitation or contribution of each mode to the cost function given an impulsive disturbance to each vehicle. The modal cost is used to compare

communication structures for their disturbability, where communication structures with lower disturbability measures are desired. In this section, the cost analysis is presented for the structural system in physical coordinates written in its first-order form. The component cost is also presented followed by the modal-cost analysis for the structural system. The application to the multivehicle formation control problem is discussed and a modal-cost measure is presented, which is used to compare the disturbability of different communication structures.

a. Cost Analysis for Physical Coordinates

The second-order equations of motion for the multivehicle system can be written in a first-order form. Note that in this analysis, the forcing terms in the closed-loop equations of motion are set equal to zero. The disturbance-effects analysis for the unforced system also holds for a translating formation that is tracking a reference trajectory.

$$\dot{\boldsymbol{z}} = A\boldsymbol{z} + B\boldsymbol{u}; \quad A = \left[\begin{array}{c:c} 0 & I \\ \hdashline -M^{-1}K & -M^{-1}C \end{array}\right], \quad B = \left[\begin{array}{c} I \\ \hdashline 0 \end{array}\right], \quad \boldsymbol{z} = \left[\begin{array}{c} \boldsymbol{x} \\ \hdashline \boldsymbol{v_x} \end{array}\right] \tag{6.9}$$

The position and velocity vectors are of dimension $n \times 1$; therefore, $\boldsymbol{z} \in R^{2n}$. Each vehicle in the system is subjected to impulsive disturbances; thus, $\boldsymbol{u}$ is also an $n \times 1$ vector. Note that the disturbances act at the kinematics level as described in the previous section, which dictates this form of the control influence matrix, B.

A cost function is defined to represent system performance when subjected to the disturbance inputs.

$$V = \sum_{i=1}^{n} \int_0^\infty {y_d^i}^T(t) Q_v y_d^i(t) dt; \quad y_d^i(t) = C_d x^i(t) \tag{6.10}$$

Here, $y_d^i(t)$ models a desired output using the matrix C_d; the matrix Q_v is a weighting

matrix; and, $\boldsymbol{x}^i(t)$ is the system response to a unit impulse to the ith vehicle. The impulses are assumed to be applied at $t = 0$ with initial conditions equal to zero. The cost function, V, is the system's output "energy" over the n disturbance inputs. Computation of the cost function is eased by the analytical solution to Equation (6.9) for an impulsive input to the ith vehicle.

$$\boldsymbol{x}^i(t) = e^{At}\boldsymbol{x}(0) + \int_0^t e^{A(t-\tau)}Bu(\tau)d\tau = e^{At}\boldsymbol{b}_i \tag{6.11}$$

The $n \times 1$ vector b_i is the ith column of the B matrix. Junkins and Kim show that the cost function can be rewritten using a matrix identity and Equation (6.11) [29].

$$\begin{aligned} V &= \text{trace}\left[Q_v C_d \left(\sum_{i=1}^{n}\int_0^\infty e^{At}\boldsymbol{b}_i\boldsymbol{b}_i^T e^{A^T t}dt\right) C_d^T\right] \\ &= \text{trace}\left[Q_v C_d \left(\int_0^\infty e^{At}BB^T e^{A^T t}dt\right) C_d^T\right] \end{aligned} \tag{6.12}$$

The parenthetical term above is the controllability grammian, X, which is an indicator of the controllability of the linear system in Equation (6.9). A system is controllable if the controllability grammian is full rank [29, 35].

$$X \equiv \int_0^\infty e^{At}BB^T e^{A^T t}dt \tag{6.13}$$

The controllability grammian satisfies the Lyapunov equation.

$$XA^T + AX = -BB^T \tag{6.14}$$

Therefore, the cost function can be determined using the $n \times n$ matrix, X.

$$V = \text{trace}\left(Q_v C_d X C_d^T\right) \tag{6.15}$$

b. Component Cost

The cost function can be decomposed into the individual contributions of each state, where the contributions of the ith state, $\boldsymbol{x}_i$, are related to the cost V [29].

$$V_{x_i} \equiv \frac{1}{2}\frac{\partial V}{\partial x_i}x_i; \quad V = \sum_{i=1}^{n} V_{x_i} \tag{6.16}$$

The component cost is also computed using the controllability grammian.

$$V_{x_i} = \left[XC_d^T Q_v C_d\right]_{ii} \tag{6.17}$$

Proofs of these results are presented in Junkins and Kim [29].

c. Cost Analysis for Modal Coordinates

Computing the modal cost of a system has several advantages over evaluating the cost using physical coordinates. Each component cost is the modal cost; therefore, the modal cost indicates which modes are most excited when the system is subjected to a disturbance. The computation of the system cost is similar to the development for the physical-coordinate cost. The first-order system has the same form as Equation (6.9); the A matrix is redefined using the diagonalized stiffness and damping matrices; the B matrix is transformed to relate the individual vehicle inputs to each mode; and, $\boldsymbol{z}$ is a vector of modal positions and velocities.

$$A = \left[\begin{array}{c:c} 0 & I \\ \hdashline -\tilde{K} & -\tilde{C} \end{array}\right]; \quad B = \left[\begin{array}{c} \Phi^{-1} \\ \hdashline 0 \end{array}\right]; \quad \boldsymbol{z} = \left[\begin{array}{c} \boldsymbol{\eta} \\ \hdashline \dot{\boldsymbol{\eta}} \end{array}\right] \tag{6.18}$$

The cost function is the same as in Equation (6.10), where the input u_i is an impulse to the ith vehicle. The output $y_d(t)$ is related to the modal coordinates.

$$\begin{aligned} y_d(t) &= C_d \left[\begin{array}{c} \boldsymbol{x}(t) \\ \hdashline \boldsymbol{v_x}(t) \end{array}\right] = \left[\begin{array}{c:c} C_{d_{\boldsymbol{x}}} & 0 \\ \hdashline 0 & C_{d_{\boldsymbol{v_x}}} \end{array}\right] \left[\begin{array}{c} \boldsymbol{x}(t) \\ \hdashline \boldsymbol{v_x}(t) \end{array}\right] \\ &= C_d \left[\begin{array}{c} \Phi\boldsymbol{x}(t) \\ \hdashline \Phi\boldsymbol{v_x}(t) \end{array}\right] = \left[\begin{array}{c:c} C_{d_{\boldsymbol{x}}}\Phi & 0 \\ \hdashline 0 & C_{d_{\boldsymbol{v_x}}}\Phi \end{array}\right] \left[\begin{array}{c} \boldsymbol{\eta}(t) \\ \hdashline \dot{\boldsymbol{\eta}}(t) \end{array}\right] \end{aligned} \tag{6.19}$$

The weighting matrix, Q_v, is also partitioned into parts related to $\boldsymbol{x}$ and $\boldsymbol{v_x}$.

$$Q_v = \left[\begin{array}{c:c} Q_{\boldsymbol{x}} & 0 \\ \hdashline 0 & Q_{\boldsymbol{v_x}} \end{array}\right] \tag{6.20}$$

The modal cost for the ith mode is comprised of costs related to both the modal position and the modal velocity.

$$V_i = V_{\boldsymbol{\eta_i}} + V_{\dot{\boldsymbol{\eta}}_i} \tag{6.21}$$

Costs V_{η_i} and $V_{\dot{\eta}_i}$ are determined by appropriately substituting for C_d, Q_v, and X in Equation (6.17). The controllability grammian is still determined using the Lyapunov equation, and the resulting matrix can be partitioned into four parts.

$$X = \left[\begin{array}{c:c} X_{\boldsymbol{\eta\eta}} & X_{\boldsymbol{\eta\dot{\eta}}} \\ \hdashline X_{\boldsymbol{\dot{\eta}\eta}} & X_{\boldsymbol{\dot{\eta}\dot{\eta}}} \end{array}\right] \tag{6.22}$$

The diagonal blocks of X are used to compute the modal cost.

$$V_{\boldsymbol{\eta_i}} = \left[X_{\boldsymbol{\eta\eta}}\Phi^T C_{d_{\boldsymbol{x}}}^T Q_{\boldsymbol{x}} C_{d_{\boldsymbol{x}}}\Phi\right]_{ii}; \quad V_{\dot{\boldsymbol{\eta}}_{\boldsymbol{i}}} = \left[X_{\dot{\boldsymbol{\eta}}\dot{\boldsymbol{\eta}}}\Phi^T C_{d_{\dot{\boldsymbol{x}}}}^T Q_{\dot{\boldsymbol{x}}} C_{d_{\dot{\boldsymbol{x}}}}\Phi\right]_{ii} \tag{6.23}$$

If the output matrix, C_d, and the weighting matrix, Q_v, are chosen as identity, then the cost function in Equation (6.10) evaluates the disturbability of each mode from

the equilibrium position.

d. Modal-Cost Measure

A modal-cost measure α is developed in order to compare communication structures when each vehicle is subjected to an impulsive disturbance. Therefore, the measure is defined to quantify the disturbability of the whole system. Here, the L_2 norm is used find the scalar quantity α.

$$\alpha = \sqrt{\left(\frac{V_1}{V}\right)^2 + \left(\frac{V_2}{V}\right)^2 + ... + \left(\frac{V_n}{V}\right)^2} \tag{6.24}$$

The communication structure with the smallest value of α is the least disturbable system.

2. Frequency Response Functions

Frequency response functions (FRFs) describe the steady-state response of a system to harmonic excitation for a given input frequency [45, 51]. For single degree-of-freedom (DOF) systems, the FRF can be used to design controllers and select control gains to stabilize the open-loop system, and the closed-loop FRF provides information about low-frequency input tracking and high-frequency noise rejection. Here, the multi-DOF FRFs are used to evaluate disturbance effects on the formation. The developments in this section show that string stability of the formation can be determined using frequency-response information to find the steady-state errors between adjacent vehicles. This approach allows communication structures to be evaluated and compared for string stability in disturbance environments.

In this section, frequency-response functions for single- and multi-DOF systems are reviewed. The steady-state solutions are developed for the multi-DOF systems, and the analogy to string stability is presented. The frequency-response analysis for

the structurally-analogous system has some relation to previous work in graph theory, and this relationship is also discussed.

a. Single-Degree-of-Freedom Systems

The steady-state response of linear, damped, second-order systems to harmonic excitation is also harmonic with the same frequency as the excitation with a different amplitude and a phase shift. For example, the system below has a steady-state solution of the form $x_{ss} = X\cos(\sigma t - \alpha)$ [45].

$$m\ddot{x} + c\dot{x} + kx = f\cos(\sigma t) \tag{6.25}$$

The steady-state solution can be rewritten as $x_{ss} = X\left[\cos(\sigma t)\cos(\alpha) + \sin(\sigma t)\sin(\alpha)\right]$. Substituting x_{ss} into Equation (6.25) yields two equations, which are the $\sin(\sigma t)$ and $\cos(\sigma t)$ terms.

$$(k^2 - m\sigma^2)\sin\alpha - c\sigma\cos\alpha = 0 \tag{6.26}$$

$$(k^2 - m\sigma^2)\cos\alpha + c\sigma\sin\alpha = \frac{f}{X} \tag{6.27}$$

The phase angle α is found from Equation (6.26).

$$\alpha = \tan^{-1}\left(\frac{c\sigma}{k^2 - m\sigma^2}\right) \tag{6.28}$$

The amplitude of the steady-state solution, X, is found by squaring and adding Equations (6.26) and (6.27).

$$X = \frac{f}{\sqrt{(k^2 - m\sigma^2)^2 + (c\sigma)^2}} \tag{6.29}$$

The FRF is composed of two parts: the ratio of the steady-state amplitude to the static response, $H(\sigma)$, and the phase of the response, α [45]. The static response of

the system in Equation (6.25) is $x_{static} = f/k$.

$$H(\sigma) = \frac{X}{x_{static}} = \frac{k}{\sqrt{(k^2 - m\sigma^2)^2 + (c\sigma)^2}} \tag{6.30}$$

Equation (6.25) can also be written in terms of the natural frequency and damping ratio.

$$\ddot{x} + 2\zeta\omega\dot{x} + \omega^2 x = f\cos(\sigma t) \tag{6.31}$$

Here, $\omega^2 = k/m$ and $2\zeta\omega = c/m$. Equations (6.28) and (6.30) are rewritten in terms of the damping ratio, natural frequency, and the ratio of the excitation frequency to the natural frequency, $r = \sigma/\omega$.

$$H(r) = \frac{1}{\sqrt{(1 - r^2)^2 + (2\zeta r)^2}}; \quad \alpha = \tan^{-1}\left(\frac{2\zeta r}{1 - r^2}\right) \tag{6.32}$$

Of greater interest in this case is the receptance function, which is the ratio of the steady-state amplitude to the excitation amplitude.

$$\frac{X}{f} = \frac{1}{\sqrt{(\omega^2 - \sigma^2)^2 + (2\zeta\omega\sigma)^2}} \tag{6.33}$$

Equation (6.33) determines the amplification of the disturbance by the system. Ideally, one would choose system parameters such that the ratio X/f is less than one for all excitation frequencies.

b. Multi-Degree-of-Freedom Systems

Receptance functions for multi-DOF systems relate steady-state amplitudes of the jth output to the kth input. The multi-DOF receptance functions are determined using modal coordinates and appropriate transformations to express ratios in terms of physical coordinates. The structural system is expressed in the familiar first-order

form with a disturbance acting at the kinematics level.

$$\dot{\boldsymbol{z}} = \left[\begin{array}{c:c} 0 & I \\ \hdashline -M^{-1}K & -M^{-1}C \end{array}\right] \boldsymbol{z} + \left[\begin{array}{c} \boldsymbol{f}\cos(\sigma t) \\ \hdashline 0 \end{array}\right]; \quad \boldsymbol{z} = \left[\begin{array}{c} \boldsymbol{x} \\ \hdashline \boldsymbol{v_x} \end{array}\right] \tag{6.34}$$

Note that the control, which is represented by the lower partition of Equation (6.34), is a function of the position and ideal velocity because the disturbance is assumed unknown. Equation (6.34) is decoupled using a modal-coordinate transformation.

$$\dot{\boldsymbol{z}}_{\boldsymbol{\eta}} = \left[\begin{array}{c:c} 0 & I \\ \hdashline -\tilde{K} & -\tilde{C} \end{array}\right] \boldsymbol{z}_{\boldsymbol{\eta}} + \left[\begin{array}{c} \tilde{\boldsymbol{f}}\cos(\sigma t) \\ \hdashline 0 \end{array}\right]; \quad \boldsymbol{z} = \left[\begin{array}{c} \boldsymbol{\eta_1} \\ \hdashline \boldsymbol{\eta_2} \end{array}\right] \tag{6.35}$$

The diagonal matrices $\tilde{K} = \Phi^{-1}K\Phi$ and $\tilde{C} = \Phi^{-1}C\Phi$, and the transformed disturbance input $\tilde{\boldsymbol{f}} = \Phi^{-1}\boldsymbol{f}$. The ith mode can be described by a set of first-order equations.

$$\dot{\eta}_{i,1} = \eta_{i,2} + \tilde{f}_i\cos(\sigma t) \tag{6.36}$$

$$\dot{\eta}_{i,2} = -\tilde{K}_i\eta_{i,1} - \tilde{C}_i\eta_{i,2} \tag{6.37}$$

To be rigorous in terminology, $\dot{\eta}_{i,1}$ is the true modal velocity, and $\eta_{i,2}$ is the ideal modal velocity. A derivative is taken of Equation (6.36) and appropriate substitutions are made in order to write the equations of motion for the ith mode in a second-order form.

$$\begin{aligned} \ddot{\eta}_{i,1} &= \dot{\eta}_{i,2} - \sigma\tilde{f}_i\sin(\sigma t) \\ &= -\tilde{K}_i\eta_{i,1} - \tilde{C}_i\eta_{i,2} - \sigma\tilde{f}_i\sin(\sigma t) \\ &= -\tilde{K}_i\eta_{i,1} - \tilde{C}_i\left(\dot{\eta}_{i,1} - \tilde{f}_i\cos(\sigma t)\right) - \sigma\tilde{f}_i\sin(\sigma t) \end{aligned} \tag{6.38}$$

Thus, the second-order equation that describes the ith modal dynamics subject to a kinematic disturbance has two excitation terms on the right-hand side.

$$\ddot{\eta}_{i,1} + \tilde{C}_i\dot{\eta}_{i,1} + \tilde{K}_i\eta_{i,1} = \tilde{C}_i\tilde{f}_i\cos(\sigma t) - \sigma\tilde{f}_i\sin(\sigma t) \tag{6.39}$$

The steady-state solution to the above expression is written as a sum of the steady-state solutions for the $\cos(\cdot)$ and $\sin(\cdot)$ excitation terms.

$$\eta_{i,ss} = N_i^I\cos(\sigma t - \alpha_i^I) + N_i^{II}\sin(\sigma t - \alpha_i^{II}). \tag{6.40}$$

The receptance functions and phases for each term in the solution are found using the same approach described for single-DOF systems, where r_i is the ratio of the excitation frequency to the ith natural frequency.

$$\frac{N_i^I}{\tilde{f}_i} = \frac{\tilde{C}_i}{\omega_i^2\sqrt{(1-r_i^2)^2 + (2\zeta_i r_i)^2}}; \quad \alpha_i^I = \tan^{-1}\left(\frac{2\zeta_i\omega_i\sigma}{\omega_i^2 - \sigma^2}\right) \tag{6.41}$$

$$\frac{N_i^{II}}{\tilde{f}_i} = \frac{\sigma}{\omega_i^2\sqrt{(1-r_i^2)^2 + (2\zeta_i r_i)^2}}; \quad \alpha_i^{II} = \tan^{-1}\left(\frac{-2\zeta_i\omega_i\sigma}{\sigma^2 - \omega_i^2}\right) \tag{6.42}$$

The steady-state amplitudes in modal coordinates are transformed to the steady-state amplitudes in physical coordinates using the modal matrix.

$$\boldsymbol{X} = \Phi(\boldsymbol{N}^I + \boldsymbol{N}^{II}) \tag{6.43}$$

The vectors of modal amplitudes are defined as $\boldsymbol{N}^I = D^I\Phi^{-1}\boldsymbol{f}$ and $\boldsymbol{N}^{II} = D^{II}\Phi^{-1}\boldsymbol{f}$, where D^I and D^{II} are defined below.

$$D^I = \text{diag}\left(\frac{\tilde{C}_1}{\omega_1^2 s_1}, \frac{\tilde{C}_2}{\omega_2^2 s_2}, ..., \frac{\tilde{C}_n}{\omega_n^2 s_n}\right); \quad D^{II} = \text{diag}\left(\frac{\sigma}{\omega_1^2 s_1}, \frac{\sigma}{\omega_2^2 s_2}, ..., \frac{\sigma}{\omega_n^2 s_n}\right) \tag{6.44}$$

The term s_i is the square root term in Equations (6.41) and (6.42).

$$s_i = \sqrt{(1-r_i^2)^2 + (2\zeta_i r_i)^2} \tag{6.45}$$

The receptance functions for the multi-DOF system in physical coordinates are determined via appropriate substitutions.

$$H_{jk} \equiv \frac{X_j}{f_k} = \left[\Phi(D^I + D^{II})\Phi^{-1}\right]_{jk} \tag{6.46}$$

Here, H is an $n \times n$ matrix, and the (j,k)th element of H is the ratio of the jth output to the kth input. More specifically for the multivehicle-control application, H_{jk} is the ratio of the steady-state amplitude of the jth vehicle to the amplitude of the disturbance to the kth vehicle. The matrix H is symmetric if the eigenvector matrix Φ is symmetric (if the stiffness matrix K is symmetric).

To illustrate the use of the receptance functions as an analysis tool, an example receptance function is presented and interpreted here. Figure 20 shows the receptance functions for the cooperative control of a three-vehicle system, where the H matrix is not symmetric.

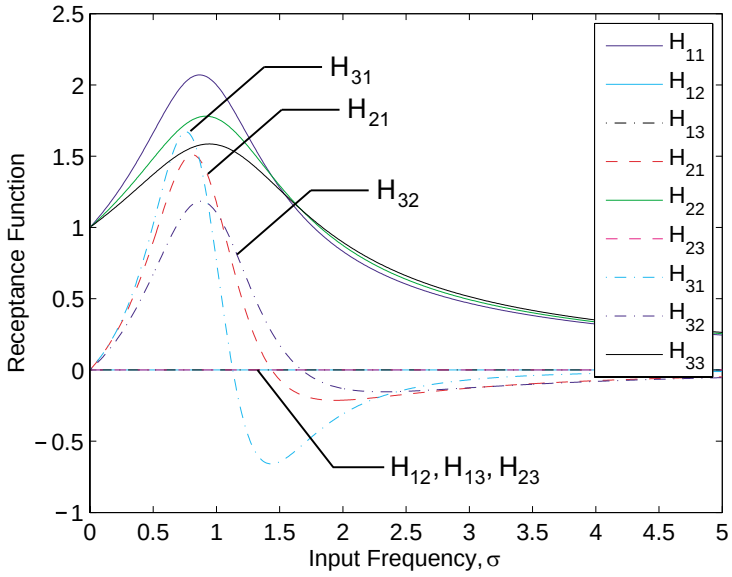

Fig. 20.: Example receptance function for a three-vehicle system.

The behavior of H_{31} and H_{32} reveals notable behavior in the motion of the multivehicle system. As previously defined, the functions H_{31} and H_{32} describe the motion of vehicle 3 due to disturbances to vehicles 1 and 2, respectively. The peak magnitude of H_{31} is greater than the peak magnitude of H_{32}, which indicates that disturbances to vehicle 1 have a greater effect on vehicle 3 than the disturbances to vehicle 2 have on vehicle 3. String instabilities are essentially defined as the growth of errors through a system of vehicles; hence, Figure 20 may indicate that errors are propagated through the vehicle string for this cooperative control law. For this example, the cooperative control laws are in fact string unstable.

The frequency-response information provides a way to analyze formation dynamics in disturbance environments, and the interpretation of the example receptance functions shows that the receptance functions may reveal string stabilities or instabilities. However, the receptance functions alone may not reveal instabilities; therefore to more fully analyze the string stability of communication structures, the steady-state errors between vehicles must be determined. Whereas the receptance functions show the magnitudes of the steady-state responses relative to disturbance inputs from each vehicle, the steady-state amplitude of the jth vehicle is determined using the steady-state modal amplitudes and the phase information.

c. Steady-State Solution from Frequency-Response Functions

The steady-state response of the ith vehicle in physical coordinates can be expressed using the superposition of the modal-coordinate responses.

$$x_{i,ss} = x^I_{i,ss} + x^{II}_{i,ss} = \Phi_{ij}\left[N^I_j \cos(\sigma t - \alpha^I_j) + N^{II}_j \sin(\sigma t - \alpha^{II}_j)\right] \tag{6.47}$$

The first term in Equation (6.47) can be expanded and rearranged as shown.

$$\begin{aligned} x^I_{i,ss} &= \Phi_{i1}N^I_1 \cos(\sigma t - \alpha^I_1) + \Phi_{i2}N^I_2 \cos(\sigma t - \alpha^I_2) + ... + \Phi_{in}N^I_n \cos(\sigma t - \alpha^I_n) \\ &= \Phi_{i1}N^I_1 \left[\cos(\sigma t)\cos(\alpha^I_1) + \sin(\sigma t)\sin(\alpha^I_1)\right] + \\ &\quad + \Phi_{i2}N^I_2 \left[\cos(\sigma t)\cos(\alpha^I_2) + \sin(\sigma t)\sin(\alpha^I_2)\right] + ... \\ &\quad ... + \Phi_{in}N^I_n \left[\cos(\sigma t)\cos(\alpha^I_n) + \sin(\sigma t)\sin(\alpha^I_n)\right] \\ &= \sin(\sigma t)\left[\Phi_{i1}N^I_1 \sin(\alpha^I_1) + \Phi_{i2}N^I_i \sin(\alpha^I_2) + ... + \Phi_{in}N^I_n \sin(\alpha^I_n)\right] + \\ &\quad + \cos(\sigma t)\left[\Phi_{i1}N^I_1 \cos(\alpha^I_1) + \Phi_{i2}N^I_i \cos(\alpha^I_2) + ... + \Phi_{in}N^I_n \cos(\alpha^I_n)\right] \end{aligned} \tag{6.48}$$

The response is written as $x^I_{i,ss} = A_i \sin(\sigma t) + B_i \cos(\sigma t)$.

$$A_i = \Phi_{i1}N^I_1 \sin(\alpha^I_1) + \Phi_{i2}N^I_i \sin(\alpha^I_2) + ... + \Phi_{in}N^I_n \sin(\alpha^I_n) \tag{6.49}$$

$$B_i = \Phi_{i1}N^I_1 \cos(\alpha^I_1) + \Phi_{i2}N^I_i \cos(\alpha^I_2) + ... + \Phi_{in}N^I_n \cos(\alpha^I_n) \tag{6.50}$$

The second term in Equation (6.47) can be rearranged similarly.

$$\begin{aligned} x^{II}_{i,ss} &= \sin(\sigma t)\left[\Phi_{i1}N^{II}_1 \cos(\alpha^{II}_1) + \Phi_{i2}N^{II}_2 \cos(\alpha^{II}_2) + ... + \Phi_{in}N^{II}_n \cos(\alpha^{II}_n)\right] + \\ &\quad + \cos(\sigma t)\left[\Phi_{i1}N^{II}_1 \sin(\alpha^{II}_1) + \Phi_{i2}N^{II}_2 \sin(\alpha^{II}_2) + ... + \Phi_{in}N^{II}_n \sin(\alpha^{II}_n)\right] \end{aligned} \tag{6.51}$$

Here, $x_{i,ss}^{II} = C_i \sin(\sigma t) - D_i \cos(\sigma t)$.

$$C_i = \Phi_{i1} N_1^{II} \cos(\alpha_1^{II}) + \Phi_{i2} N_2^{II} \cos(\alpha_2^{II}) + ... + \Phi_{in} N_n^{II} \cos(\alpha_n^{II}) \tag{6.52}$$

$$D_i = \Phi_{i1} N_1^{II} \sin(\alpha_1^{II}) + \Phi_{i2} N_2^{II} \sin(\alpha_2^{II}) + ... + \Phi_{in} N_n^{II} \sin(\alpha_n^{II}) \tag{6.53}$$

Therefore, the steady-state response of the ith vehicle is expressed as the sum of $x_{i,ss}^{I}$ and $x_{i,ss}^{II}$.

$$x_{i,ss} = (A_i + C_i) \sin(\sigma t) + (B_i - D_i) \cos(\sigma t). \tag{6.54}$$

The amplitude of the steady-state solution is: $X_{i,ss} = \sqrt{(A_i + C_i)^2 + (B_i - D_i)^2}$. Vector expressions for A, B, C, and D can be found using the following expressions.

$$\boldsymbol{A} = \Phi \ \mathrm{diag}(\boldsymbol{N}^I) \sin(\boldsymbol{\alpha}^I) \tag{6.55}$$

$$\boldsymbol{B} = \Phi \ \mathrm{diag}(\boldsymbol{N}^I) \cos(\boldsymbol{\alpha}^I) \tag{6.56}$$

$$\boldsymbol{C} = \Phi \ \mathrm{diag}(\boldsymbol{N}^{II}) \cos(\boldsymbol{\alpha}^{II}) \tag{6.57}$$

$$\boldsymbol{D} = \Phi \ \mathrm{diag}(\boldsymbol{N}^{II}) \sin(\boldsymbol{\alpha}^{II}) \tag{6.58}$$

Whereas the receptance function, H, shows how vehicles are affected by the disturbances to other vehicles, the steady-state solution can be used to find the maximum steady-state amplitude of each vehicle. The steady-state errors between adjacent vehicles can also be found using the steady-state solutions.

$$e_{(i,i+1),ss} = (A_i + C_i - A_{i+1} - C_{i+1}) \sin(\sigma t) + (B_i - D_i - B_{i+1} + D_{i+1}) \cos(\sigma t) \tag{6.59}$$

The amplitude of the steady-state errors is easily found.

$$E_{(i,i+1),ss} = \sqrt{(A_i + C_i - A_{i+1} - C_{i+1})^2 + (B_i - D_i - B_{i+1} + D_{i+1})^2}. \tag{6.60}$$

To illustrate the theory presented in this section, the steady-state vehicle amplitudes and the steady-state errors between vehicles are shown in Figure 21 for the

receptance functions presented in Figure 20. Figure 21(a) shows that the steady-state amplitudes of the vehicle motion grow along the string, and the steady-state errors also grow as shown in Figure 21(b). Therefore, the behavior of the steady-state errors reveals that the cooperative control laws for the three-vehicle systems are string unstable in this example.

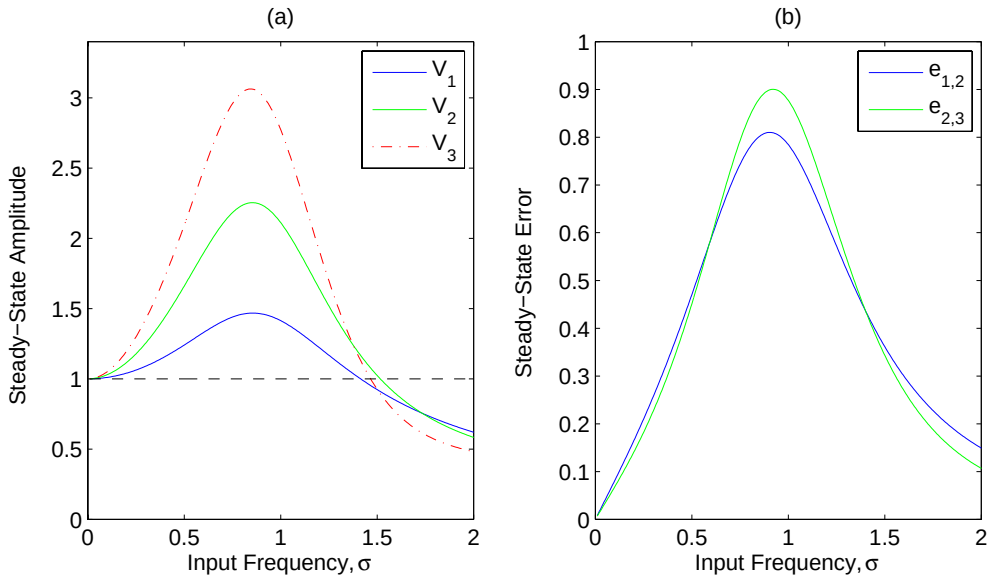

Fig. 21.: Example steady-state amplitudes (a) and errors (b) for a three-vehicle system.

In Section D, simulation results will be used to illustrate the evidence of string instabilities in the frequency-response information. In addition, the influence of control gains on system response can be evaluated using the frequency-response analysis, and the analysis tools can aid in the selection of control gains for stability and performance.

d. Relationship to Previous Work

As described in Chapter I, Fax and Murray investigated information flow in decentralized, cooperative systems to evaluate formation stability for linear, homogeneous systems [11]. Information flow between vehicles is described using a directed graph from which the *Laplacian* of the graph is easily found. A dynamic compensator is used for relative position control, and the closed-loop equations of motion include the Laplacian. Formation stability is evaluated by decoupling the equations of motion through a Schur transformation [29] of the Laplacian. The decoupled system is a function of the eigenvalues of the Laplacian; therefore, the control law stabilizes the formation if it stabilizes the decoupled system for each of the eigenvalues. Stability is alternatively proved using the Nyquist-stability criterion. Here, the Laplacian is analogous to the structure of the stiffness matrix, which has been shown in Chapter V to represent the communication structure of the multivehicle system.

Extensions to the work by Fax and Murray investigated the effects of disturbances on formation stability. Jin and Murray investigated string stability for a look-ahead formation, where control inputs are functions of preceding vehicles' states only, using a transfer function matrix to relate spacing errors in the formation [52]. That approach has some similarities to the frequency-response string-stability analysis described by Swaroop and Hedrick [15] and the multi-DOF receptance functions and subsequent string-stability analysis presented here. Gattami and Murray extended the Nyquist-stability criterion to explore formation stability when the system is subject to multiplicative uncertainties [12].

Yadlapalli, et al. investigated the effects of information flow on rigid formations, where "rigid" links between vehicles are designed to maintain a rigid formation during translational maneuvers [43]. In that reference, the researchers made the connection

between the undirected Laplacian matrix from the information-flow graph and a stiffness matrix comprised of springs with unit stiffnesses. The propagation of spacing errors was studied to investigate constraints on the information flow to achieve bounded spacing errors independent of the number of vehicles in the formation. Analysis of the spacing errors employed a frequency-domain approach using the decoupled system (similar to the approach used by Fax and Murray) in order to determine a bound on the degree of the information flow that permits a scalable controller.

In the present work, the use of structural analogies in the stability analysis of multivehicle systems does show some similarities to the aforementioned research approaches. Most notably, the Laplacian matrix has been shown to be analogous to the structure of the stiffness matrix, and this analogy was exploited by Yadlapalli, et al. The Laplacian matrix used by Yadlapalli was derived from an undirected graph indicating bidirectional communication, which can be physically represented by masses connected by springs. In contrast, the Laplacian matrix used by Fax and Murray was directed and therefore does not necessarily yield a physical representation; similar to that work, the communication structures in this research are not constrained to be physically representative. In this research, the structural analogy has been further investigated to demonstrate the use of structural design methodologies to achieve desired system behaviors and performance.

C. Communication Structures and Control-Law Design

In Chapter V and throughout this chapter, the communication structure and its impact on the form of the stiffness matrix have been discussed. There are two factors to consider when selecting the communication structure: (1) system constraints and (2) design considerations. The system constraints may arise due to limitations on

which vehicles can communicate based upon separation distances or processing speeds of communication between vehicles. Design considerations may determine the selected communication structure in order to mitigate disturbance effects on the formation.

As the previous sections described, the modal cost can be used to select a communication structure based upon its disturbability, and the frequency-response characteristics of the system can be used to analyze string stability and determine control gains. Whereas there is no specific order for the application of these analysis and design tools, they can be used in combination and iteratively to meet application-specific objectives.

1. Communication Structures

Figure 22 illustrates seven different communication structures for a three-vehicle formation. In the figure, vehicle 1 is the platoon lead, which tracks a reference trajectory, and vehicles 2 and 3 are trailing vehicles. Whereas the general cooperative control law in Equation (3.6) assumes that each vehicle in the formation has knowledge of the reference trajectory, the communication structures in Figure 22 assume that only the first vehicle has knowledge of the reference trajectory. The arrow heads point to the vehicle receiving state information from where the arrow originates. The two-headed arrows indicate bidirectional communication, i.e., each vehicle has information about the other vehicle. An arrow with only one head indicates a single connection. Double-headed arrows can also be represented by springs or dampers; however, single-headed arrows do not have an equivalent physical representation.

These communication-structure concepts can be extended to an n-vehicle formation based upon the descriptions in the figure. A fully-connected communication structure, for example, means that all vehicles in the formation have information about all of the other vehicles. In communication structures 2 through 4, the sec-

ond through nth vehicles have information about the formation lead, and the trailing vehicles communicate as described in Figure 22.

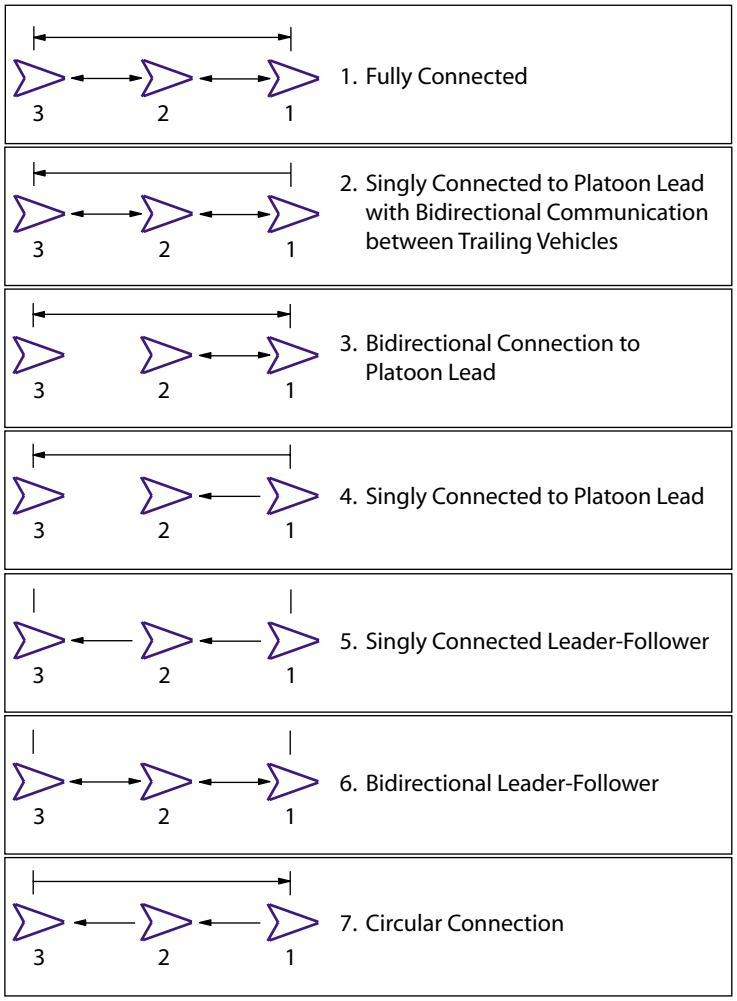

Fig. 22.: Seven possible communication structures for multivehicle formation control.

In some decentralized applications, vehicles will broadcast packets containing current state information for use by other vehicles, and equivalently, vehicles will receive and process packets from other vehicles in order to determine control inputs. Whereas the modal-cost and frequency-response analysis tools can be used to compare the disturbability and assess the string-stability characteristics of each communica-

tion structure, two other quantities are defined that may be a contributing factor in the selection of a communication structure. The first quantity is the total number of received packets by the entire n-vehicle system at each time step, and the second quantity is the maximum number of packets processed by one vehicle in the formation. The second quantity gives an indication of the onboard processing requirements necessary for a particular communication structure. Table II show the two quantities for each communication structure.

Table II.: Packet Processing for the Communication Structures.

Comm. Structure	# of Packets (n-vehicles)	Max # of Packets Processed by 1 Veh.	Veh.(s) Processing Max # of Packets
1	$\sum_{j=1}^{n} 2(n-j)$	$n-1$	all
2	$2(n-1)+(n-2)$	2, $n=3$ 3, $n>3$	2,...,n
3	$2(n-1)$	$n-1$	1
4	$n-1$	1	2,...,n
5	$n-1$	1	2,...,n
6	$2(n-1)$	2	2,...,(n-1)
7	n	1	all

2. Control-Law Design

Following the design approach developed in Chapter III, where cooperative control inputs are functions of spacing errors as determined by the communication structure,

error terms are defined between all vehicles. The number of error terms in an n-vehicle system is $n_e = \left(\sum_{j=1}^{n-1} j\right) + 1$. For example, in a three-vehicle formation, there are four error terms.

$$\begin{aligned}
e_{r1} &= x_r - x_1 - d_{r1}; \quad & \dot{e}_{r1} &= \dot{x}_r - \dot{x}_1; \quad & \ddot{e}_{r1} &= \ddot{x}_r - u_1 \\
e_{12} &= x_1 - x_2 - d_{12}; \quad & \dot{e}_{12} &= \dot{x}_1 - \dot{x}_2; \quad & \ddot{e}_{12} &= u_1 - u_2 \\
e_{13} &= x_1 - x_3 - d_{13}; \quad & \dot{e}_{13} &= \dot{x}_1 - \dot{x}_3; \quad & \ddot{e}_{13} &= u_1 - u_3 \\
e_{23} &= x_2 - x_3 - d_{23}; \quad & \dot{e}_{23} &= \dot{x}_2 - \dot{x}_3; \quad & \ddot{e}_{23} &= u_2 - u_3
\end{aligned} \tag{6.61}$$

The notation of the error variables in Equation (6.61) is slightly different from the notation introduced in Chapter III. Here, the two subscripts denote each vehicle in the spacing-error definition because the error variables are no longer limited to adjacent vehicle pairs. It should be noted that the errors and desired distances between vehicles are constrained; e.g., $e_{13} = e_{12} + e_{23}$, and equivalently, $d_{13} = d_{12} + d_{23}$. The control inputs are functions of the error terms as defined by the communication structure, and the stiffness, damping, and forcing matrices can be determined accordingly.

Consider the control inputs for a three-vehicle formation using the fully-connected communication structure (communication structure 1 in Figure 22).

$$\begin{aligned}
u_1 &= -k_{12}(x_1 - x_2) - c_{12}(\dot{x}_1 - \dot{x}_2) - k_{13}(x_1 - x_3) - c_{13}(\dot{x}_1 - \dot{x}_3) + \\
&\qquad + k_r(x_r - x_1) + c_r(\dot{x}_r - \dot{x}_1) \\
u_2 &= k_{12}(x_1 - x_2) + c_{12}(\dot{x}_1 - \dot{x}_2) - k_{23}(x_2 - x_3) - c_{23}(\dot{x}_2 - \dot{x}_3) \\
u_3 &= k_{13}(x_1 - x_3) + c_{13}(\dot{x}_1 - \dot{x}_3) + k_{23}(x_2 - x_3) + c_{23}(\dot{x}_2 - \dot{x}_3)
\end{aligned} \tag{6.62}$$

It is assumed that the control gain k_{ij} (c_{ij}) on the spacing error e_{ij} ($\dot{e}_{ij}$) is the same wherever it is used. This assumption reduces some of the design degrees of freedom, but it is not a necessary constraint in the developments here. The stiffness matrix is

found from the control inputs.

$$K = \begin{bmatrix} k_r + k_{12} + k_{13} & -k_{12} & -k_{13} \\ -k_{12} & k_{12} + k_{23} & -k_{23} \\ -k_{13} & -k_{23} & k_{13} + k_{23} \end{bmatrix} \tag{6.63}$$

The damping matrix has the same form and is proportional to the stiffness matrix: $C = \beta K$. By comparing Equations (6.62) and (6.63), it can be seen that the stiffness matrix can be determined by inspection from the communication structures, and the damping and forcing matrices can be found similarly. Appendix E lists the stiffness and forcing matrices for the seven communication structures in Figure 22.

D. Design Problem: Use of Analysis Tools

Simulation examples are used to illustrate the use of the modal-cost and frequency-response analysis and design tools.

1. Modal Cost to Compare Communication Structures

The seven communication structures are compared using the modal-cost measure in Equation (6.24). The control gains in the stiffness matrices are assumed equal to one; however, because communication structures 2, 4, 5, and 7 are asymmetric, the invertibility of the Φ matrix must be explored. The gains in communication structures 2 and 7 do not need to be perturbed to allow invertibility of the Φ matrix, but the gains in communication structures 4 and 5 must be perturbed. In communication structure 4, the stiffness matrix has a lower diagonal form with k_{1j} gains, where $j = 2, ..., n$, along the diagonal. These gains are perturbed by 0.01 such that $k_{1j} = 1 + 0.01(j-1)$, and this yields n distinct eigenvalues and a full-rank eigenvector matrix. The stiffness matrix for communication structure 5 is also a lower-diagonal matrix, and the diagonal

gains are perturbed to yield n distinct eigenvalues. Here, the $k_{j(j+1)}$ gains, for $j = 1, ..., n-1$, are perturbed by 0.25 to get $k_{j(j+1)} = 1 + 0.25j$. The damping matrices are assumed proportional to the stiffness matrices with $\beta = 1$. Table III shows the modal-cost measures for each communication structure for formations of 3, 5, and 10 vehicles.

Table III.: Comparison of Communication Structures using Modal-Cost Measure α.

Communication Structure	α (n = 3)	α (n = 5)	α (n = 10)
1	0.6379	0.5406	0.4516
2	0.6166	0.4956	0.3864
3	0.6232	0.5076	0.3997
4	8.6874	6.5425	4.2205
5	0.8440	7.9597	114.3824
6	0.6562	0.6132	0.6387
7	0.6340	0.5037	unstable

In each case, communication structure 2 is the least disturbable. The large values for communication structures 4 and 5 are related to the perturbations in the gains. Choosing different values for the gain perturbations will yield different values for the modal-cost measure; however, the costs still remain greater than the costs for the other communication structures. Communication structure 7 becomes unstable, where the closed-loop A matrix has at least one pair of eigenvalues in the right-half plane, for six or more vehicles in the formation.

Based upon these results, communication structures 1, 2, and 3 are similar in terms of the magnitude of the modal-cost measure. From the modal-cost results

alone, one would likely choose the second or third communication structure over the first because fewer packets need to be processed by the system. Communication structure 3 requires the formation lead vehicle to process $n-1$ packets at each time step; however, the second through nth vehicles only process one packet at each time. Therefore, different processing requirements will allow lesser-equipped, or cheaper, vehicles to be integrated with better-equipped vehicles.

2. Frequency-Response Analysis for String Stability

The modal-cost analysis can be used to compare communication structures for disturbablity; however, this analysis does not give an indication of string stability. The frequency-response analysis is used to analyze the string stability of each of the communication structures.

a. Receptance Functions

Figures 23 through 29 show the receptance functions for the seven communication structures in Figure 22 assuming a three-vehicle formation. The receptance functions for communication structure 1, the fully-connected system, are symmetric due to the symmetry of the stiffness matrix. Recall that the (j,k)th element of the receptance function is the ratio of the jth vehicle's output to the kth vehicle's disturbance input. Because the gains k_{13} and k_{23} are equal, the disturbance effects from vehicles 2 and 3 equally affect vehicle 1. The peak of H_{11} is smaller due to the additional gain from the reference tracking. The receptance function only exhibits one resonant frequency at the first mode, which has a damping ratio of 0.26; the other modes have damping ratios closer to one.

The receptance functions for communication structures 2 and 3 display similarities to the results for communication structure 1. Differences in the receptance

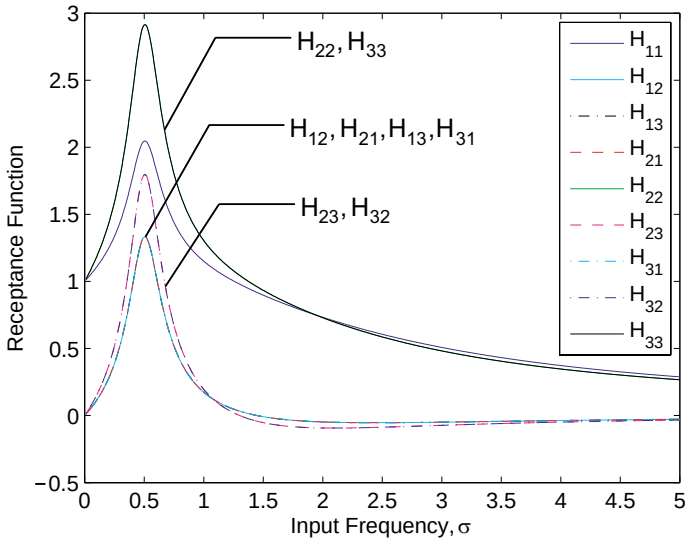

Fig. 23.: Receptance function for communication structure 1.

functions are, of course, attributed to the differences in the stiffness matrices. Communication structure 4 in Figure 26 shows different behavior in that some vehicles are unaffected by disturbances to other vehicles, and those elements of H are zero for all disturbance frequencies; e.g., vehicle 3 is unaffected by disturbances to vehicle 2, and vice versa. The receptance functions for each of these communication structures do not give an indication of string instabilities based upon the interpretation of the receptance functions presented previously.

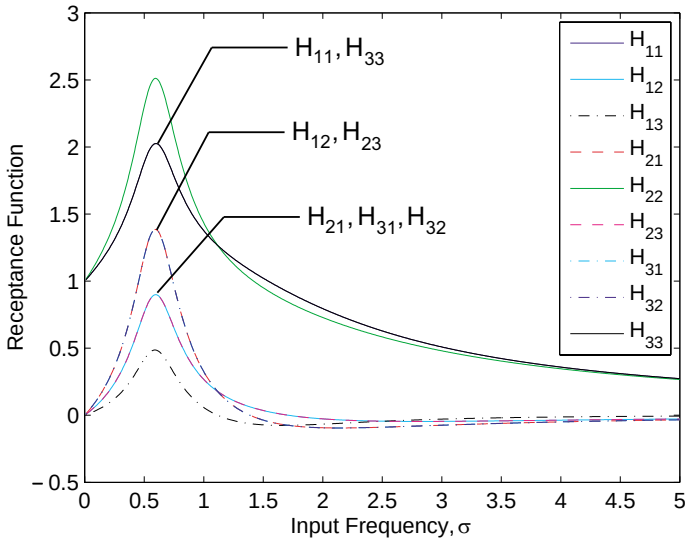

Fig. 24.: Receptance function for communication structure 2.

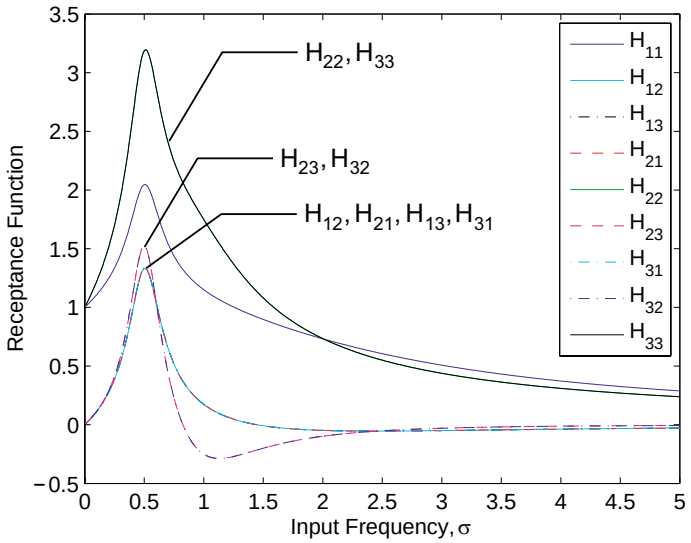

Fig. 25.: Receptance function for communication structure 3.

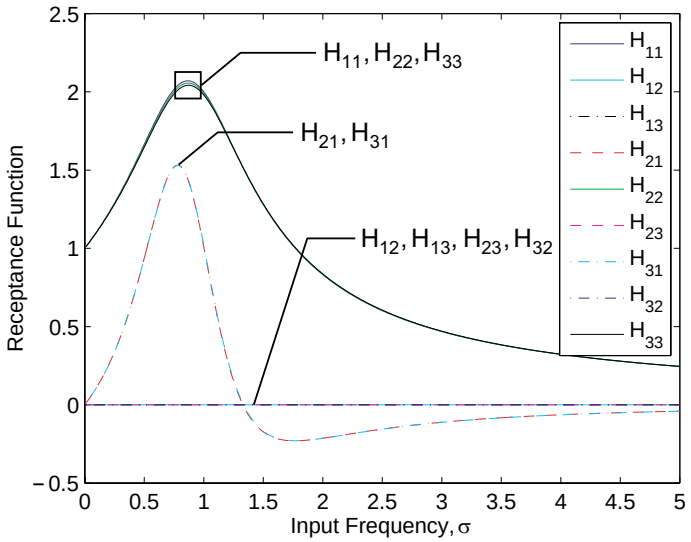

Fig. 26.: Receptance function for communication structure 4.

The receptance functions for communication structure 5 are shown in Figure 27, which is the same figure as the example in Figure 20. Recall that the string instabilities become evident by examining the behavior of H_{31} and H_{32}. This suggests that disturbances to vehicle 1 have a greater effect than disturbances to vehicle 2 on the motion of vehicle 3. In the analysis here, it is known that vehicle 3 is connected to vehicle 2 through its control input, but it is not connected to vehicle 1.

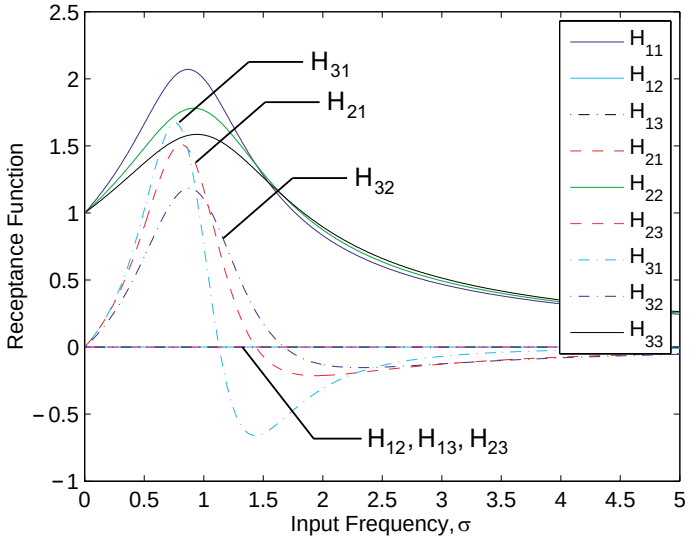

Fig. 27.: Receptance function for communication structure 5.

Communication structure 6 displays similar behavior to communication structures 1, 2, and 3; however, the peak magnitudes are much greater. Thus, disturbances near the resonant frequency are amplified more for this communication structure. String instabilities are not evident in this figure, and further examination of the steady-state errors indicates that this communication structure yields string-stable cooperative control laws.

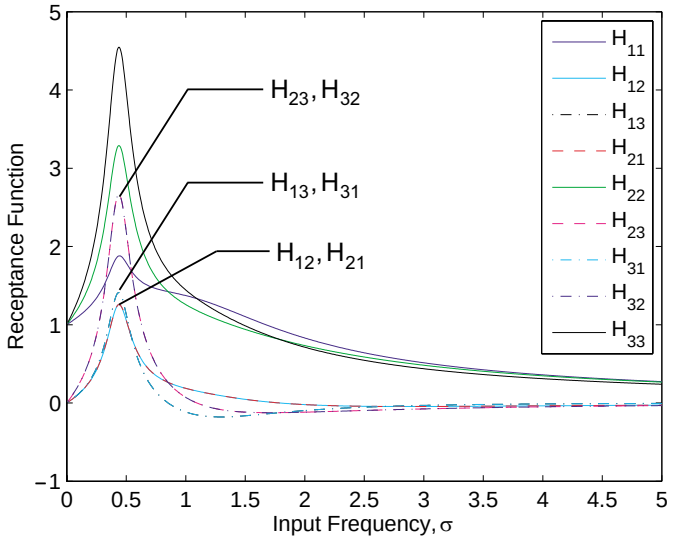

Fig. 28.: Receptance function for communication structure 6.

The receptance functions for communication structure 7 do not immediately indicate string instabilities for this communication structure; however, the peak magnitude of H_{32} is greater than H_{21}, which may indicate that the errors amplify through the vehicle string. However, a priori knowledge of the communication structure would suggest that error growth would be evident if H_{13} is greater than H_{32}. This is not the case here, and this communication structure is in fact string stable.

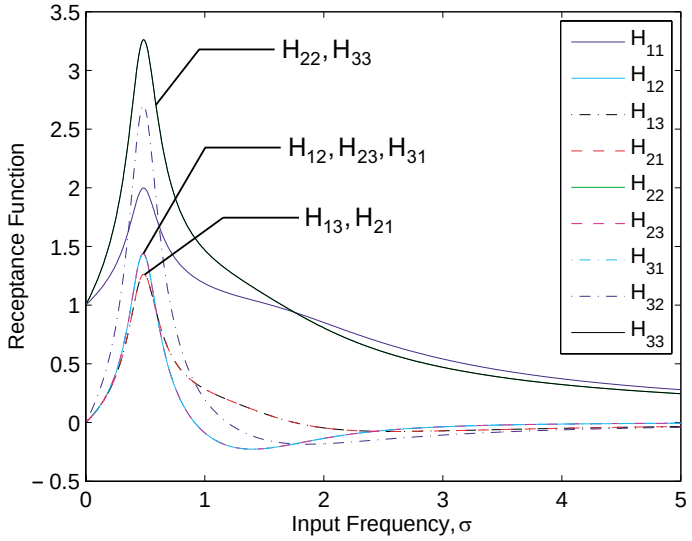

Fig. 29.: Receptance function for communication structure 7.

b. Steady-State Solution to Evaluate String Stability

Communication structures 1, 2, and 5 are further explored here to illustrate the evidence of string stability or instability in the receptance functions. Ten-vehicle formations are used to further show the string-stability characteristics for the selected communication structures.

The receptance functions in Figure 23 for a three-vehicle formation indicate that communication structure 1 leads to string-stable control laws. The receptance functions for the tenth vehicle shown in Figure 30 show that the tenth vehicle is equally affected by disturbances to vehicles 2 through 9. Figure 31(a) shows the steady-state amplitudes of the vehicle positions for communication structure 1, and this figure shows that the steady-state amplitudes of vehicles 2 through 10 are equal. Thus, the steady-state errors between all adjacent vehicle pairs are zero with the exception of the error between the first and second vehicles as shown in Figure 31(b). The errors between vehicles pair do not grow along the vehicle string, which satisfies the definition of string stability.

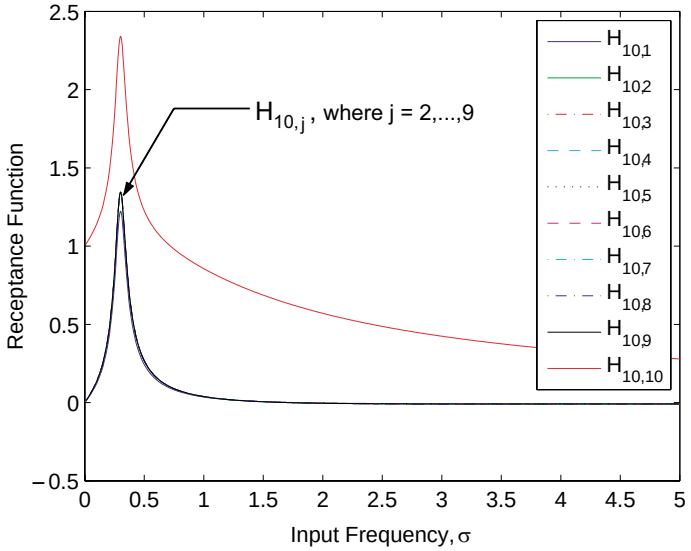

Fig. 30.: Receptance functions for the tenth vehicle (communication structure 1).

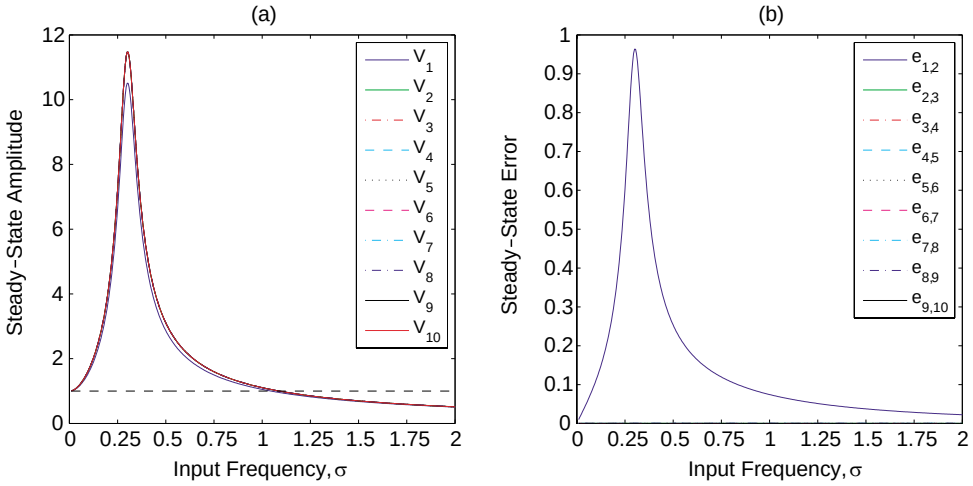

Fig. 31.: Steady-state amplitudes of the vehicle positions (a) and steady-state errors (b) for communication structure 1.

Figures 32 and 33 show the receptance functions for the tenth vehicle and the steady-state errors for communication structure 2, respectively. For this communication structure, the disturbances to other vehicles do not equally affect the tenth vehicle as was the case for communication structure 1. Here, it is not clear whether the receptance function indicates string instabilities; therefore, the steady-state errors are investigated. Figure 33 shows that this communication structure is in fact string stable. This communication structure does exhibit a wider frequency band where the error between the first and second vehicles is affected. Thus, it can be seen how communication structure 1 may be more advantageous for some disturbance frequencies.

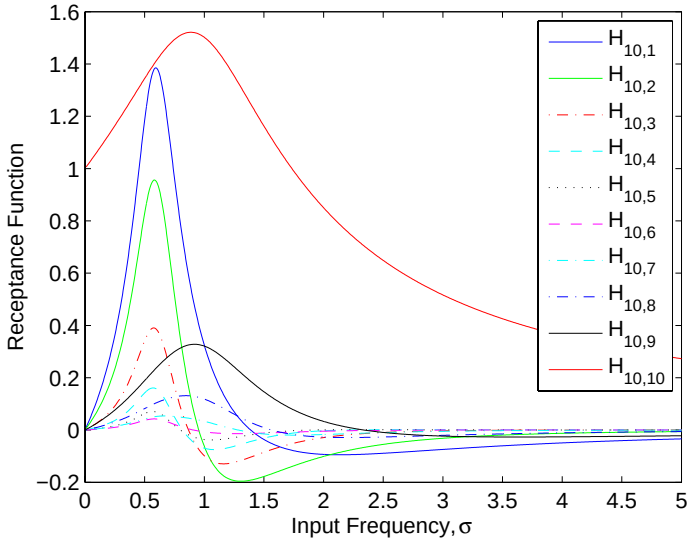

Fig. 32.: Receptance functions for the tenth vehicle (communication structure 2).

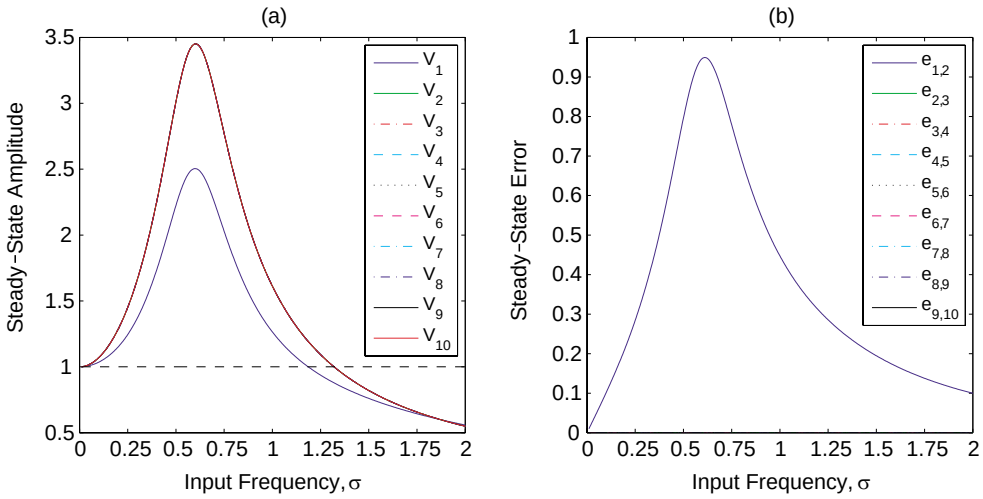

Fig. 33.: Steady-state amplitudes of the vehicle positions (a) and steady-state errors (b) for communication structure 2.

The receptance functions for communication structure 5 exhibit string instabilities for the three-vehicle example in Figure 27. For this communication structure, the receptance functions are plotted for all ten vehicles to show how the disturbance effects grow along the string of vehicles (Figure 34). The string instabilities are obvious from the receptance functions and a priori knowledge of the communication structure. Figure 35 shows the steady-state vehicle amplitudes (a) and steady-state errors between vehicles (b). The errors between trailing vehicle pairs increase for a range of input frequencies, and hence, this particular communication structure leads to string instabilities.

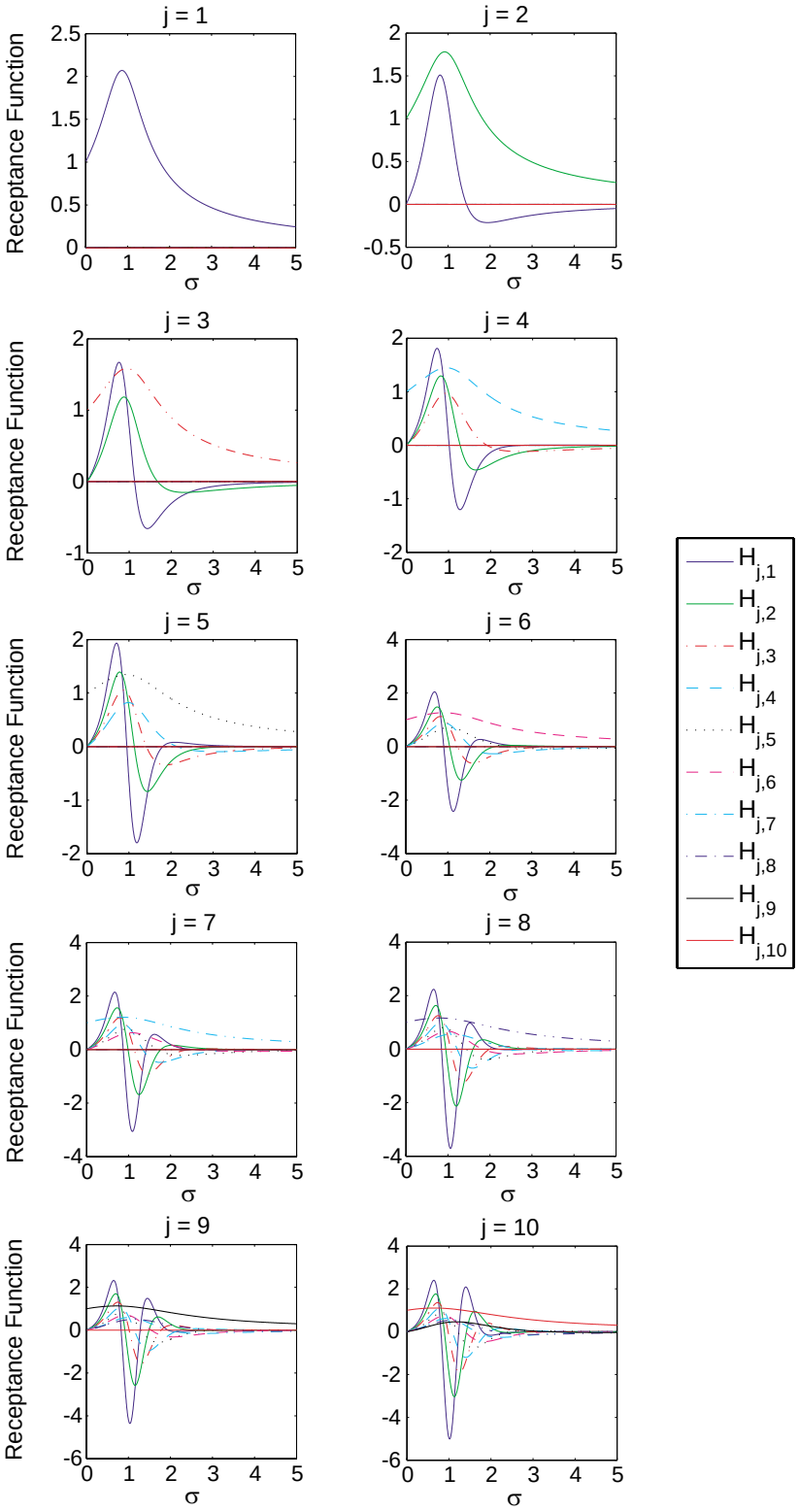

Fig. 34.: Receptance functions for all ten vehicles (communication structure 5).

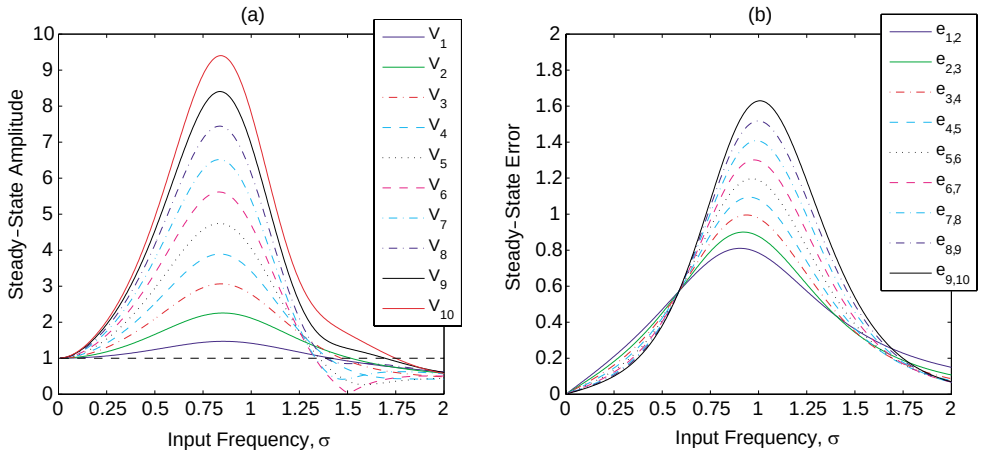

Fig. 35.: Steady-state amplitudes of the vehicle positions (a) and steady-state errors (b) for communication structure 5.

The ten-vehicle formation is simulated for a reference trajectory along the x axis with $\dot{x}_r = 5$ DU/TU. The desired spacing between vehicles is 1 DU in the x direction. Disturbances are of the form $d_{x,y} = \cos(\sigma t)$, where $\sigma = 1$ is the first natural frequency, or the resonant frequency, of the system. Figure 36 shows that the errors grow between vehicle pairs along the vehicle string as predicted by the frequency-response results in Figure 35(b). Figure 37 shows the calculated control inputs necessary to maintain the formation. If these control inputs were bounded, some vehicles in the formation may not be able to maintain their position. Therefore, this communication structure could not be used for an infinite string of vehicles.

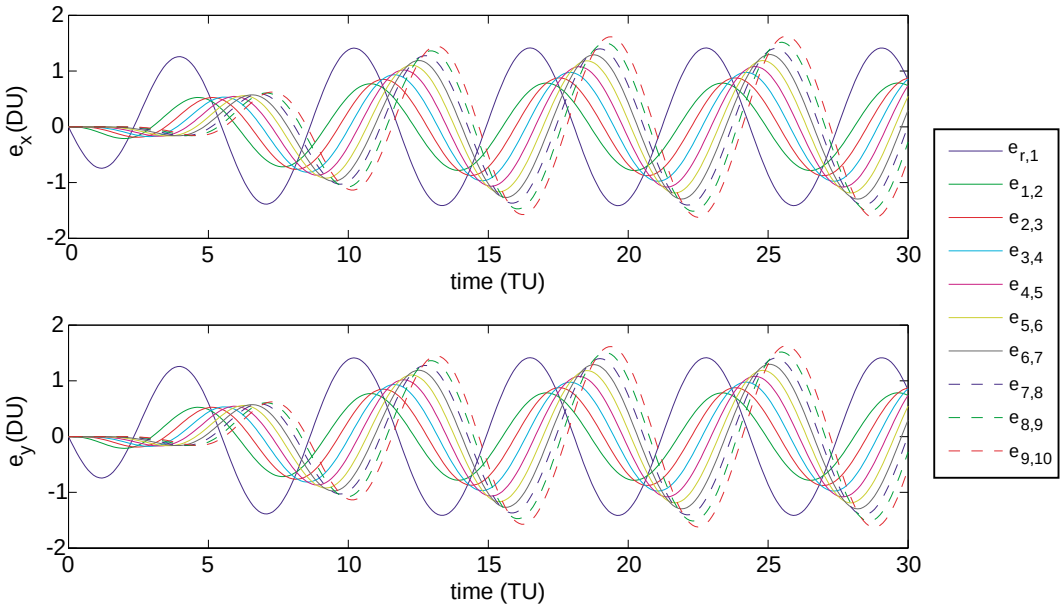

Fig. 36.: Spacing errors between vehicles (communication structure 5).

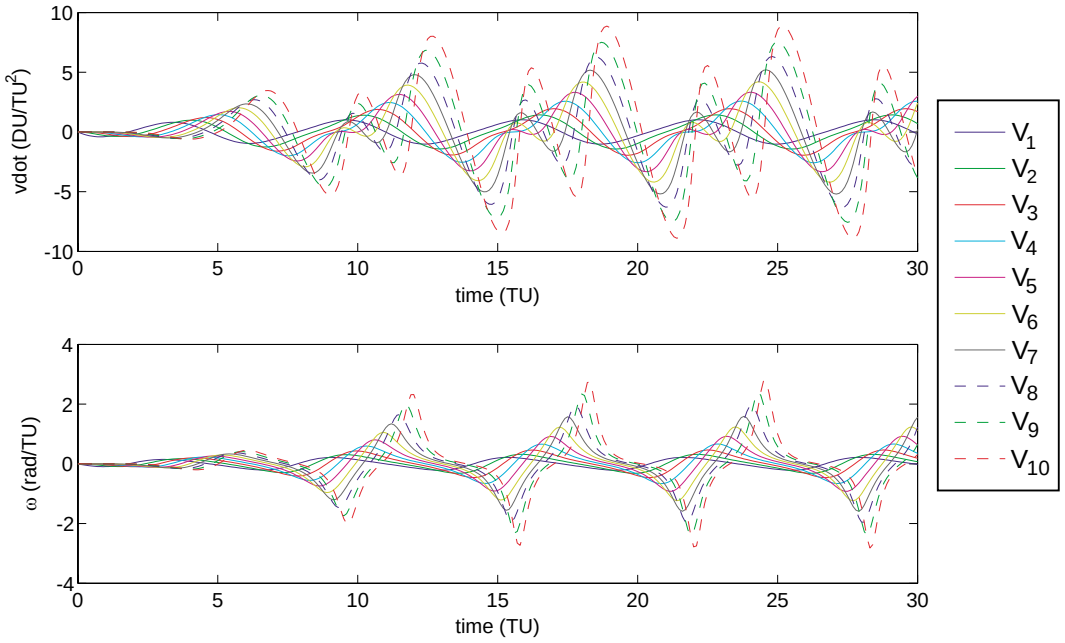

Fig. 37.: Control inputs, $\dot{v}$ and ω, to each vehicle in the formation (communication structure 5).

E. Design Problem: Gain Selection for Performance

The modal-cost and frequency-response-function tools can be used to compare communication structures for disturbability and string stability, respectively. Once a communication structure has been selected, the frequency-response analysis can be used to determine the effects of gain changes on string stability and system response. Some design considerations that may be taken into account are the resonant frequency, the steady-state amplitudes from the receptance functions, and string stability.

There are several ways to affect system performance. The nominal control gains in the stiffness matrix can be changed, which will change the natural frequencies of the system. Individual gains in the stiffness matrix can be perturbed to change one or more natural frequencies in a desired manner. The damping constant, β, can be changed, which affects the steady-state amplitudes and steady-state errors of the system. Changing the value of β can also lead to string stability for a previously string-unstable control form. To this point, it has been assumed that the damping matrix is proportional to the stiffness matrix with constant, β; however, damping matrices of the form $C = \alpha M + \beta K$ do not alter the frequency-response theory developed previously. As was described in the previous chapter, the constants α and β can be chosen using a minimum-norm solution for a desired set of damping ratios; however, non-zero values for α may lead to steady-state errors between vehicles by introducing non-homogeneous terms to the error dynamics.

Simulation examples are used here to illustrate the use of the analysis tools in the selection of control gains. In the previous section, communication structure 5 was shown to be string unstable for the nominal gain of one. Changing the nominal gain to two, which will be denoted as $k = 2$, decreases the steady-state amplitudes and errors as shown in Figure 38. Figure 38(b) still indicates that the cooperative control

laws are not string stable; however, a simulation of the ten-vehicle formation shows that the required control efforts to maintain the formation are approximately halved for $k = 2$ in comparison to the control efforts in Figure 37 for $k = 1$.

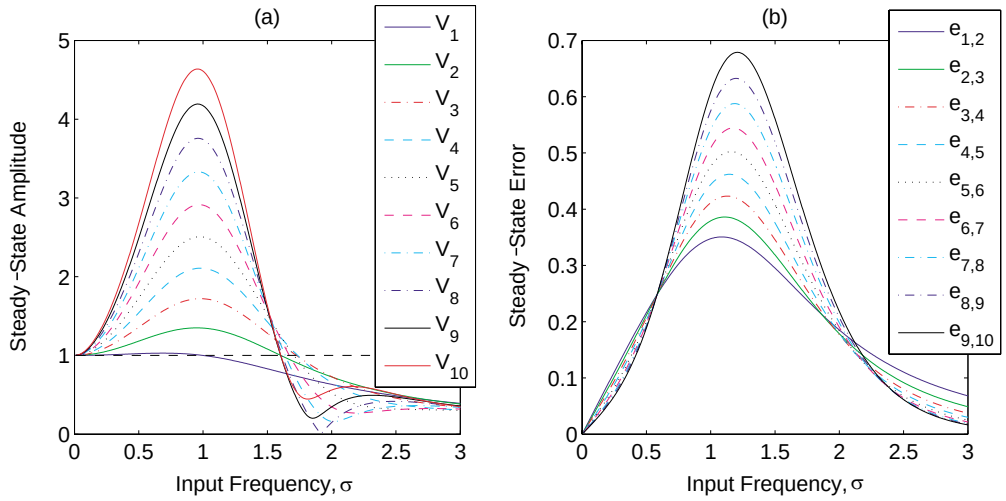

Fig. 38.: Steady-state amplitudes of the vehicle positions (a) and steady-state errors (b) for communication structure 5 (k = 2, $\beta = 1$).

Figure 39 shows the steady-state amplitudes and errors for a nominal gain of $k = 1$ with a damping constant $\beta = 2$. Figure 39(b) indicates that this choice of gains leads to a string-stable cooperative control law. Whereas the steady-state errors do not grow along the vehicle string, the amplitudes of the vehicle positions still increase along the string. This behavior can be contrasted to the steady-state amplitudes in Figures 31 and 33 for communication structures 1 and 2, respectively. In those cases, the steady-state amplitudes of vehicles 2 through 10 are equal and do not grow along the vehicle string. Communication structures 3 and 4 exhibit similar behavior, which indicates that a connection to the first vehicle can help to prevent large amplitudes along the string. This should be not be confused with string stability

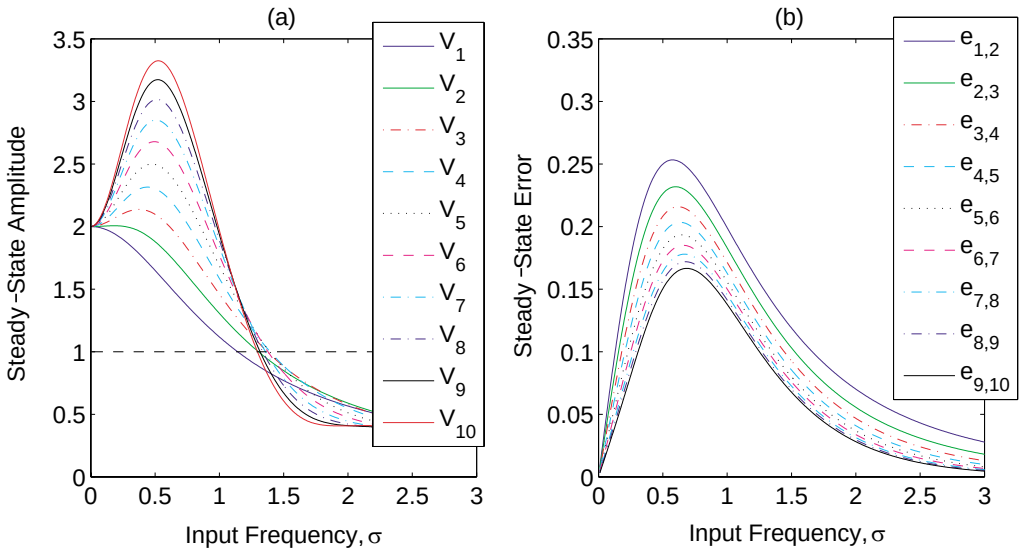

Fig. 39.: Steady-state amplitudes of the vehicle positions (a) and steady-state errors (b) for communication structure 5 (k = 1, $\beta = 2$).

however, which is defined as the propagation of errors through the string.

The growth in steady-state amplitudes corresponds to increased control inputs along the string. Therefore, a control form may be string stable, but a growth in required control inputs along the string indicates that the communication structure cannot be implemented for a string with an infinite number of vehicles. Communication structure 5 with $k = 1$ and $\beta = 2$ can be considered a quasi-string-stable control form.

The results presented here appear to contradict the string-stability results presented by Swaroop and Hedrick for a lead-vehicle-only control form. The results, which were also presented in Chapter IV, indicate that a control law using position and velocity errors from an immediately preceding vehicle is string unstable for all position and velocity control gains greater than zero. However, in this case the perturbations in the gains to permit invertibility of the Φ matrix lead to a string-stable

control form. The perturbations were implemented such that the gains increase along the string; and therefore, the trailing vehicles are more aggressive. If the gains are perturbed such that the vehicles are less aggressive along the string, then the string-instabilities remain.

Individual gains can be perturbed to change a natural frequency in a desired way. The eigenvalue sensitivities can aid in the selection of gains to perturb. For communication structure 5, which has a lower-diagonal form, the eigenvalues of the system are equal to the gains along the diagonal. Therefore, the ith natural frequency can be perturbed by perturbing the control gain $k_{i-1,i}$. Other communication structures do not have this same decoupled relationship between control gains and the system eigenvalues.

Communication structure 6 is used to show how the eigenvalue sensitivities can be used to change the system's natural frequencies. Figure 40 shows the steady-state amplitudes and errors. The first natural frequency is $\omega_1 = 0.1495$ rad/sec with a damping ratio $\zeta = 0.0747$. To change the first natural frequency, the eigenvalue sensitivities are determined for perturbations to the control gains. The more sensitive gains are then used to perturb the first natural frequency. In communication structure 5, perturbing one control gain only affects one natural frequency; however, the relationship between control gains and natural frequencies is coupled for communication structure 6. The vectors shown below are the sensitivities of the eigenvalues for perturbations to the k_r and k_{12} control gains. These two vectors have the greatest sensitivity to the first natural frequency.

$$\frac{\partial \boldsymbol{\lambda}}{\partial k_r} = [0.0040, 0.0231, 0.0191, 0.0000, 0.0558, 0.2503, 0.4944, 0.5878, 0.4253, 0.1402]^T$$
$$\frac{\partial \boldsymbol{\lambda}}{\partial k_{12}} = [0.0042, 0.0359, 0.0881, 0.1429, 0.1810, 0.1894, 0.1651, 0.1164, 0.0604, 0.0165]^T$$

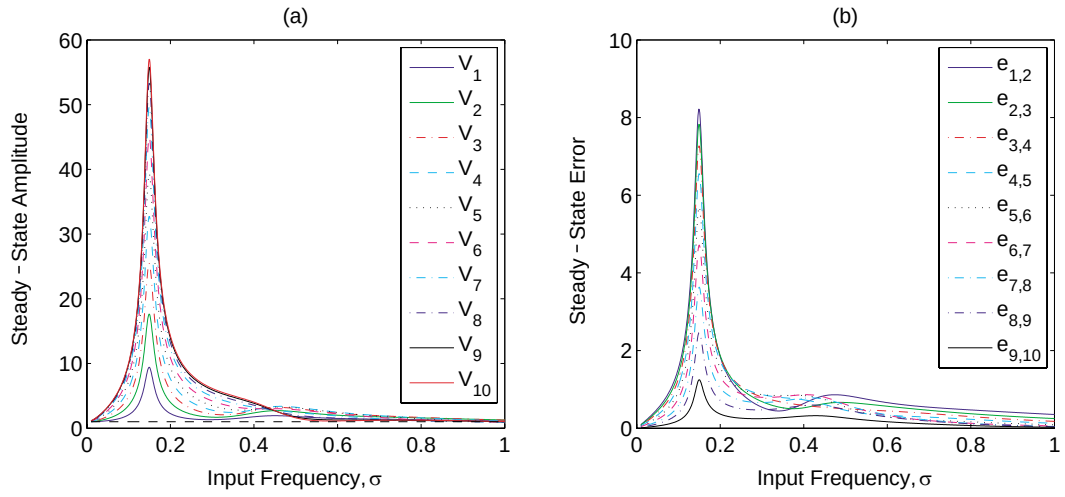

Fig. 40.: Steady-state amplitudes of the vehicle positions (a) and steady-state errors (b) for communication structure 6.

Perturbations to these gains will not only alter the first natural frequency, but will have an effect on the other frequencies as well due to the structure of the stiffness matrix for this communication structure. By perturbing k_r and k_{12} by 0.1, the first natural frequency is now equal to 0.1520 rad/sec, which is a small change. This approach seems to have limited utility except for fine tuning frequencies, which is complicated by the coupled nature of the sensitivities.

Another design technique is to select damping ratios such that certain modes are more highly damped while not significantly changing the damping ratios of other modes. Figure 40 shows that the first mode is very lightly damped, and thus, the steady-state amplitudes and errors at the resonant frequency are large. It may be desirable to increase the damping of the lower-frequency modes, while maintaining the damping ratios of the higher-frequency modes. The damping ratios for the case

when $k = \beta = 1$ are shown below.

$$\zeta = [0.0747, 0.2225, 0.3653, 0.5000, 0.6235, 0.7331, 0.8262, 0.9010, 0.9556, 0.9888]^T$$

A vector of the desired damping ratios is used to find the proportional damping constants, α and β.

$$\zeta_d = [0.3500, 0.4000, 0.4500, 0.5000, 0.6235, 0.7331, 0.8262, 0.9010, 0.9556, 0.9888]^T$$

Using the minimum-norm solution, $\alpha = 0.0909$ and $\beta = 0.9713$. The resulting steady-state amplitudes and errors are shown in Figure 41. As expected, the steady-state amplitudes and errors are smaller; however, the steady-state errors at $\sigma = 0$ are not zero. Using proportional damping with $\alpha \neq 0$ leads to steady-state errors between vehicles even when disturbances are not present. This is caused by the non-zero term on the right-hand side of the error dynamics equations, which leads to non-zero equilibrium points for the errors.

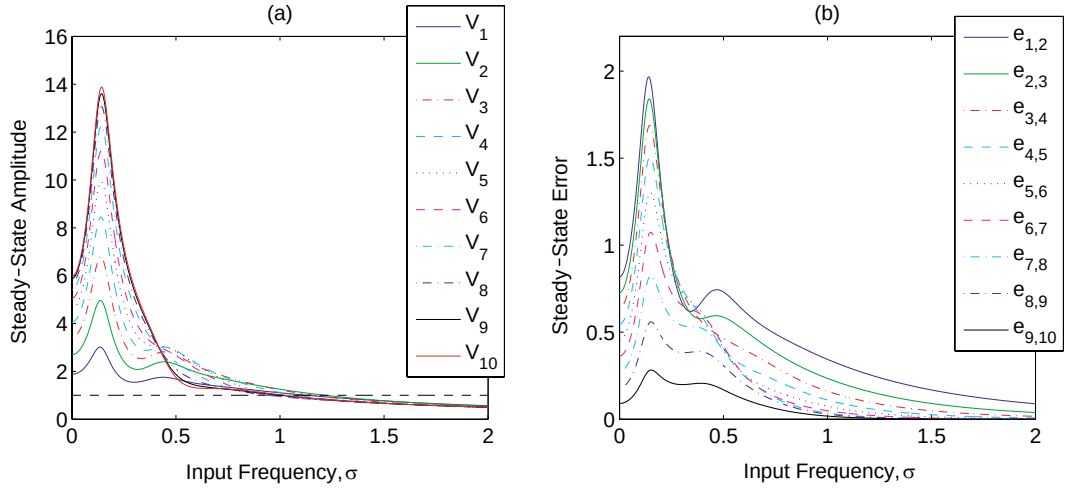

Fig. 41.: Steady-state amplitudes of the vehicle positions (a) and steady-state errors (b) for communication structure 6 ($k = 1$, $\alpha = 0.0909$, $\beta = 0.9713$).

F. Gain Selection Using Nonlinear Programming

One last design approach is explored to select control gains for the different stiffness matrices. A nonlinear-programming problem (NLP) is formulated to determine control gains in the stiffness matrix to yield a set of desired natural frequencies. The optimization variables are the $n \times n$ components of the eigenvector matrix, Φ, and n natural frequencies that together yield a stiffness matrix of the desired form. Each communication structure has a stiffness matrix of a certain form, and *communicability constraints* can be defined to ensure that stiffness matrices are representative of the desired communication structure.

The objective function seeks to minimize the condition number of Φ, $\kappa(\Phi)$, and the errors between the vector of natural frequencies from the resulting stiffness matrix, $\boldsymbol{\omega}$, and the vector of desired natural frequencies, $\boldsymbol{\omega}_d$.

$$J\left(\Phi, \boldsymbol{\omega}\right) = \alpha_1 \kappa(\Phi) + \alpha_2 \left(\boldsymbol{\omega} - \boldsymbol{\omega}_d\right)^T \left(\boldsymbol{\omega} - \boldsymbol{\omega}_d\right) \tag{6.64}$$

The constants α_1 and α_2 are weights. The condition number of a matrix is the ratio of the maximum and minimum singular values of a matrix, where orthogonal matrices have a condition of one, and rank-deficient matrices have an infinite condition number [29]. The matrix Φ and vector of natural frequencies, $\boldsymbol{\omega}$, are subject to equality constraints for a desired communication structure, such that $K = \Phi \left[\text{diag}(\boldsymbol{\omega})\right] \Phi^{-1}$ belongs to the subset of K^*, where K^* has the form of the desired communication structure. The NLP is stated below.

$$\begin{aligned} \min_{\Phi \in \mathbf{R^{n \times n}}, \boldsymbol{\omega} \in \mathbf{R^n}} \quad & J(\Phi, \boldsymbol{\omega}) \\ \text{Subject to:} \quad & \boldsymbol{f}(\Phi, \boldsymbol{\omega}) = 0 \\ & \boldsymbol{g}(\Phi, \boldsymbol{\omega}) \leq 0 \end{aligned}$$

Inequality constraints are used to force the sign of the control gains to be greater

than zero. As described previously, the equality or communicability constraints are used to find K of the form K^*.

The following communicability constraints would be imposed for a three-vehicle system assuming a fully-connected communication structure (see Appendix E for the form of the stiffness matrix). The $K(i,j)$ refers to the element in the ith row and jth column of the stiffness matrix.

$$\begin{aligned} g_1 &= -K(1,2) \leq 0 \\ g_2 &= -K(1,3) \leq 0 \\ g_3 &= -K(2,3) \leq 0 \end{aligned} \tag{6.65}$$

$$\begin{aligned} f_1 &= K(1,2) - K(2,1) = 0 \\ f_2 &= K(1,3) - K(3,1) = 0 \\ f_3 &= K(2,3) - K(3,2) = 0 \end{aligned} \tag{6.66}$$

$$\begin{aligned} f_4 &= K(2,2) - [K(2,1) + K(2,3)] = 0 \\ f_5 &= K(3,3) - [K(3,1) + K(3,2)] = 0 \end{aligned} \tag{6.67}$$

The constraints in Equation (6.66) enforce the symmetry of the K matrix for communication structure 1, and the constraints in Equation (6.67) constrain the diagonal terms to be equal to the sum of the other terms in that row for rows 2 and 3.

The NLP is implemented using *fmincon* in MATLAB. Results for a five-vehicle system assuming communication structure 1 are shown in Table IV, where the constants in the cost function are $\alpha_1 = 0.1$ and $\alpha_2 = 100$. The table shows the resulting natural frequencies ($\boldsymbol{\omega}_f$), starting cost (J_0), final cost (J_f), and the number of function evaluations for five different cases of desired natural frequencies. The initial guess for Φ and $\boldsymbol{\omega}$ is the eigenvector matrix and natural frequencies for the stiffness matrix

with unity gains ($k = 1$).

$$\boldsymbol{\omega}_0 = [0.4142, 2.2361, 2.2361, 2.2361, 2.3800]^T$$

The desired natural frequencies for cases 1 and 2 are chosen by adding a random number from a normal distribution to $\boldsymbol{\omega}_0$. In case 3, $\boldsymbol{\omega}_d = \boldsymbol{\omega}_0 + 0.5$, and in cases 4 and 5, $\boldsymbol{\omega}_d$ is arbitrarily chosen. In each case, the minimum possible cost is $J_f = 0.1$.

Table IV.: NLP Solutions for Communication Structure 1 ($n = 5$).

Case	$\boldsymbol{\omega}_d$, $\boldsymbol{\omega}_f$	J_0, J_f	# func evals
1	$[0.1979, 1.4033, 1.8410, 2.2987, 2.3799]^T$	90.2521	7707
	$[0.1979, 1.4033, 1.8409, 2.2987, 2.3800]^T$	0.1000	
2	$[1.2768, 1.3842, 1.9762, 2.3303, 3.1096]^T$	203.3875	5455
	$[0.7630, 1.3836, 1.9776, 2.3297, 2.2325]^T$	41.3014	
3	$[0.9142, 2.7361, 2.7361, 2.7361, 2.9142]^T$	125.1000	2590
	$[0.6810, 2.7058, 2.7217, 2.7217, 2.9895]^T$	6.2495	
4	$[0.5000, 1.8000, 2.2000, 2.4000, 2.6000]^T$	26.1206	9024
	$[0.5000, 1.8000, 2.1999, 2.4000, 2.6000]^T$	0.1000	
5	$[1.0000, 2.0000, 3.0000, 4.0000, 5.0000]^T$	1078.1214	5457
	$[1.0000, 2.0001, 3.0000, 4.0000, 5.0000]^T$	0.1000	

Table IV shows that for some choices of $\boldsymbol{\omega}_d$, a stiffness matrix can be found that satisfies the communicability constraints and places the eigenvalues of the stiffness matrix at the desired locations. The communicability constraints for communication structure 1 enforce the symmetry of the stiffness matrix, which results in an orthogonal set of n eigenvectors by the finite-dimensional spectral theorem [46]. Therefore,

$\kappa(\Phi) = 1$ in all of the cases in Table IV.

Communication structure 5 does not yield a symmetric stiffness matrix, which poses challenges in finding a set of linearly-independent eigenvectors. This results in interesting NLP results. Table V shows the results for three cases where $\boldsymbol{\omega}_d = \boldsymbol{\omega}_0$, i.e., the desired natural frequency is the same as the starting value.

$$\boldsymbol{\omega}_0 = [1.0000, 1.1180, 1.2247, 1.3229, 1.4142]^T$$

The constants in the cost function are varied to show the effects on the problem solution. Table V shows how increasing α_1 leads to smaller condition numbers for Φ. Therefore, the NLP can be used to determine perturbed control gains to yield an invertible eigenvector matrix. In each case, the number of function evaluations is less than 4000.

Table V.: NLP Solutions for Communication Structure 5 ($n = 5$) with Varying α_1 and α_2.

Case	α_1,α_2	$\boldsymbol{\omega}_f$	J_0, J_f	$\kappa(\Phi)$
1	0.1	$[0.8044, 0.9480, 1.1795, 1.4148, 1.5687]^T$	144.2127	131.1256
	100		23.2643	
2	1	$[0.5999, 0.7794, 1.0974, 1.4469, 1.6896]^T$	1442.1270	44.2406
	100		82.4646	
3	10	$[0.1560, 0.4329, 0.7406, 1.1369, 1.7145]^T$	14421.2695	15.5277
	100		309.3246	

The NLP solution enables comparison of the different communication structures for the same set, or close to the same set, of natural frequencies. The NLP is used

to determine the control gains in the stiffness matrices for communication structures 1-6 in order to yield the arbitrary set of desired natural frequencies:

$$\boldsymbol{\omega}_d = [1.0000, 2.0000, 3.0000, 4.0000, 5.0000]^T.$$

Because the natural frequencies of communication structure 7 are complex, communication structure 7 is not included in the comparison here. The modal-cost analysis is repeated for a five-vehicle system and results are presented in Table VI ($\alpha_1 = 0.1$ and $\alpha_2 = 100$). For some communication structures, the NLP is not able to determine control gains to achieve the desired natural frequencies. However, this is a result of the communicability constraints, which do not allow for arbitrary selection of natural frequencies in all communication structures. The results here indicate that communication structure 1 has the smallest modal-cost measure, α; therefore, communication structure 1 is the least disturbable control form. In contrast, communication structure 5 is the most disturbable.

Table VI.: Modal-Cost Analysis for Communication Structures with Common Natural Frequencies.

CS	$\boldsymbol{\omega}_f$	J_f	α
1	$[1.0000, 2.0001, 3.0000, 4.0000, 5.0000]^T$	0.1000	0.4527
2	$[0.9995, 2.0000, 3.0001, 4.0000, 5.0000]^T$	0.1282	0.4533
3	$[0.6140, 1.7781, 2.7460, 2.7460, 5.8298]^T$	252.4719	0.4782
4	$[1.0000, 1.9996, 2.9985, 4.0011, 5.0002]^T$	0.5934	0.4530
5	$[0.9986, 1.9915, 2.9915, 4.0045, 5.0049]^T$	2.8882	0.5475
6	$[0.7166, 1.9688, 3.0422, 4.0410, 4.9942]^T$	8.5759	0.4665

Further research on the NLP problem is necessary; however, these examples are used to show the complexities in selecting control gains to achieve desired system behavior. The NLP problem can be used to select gains that will yield the desired, or close to desired, natural frequencies for a selected communication structure. Additionally, the NLP problem can be used to perturb gains for communication structures that require gain perturbations to yield a full-rank eigenvector matrix.

G. Chapter Summary

In this chapter, traditional structural-analysis tools were applied to the cooperative multivehicle problem in order to evaluate the disturbance-rejection properties of the different communication structures or control forms. The disturbed vehicle equations were investigated to show how disturbances affect the double-integrator vehicle representation that has been used throughout this research. Modal cost was used to evaluate the disturbability of the different control forms to impulsive disturbances applied to each vehicle. A modal-cost measure was defined to quantify the disturbability of each communication structure allowing different control forms to be compared. Frequency-response functions were used to evaluate the effect of disturbances on the multivehicle system. The steady-state response of the system follows from the frequency response and was used to determine whether a given control form was string stable. This mechanics-based approach to string-stability analysis is applicable to general cooperative control forms where the closed-loop system can be written in a structural form. One drawback to the analysis tools presented here is the requirement that the matrix of eigenvectors from the stiffness matrix is invertible. Therefore, some stiffness matrices may need to be perturbed in order to yield a full-rank eigenvector matrix.

Simulation results for seven different communication structures were shown to illustrate the use of the modal-cost and frequency-response analysis tools. The effects of control-gain choices on system stability and performance were also shown to demonstrate the use of the frequency-response analysis in the selection of control gains. There are several design degrees of freedom that influence stability and performance, and the use of an NLP to select control gains can aid in the design process.

CHAPTER VII

TIME-DELAY EFFECTS ON MULTIVEHICLE SYSTEMS

This research has investigated the design of decentralized, cooperative control laws for multivehicle systems, and these systems may be subject to time-delay effects due to delays in measurement and communication. Whereas decentralized systems are more robust to communication failures and structural reconfigurations [2], the impact of inter-vehicle communication delays on system stability and performance must also be considered.

Stability analysis of systems with delay is an important aspect to the design and control of decentralized systems. In particular, complex systems are subject to measurement, actuation, communication, and human-operator delays, and in many cases it is necessary to take these delays into account when designing control laws. Olfati-Saber and Murray investigated control laws with time-delayed feedback for dynamic agents using graph theory [10], and Subbarao and Muralidhar have approached the communication-delay problem for UAVs by designing a nonlinear MIMO state observer for output delays [53]. Much of the literature on multivehicle control does not directly address time-delay effects in feedback delays; for example, Dionne and Rabath have included communication delays in simulations, but these delay effects were not incorporated into the control design [54].

This research considers an approach to quantify stable time delays in the feedback states of decentralized, cooperative control laws. The research objective is to evaluate the maximum allowable delay for stability using delay differential equations (DDEs) to model the n-DOF closed-loop systems with delayed feedback. The equations of motion can be written in a first-order form, and the modal coordinate transformation is used to decouple the equations into $2n$ first-order, scalar equations. Here,

well-known stability results for scalar first-order DDEs are applied to determine the maximum delay of each scalar equation. This approach is a straightforward method to determine the maximum delays without solving the DDEs.

The chapter is organized as follows. Background on DDEs is presented in Section A. The stability analysis for a first-order, scalar DDE is presented in Section B, and the results presented in that section further explain DDE stability concepts introduced in the background. This theory enables the subsequent investigation of delay properties for n-DOF linear systems. Delay-independent and delay-dependent stability are investigated in Section C for the multivehicle-control application. Delay-independent stability is discussed in Section C.1 to determine whether control gains can be chosen to ensure stability for any value of the delay, and a method to determine the maximum allowable delay for an n-DOF system of equations is presented in Section C.2. Simulation results are presented in Section D for the seven communication structures introduced in the previous chapter, followed by a discussion in Section E about an underlying assumption in the theory to determine the maximum allowable delay.

A. Delay Differential Equations

Delay differential equations model systems with delay, and the literature over the past several decades has focused on analyzing the stability of this specific type of differential equation. Driver describes a DDE as a "differential equation with a retarded argument", i.e., a DDE expresses some derivative $x^{(n)}$ at time t as a function of $(x,\dot{x},...,x^{(n-1)})$ evaluated at time t and earlier instants [22].

There are two stability concepts in the analysis of DDEs: delay-independent and delay-dependent stability. Whereas delay-independent stability holds for all pos-

itive, finite delays, delay-dependent stability only holds for some values of the delays and instabilities occur when the delays are outside of the stability bounds [23–25]. In the case of linear, time-invariant DDEs, delay-independent stability criteria can be determined quite simply; however, determining bounds on delays becomes more challenging due to the need to solve a transcendental equation, which has an infinite number of solutions.

Frequency-domain methods are one approach described in the literature to analyze stability of DDEs. In the case of linear, autonomous DDEs, the roots of the transcendental characteristic function are difficult to determine, which led researchers to explore other means of analyzing the stability. Analytical methods using Pontryagin's theorem (for a single delay or a commensurable number of delays) are used to determine the number of zeros in the right-half plane, and the method of D subdivision can be applied to find the regions where the characteristic function has roots in the right-half plane as a function of the system parameters [23, 55]. Mori, et al. examined asymptotic stability of linear DDEs of the form $\dot{\boldsymbol{x}}(t) = A\boldsymbol{x}(t) + B\boldsymbol{x}(t-\tau)$, and results in the form of linear matrix inequalities (LMIs) provide both delay-independent and delay-dependent criteria [24, 25]. Niculescu investigated necessary and sufficient conditions for delay-independent and delay-dependent stability using a matrix-pencil technique [56].

Time-domain methods can also be used to show delay-independent or delay-dependent stability using an extension of Lyapunov's second method for time-delay systems [22, 23]. Driver describes the Lyapunov-Krasovskiĭ method as seeking to find a Lyapunov functional that includes information regarding the delay size, and then Lyapunov's second method can be carried through to determine stability. Dugard, et al. show that asymptotic stability can be shown using a Lyapunov-Krasovskiĭ functional that leads to the delay Riccati equation [23]. Chopra and Spong have demon-

strated delay-independent stability using the Lyapunov-Krasovskiĭ for networked passive systems with delays on the transmitted system outputs [57, 58].

Additionally, some numerical methods have been developed recently to find stability regions in the time-delay parameter space. Kalmàr-Nagy presents a method to estimate the delay-dependent stability chart using a polynomial approximation of the transcendental characteristic equation [59]. Sipahi and Olgac have developed a method to find stability regions for multiple time-delay systems using a root-clustering technique, which finds the delay regions where the roots of the transcendental characteristic equation cross the imaginary axis into the right-half plane [60–62]. The work of Asl and Ulsoy [63, 64] and Yi and Ulsoy [65] and the references therein are especially important to the work presented in this Chapter. Their focus is on a Lambert-function technique that is used to approximate the solution of a system of linear DDEs.

In all of the aforementioned methods, there are challenges in determining the delay-dependent bounds for large-dimensional systems with delays, such as solving LMIs, finding an appropriate Lyapunov-Krasovskiĭ function, or requiring extensive, problem-specific computation. The stability results for a scalar, first-order system with delay are well known, and this simplified model is exploited in this research to determine delay-dependent stability bounds for a multi-DOF, linear system of equations subject to delays in the feedback control.

B. Stability Results for a Scalar, First-Order DDE

In this section, well known results for a scalar, first-order DDE are presented. Consider the DDE given below.

$$\dot{x}(t) = ax(t) + bx(t-\tau) \tag{7.1}$$

Here, τ is a constant delay. In the parameter space, $S(0)$ is the set (a, b) where Equation (7.1) is asymptotically stable for $\tau = 0$ [23]. Thus, $S(0)$ is easily determined.

$$S(0) = \{(a, b) : a + b < 0\} \tag{7.2}$$

Assume that $a < 0$, and using a Lyapunov-Krasovskiĭ approach, the conditions on b can be found such that (a, b) corresponds to the delay-independent set, S_∞. A Lyapunov functional is defined as shown below.

$$V(t) = x^2(t) + |a| \int_{t-\tau}^{t} x^2(s)ds \tag{7.3}$$

A time-derivative of $V(t)$ reveals the condition for b.

$$\begin{aligned} \dot{V}(t) &= 2x(t) \left[ax(t) + bx(t-\tau)\right] + |a| \left[x^2(t) - x^2(t-\tau)\right] \\ &= -|a|x^2(t) - |a|x^2(t-\tau) + 2bx(t)x(t-\tau) \\ &\leq (-|a| + |b|) \left[x^2(t) + x^2(t-\tau)\right] \end{aligned} \tag{7.4}$$

Therefore, delay-independent stability is achieved for $a \leq -|b|$.

$$S_\infty = \{(a, b) : a + b < 0, a \leq -|b|\} \tag{7.5}$$

The delay-dependent set is complementary to S_∞ within $S(0)$ [23].

$$S_\tau = \{(a, b) : a + b < 0, b < -|a|\} \tag{7.6}$$

To find the stability bound in the delay-dependent region for a delay τ, the transcendental characteristic equation from Equation (7.1) is formed.

$$s - a - be^{-s\tau} = 0 \tag{7.7}$$

By substituting $s = j\omega$ and expanding using Euler's identity, the real and imaginary

parts of the characteristic equation can be written as shown.

$$-a - b\cos(\omega\tau) = 0; \quad \omega + b\sin(\omega\tau) = 0 \tag{7.8}$$

Hale [66] and Smith [67] show that the stable region, where the roots of the transcendental equation in Equation (7.7) have $Re(s) < 0$, is the open region bounded by the curves $b = -a$ and the solution to Equation (7.8) for $0 < \omega < \pi/\tau$. Figure 42 shows the delay-independent and delay-dependent stability regions for Equation (7.1) in the $(a(\omega), b(\omega))$ space for the range $0 < \omega < \pi/\tau$ and with $\tau = 0.1$ and $\tau = 1.0$. The asymptotically-stable regions are the cross-hatched areas, and the unstable regions in $S(0)$ are dotted.

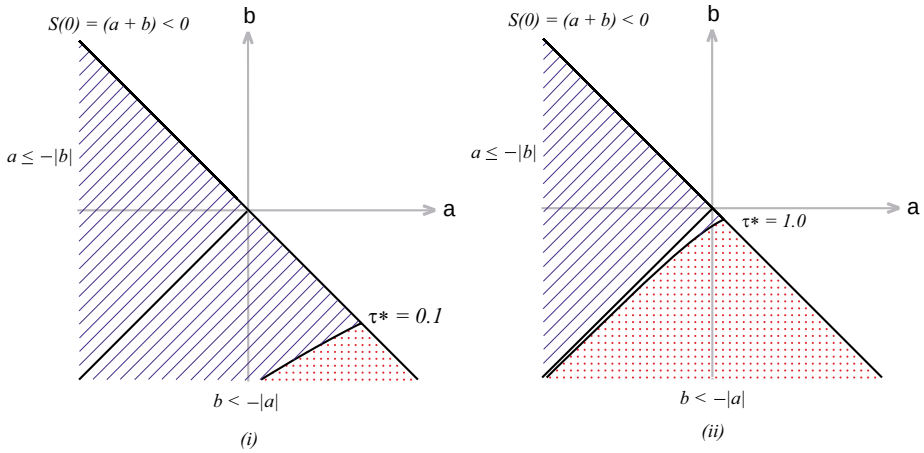

Fig. 42.: Delay-independent and -dependent stability regions for $\dot{x}(t) = ax(t) + bx(t-\tau)$.

From Equation (7.8), the stability bound on τ can be determined for any parameter set (a, b) in the delay-dependent region.

$$\tau^* = \frac{\cos^{-1}\left(\frac{-a}{b}\right)}{\sqrt{b^2 - a^2}} \tag{7.9}$$

C. Delay Analysis for the Multivehicle System

This research investigates the effect of delays on cooperative multivehicle systems when delays are introduced in the feedback control. Using the structural form to represent the closed-loop equations of motion, the delay terms are shown to affect the damping and stiffness terms that represent the cooperative control inputs.

$$M\ddot{\boldsymbol{x}} + C\dot{\boldsymbol{x}}(t-\tau) + K\boldsymbol{x}(t-\tau) = 0 \tag{7.10}$$

It is assumed that the delay τ is the same for all feedback control terms. The forcing term is set to zero for the time-delay analysis, as this term contains information about the reference trajectory and the constant desired distances between vehicle only. The delay-independent and delay-dependent stability is investigated for the system in Equation 7.10.

1. Delay-Independent Stability Analysis

Delay-independent stability was described in the previous section as the parameter space where the system is asymptotically stable independent of the delay size. Lehman and Verriest have investigated delay-independent stability for second-order DDEs with constant coefficients [68]. The DDE is written in the first-order form, where the state vector $\boldsymbol{x} \in R^2$, A and B are 2×2 matrices, and the delay $\tau \geq 0$.

$$\dot{\boldsymbol{x}}(t) = A\boldsymbol{x}(t) + B\boldsymbol{x}(t-\tau) \tag{7.11}$$

This system is asymptotically stable if the roots of the transcendental characteristic equation, found by taking the determinant of the system in the frequency domain, are shown to have real parts less than zero.

$$\det\left[sI - A - Be^{-s\tau}\right] = 0 \tag{7.12}$$

The transcendental characteristic equation of the system in Equation (7.11) has a general form.

$$f(s,\tau) = s^2 e^{s\tau} + c_1 s e^{s\tau} + c_0 e^{s\tau} + d_2 s + d_1 + d_0 e^{-s\tau} \tag{7.13}$$

Lehman and Verriest show that the characteristic equation, $f(s,\tau)$, has solutions with $Re(s) < 0$ if and only if three criteria are satisfied [68].

These criteria are applied to the multivehicle system to determine whether the control gains can be designed to achieve delay-independent stability. In Chapter V, the modal-coordinate transformation was introduced to decouple the equations of motion into n second-order, scalar equations. Therefore, the closed-loop equations of motion with feedback delays in Equation (7.10) can be expressed in the following form.

$$\ddot{\eta}_i(t) + \tilde{c}_i \dot{\eta}_i(t-\tau) + \tilde{k}_i \eta_i(t-\tau) = 0, \text{ for i = 1,...,n} \tag{7.14}$$

Equation (7.14) can be equivalently expressed in the first-order form: $\dot{\boldsymbol{\eta}}_i = A\boldsymbol{\eta}_i(t) + B\boldsymbol{\eta}_i(t-\tau)$.

$$\begin{bmatrix} \dot{\eta}_{i,1}(t) \\ \dot{\eta}_{i,2}(t) \end{bmatrix} = \begin{bmatrix} 0 & 1 \\ 0 & 0 \end{bmatrix} \begin{bmatrix} \eta_{i,1}(t) \\ \eta_{i,2}(t) \end{bmatrix} + \begin{bmatrix} 0 & 0 \\ -\tilde{k}_i & -\tilde{c}_i \end{bmatrix} \begin{bmatrix} \eta_{i,1}(t-\tau) \\ \eta_{i,2}(t-\tau) \end{bmatrix} \tag{7.15}$$

The A matrix contains the kinematic term, and the B matrix contains the feedback control gains. The transcendental characteristic equation for the system in Equation (7.15) is $f(s,\tau) = s^2 e^{s\tau} + \tilde{c}_i s + \tilde{k}_i = 0$. This system is asymptotically stable if and only if the following two criteria are satisfied (the three criteria presented by Lehman and Verriest have been simplified to match the form of the characteristic equation for the multivehicle application):

(i) $\tilde{c}_i > 0$ and $\tilde{k}_i > 0$;

(ii) the polynomial $q(y)$ is not equal to zero for any positive real y.

$$q(y) = y^4 - \tilde{c}_i^2 y^3 - \tilde{k}_i^2 y^2 \neq 0$$

Routh-Hurwitz criterion is used to show that the polynomial $q'(y) = y^2 - \tilde{c}_i^2 y - \tilde{k}_i^2$ has at least one root with a positive real part, and the quadratic equation shows that all roots of the polynomial are real. Therefore, the feedback control gains in Equation (7.15) cannot be chosen to achieve delay-independent stability.

2. Delay-Dependent Stability Analysis

It was shown that the multivehicle system cannot be designed for delay-independent stability. In this section, the delay-dependent stability is investigated, or more specifically, a method to determine the maximum delay for the multivehicle system is developed. The second-order equations of motion are written in a first-order form.

$$\dot{\boldsymbol{z}}(t) = \left[\begin{array}{c:c} 0 & I \\ \hdashline -M^{-1}K & -M^{-1}C \end{array}\right] \boldsymbol{z}(t) = A_{cl}\boldsymbol{z}(t); \quad \boldsymbol{z}(t) = \begin{bmatrix} \boldsymbol{x}(t) \\ \dot{\boldsymbol{x}}(t) \end{bmatrix} \tag{7.16}$$

Here, A_{cl} is a $2n \times 2n$ matrix, and $\boldsymbol{z}(t)$ is an $2n \times 1$ vector of positions and velocities. Suppose that $\boldsymbol{z}(t)$ is subject to delay τ due to delays on the feedback states. It is assumed that this delay also acts on the kinematics in order to simplify the first-order, closed-loop form to the expression shown below.

$$\dot{\boldsymbol{z}}(t) = A_{cl}\boldsymbol{z}(t-\tau) \tag{7.17}$$

If A_{cl} is a diagonalizable matrix, a modal transformation of the following form can be chosen [29].

$$\boldsymbol{z}(t) = \Phi\boldsymbol{\eta}(t); \quad \boldsymbol{z}(\cdot) = \Phi\boldsymbol{\eta}(\cdot) \tag{7.18}$$

Note that here Φ is an $2n \times 2n$ matrix of the eigenvectors of A_{cl}, and the modal

coordinates are a $2n \times 1$ vector. Substituting Equation (7.18) into the closed-loop form in Equation (7.17) and multiplying by Φ^{-1} yields the following $2n$ first-order differential equations with delay.

$$\dot{\boldsymbol{\eta}}(t) = A_d \boldsymbol{\eta}(t - \tau) \tag{7.19}$$

The matrix $A_d = \Phi^{-1} A_{cl} \Phi$ is diagonal; therefore, the modal transformation decouples the matrix DDE in the η coordinates.

$$\begin{aligned} \dot{\eta}_1(t) &= \lambda_1 \eta_1(t - \tau_1) \\ \dot{\eta}_2(t) &= \lambda_2 \eta_2(t - \tau_2) \\ &\vdots \\ \dot{\eta}_{2n}(t) &= \lambda_{2n} \eta_{2n}(t - \tau_{2n}) \end{aligned} \tag{7.20}$$

The coefficients λ_i in the above equations are the eigenvalues of the closed-loop matrix, A_{cl}. Therefore, the coefficients can be real or complex. A stable closed-loop matrix will have eigenvalues with negative real parts. As was the case in Chapter V, the Φ matrix must be full-rank to ensure invertibility in order to diagonalize A_{cl}.

For the case where the coefficients are real, the delay-independent and delay-dependent stability of the closed-loop system can be analyzed using the results presented in Section B for each scalar first-order DDE in Equation (7.20). In the modal form above, the coefficient a in Equation (7.1) is zero, which implies that the system is delay-independently stable for $b = \lambda_i = 0$ only. From the delay-dependent results for the optimal bound on the delay, the following relationship for each first-order DDE is derived.

$$\tau_i^* = \frac{\pi}{2|\lambda_i|} \tag{7.21}$$

In the case that the coefficients are complex, the transcendental characteristic

equation in Equation (7.7) is rewritten with $a = 0$ and b complex.

$$s - (b_R + jb_I)\, e^{-s\tau} = 0 \tag{7.22}$$

Here, b_R and b_I are the real and imaginary parts of b, respectively. The optimal bound on τ is derived by substituting $s = j\omega$ into Equation (7.22) and expanding using Euler's identity.

$$\tau_i^* = \frac{\tan^{-1}\left(\frac{-b_R}{b_I}\right)}{\sqrt{b_R^2 + b_I^2}} \tag{7.23}$$

This equation is a general expression for the DDE with $a = 0$ and b either real or complex. If $b_I = 0$, this expression is equivalent to that shown in Equation (7.21).

The optimal bounds for each DDE in Equation (7.20) are computed using the general form in Equation (7.23), and the smallest τ_i^* is the maximum allowable delay for the closed-loop system. At the maximum allowable delay, the system displays marginally stable behavior; for delays less than the maximum delay, the DDEs are asymptotically stable; and if the maximum delay is exceeded, the system will be unstable. Thus, delay bounds can be determined for a general closed-loop control form by solving an eigenvalue problem to diagonalize the closed-loop matrix. The approach presented here reduces the problem of determining delay-dependent stability bounds to an eigenvalue problem, which eliminates the rigor of other approaches that require finding a problem-specific Lyapunov function, solving LMIs, or solving computationally expensive root-finding problems.

D. Simulation Results

The maximum allowable delays were calculated for the seven communication structures shown in Figure 22. Table VII shows the delays for $n = 3$, 5, and 10 vehicles. The nominal gains are equal to one ($k = 1$), and the damping constant $\beta = 1$. The

same gain perturbations as described in Chapter VI were used here to yield a full-rank Φ matrix. Recall that communication structure 7 is unstable for $n > 6$. Whereas the maximum allowable delay decreases for communication structures 1, 2, 3, and 6 as the number of vehicles in the formation increases, the maximum delay is constant for communication structures 4 and 5.

Table VII.: Maximum Allowable Delays for Different Communication Structures

Communication Structure	τ (n = 3)	τ (n = 5)	τ (n = 10)
1	0.5058	0.3455	0.1604
2	0.5083	0.5083	0.4520
3	0.5058	0.3455	0.1604
4	0.5236	0.5236	0.5236
5	0.5236	0.5236	0.5236
6	0.5042	0.5017	0.5005
7	0.3329	0.0782	unstable

Numerical results are simulated using the DDE Runge-Kutta solver, *dde23*, in MATLAB with initial conditions held constant until the determined optimal bound, τ.

$$\boldsymbol{x}_i(t) = \boldsymbol{x}_i(0), \quad \dot{\boldsymbol{x}}_i(t) = \dot{\boldsymbol{x}}_i(0), \quad -\tau \leq t \leq 0 \tag{7.24}$$

A ten-vehicle formation is simulated tracking a constant-velocity reference trajectory in the x direction with $\dot{x}_r = 5$ DU/TU. There are no initial condition errors, but the delays affect behavior as control inputs use only the initial conditions for $t = [0, \tau]$.

Figure 43 shows the spacing errors in the x direction for the maximum allowable delay for communication structures 1 and 5. These results indicate that the time de-

lays in the feedback states have a similar effect on the formation as the disturbances. Whereas the spacing errors quickly go to zero along the vehicle string for communication structure 1, the errors grow along the string when the control is determined using communication structure 5.

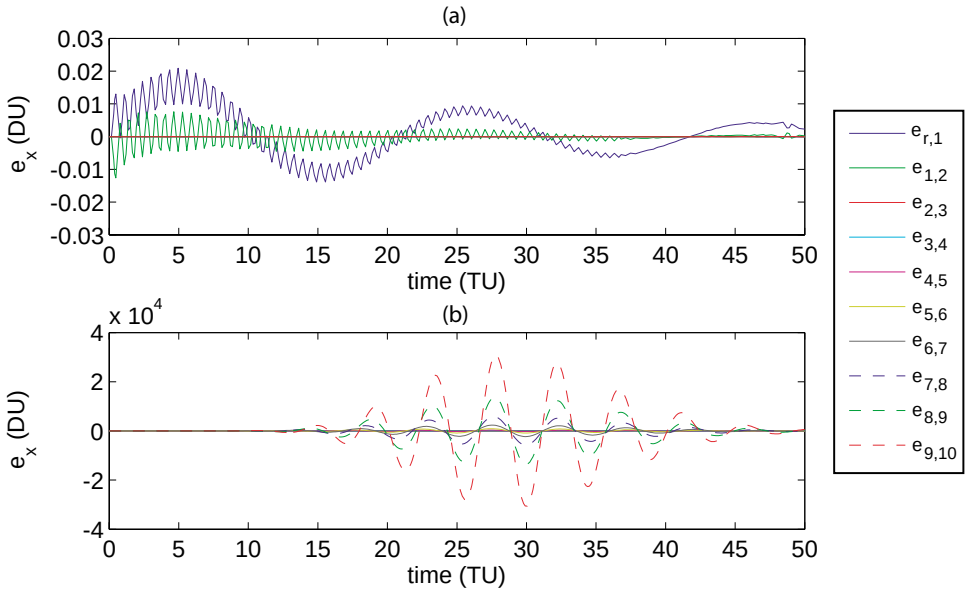

Fig. 43.: Spacing errors in the x direction for the maximum allowable delay for communication structures 1 (a) and 5 (b).

The simulation results shown in Figure 43 include the assumed delay in the kinematics, which is not representative of the physical system. Simulations of the seven communication structures confirm that the theory presented correctly predicts the maximum delay of the system in Equation (7.17). However, if zero delay is assumed in the kinematic equations, the simulations indicate that assuming delays in the kinematics in order to determine the maximum delay is not a conservative assumption. For example, communication structures 1 and 5 are stable for less than or equal to 85% and 72% of the maximum calculated delay, respectively.

Figure 44 shows the spacing error results for communication structures 1 and 5 with no assumed delays in the kinematics. Here, the spacing-error trends are consistent with the trends in Figure 43. In addition, note that the maximum spacing error between vehicles 9 and 10 for communication structure 5 is roughly 250 DU, which requires significant control inputs (maximum $\dot{v} = 2.6 \times 10^3$ DU/TU^2).

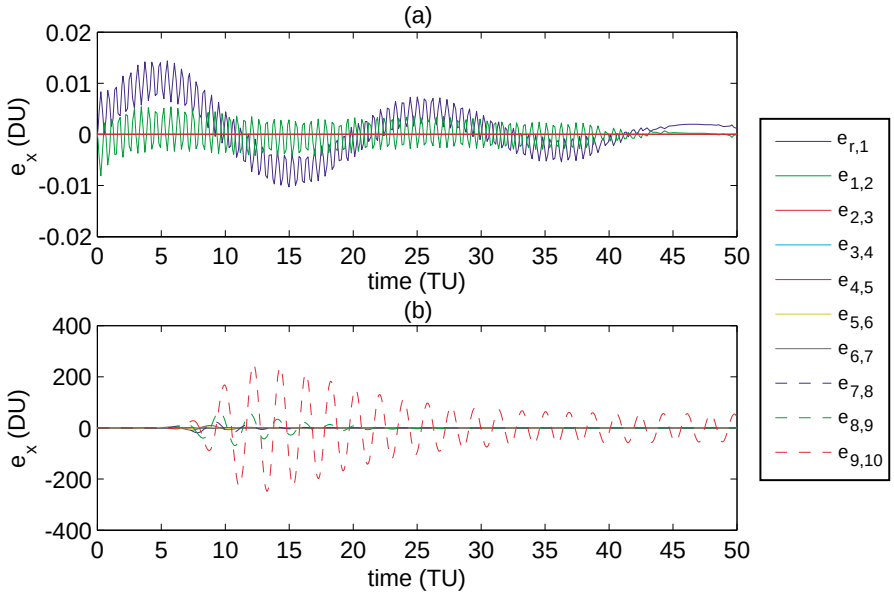

Fig. 44.: Spacing errors in the x direction at 85% and 72% of the maximum allowable delay for communication structures 1 (a) and 5 (b), respectively.

Figure 45 shows the spacing errors and control inputs for communication structure 5 at 50% of the maximum allowable delay. If the maximum delay is halved, the maximum spacing error $e_{9,10}$ is reduced to 1.25 DU, and the maximum $\dot{v} = 10$ DU/TU^2. This figure also shows that the behavior of the formation is similar to the behavior when the formation is subjected to harmonic disturbances. The spacing errors initially grow along the string with a noticeable lag before going to zero.

Table VIII shows the percentage of the maximum delay where the communi-

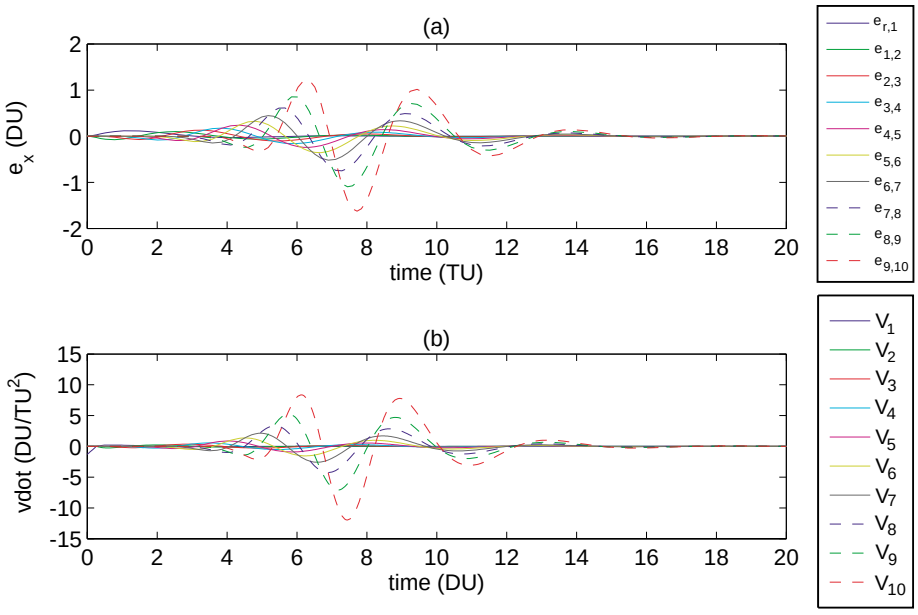

Fig. 45.: Spacing errors (a) and control inputs (b) for communication structure 5 for 50% of the maximum delay.

cation structures are stable for different numbers of vehicles in the formation. The accuracy of the maximum delay calculation increases with the number of vehicles for communication structures 1 and 3, and decreases for communication structures 5 and 6. Whereas Table VII indicates that communication structure 5 is invariant with respect the number of vehicles in the formation, the stability bound does decrease when no delay in the kinematics is assumed.

The maximum allowable delay for communication structure 4 is invariant with respect to the number of vehicles in the formation. Additionally, when no delays are assumed in the kinematics, the maximum delay is greater than the calculated delay. The percentage of maximum-delay for stability is also invariant with respect to the number of vehicles. Figure 46 shows the spacing errors in the x direction for 130% and 100% of the maximum delay. At 100% of the maximum calculated delay, the

Table VIII.: Percentage of Maximum Delay for Stability (No Delays in Kinematics)

Communication Structure	% (n = 3)	% (n = 5)	% (n = 10)
1	67	69	85
2	83	61	64
3	67	69	85
4	133	134	131
5	115	99	72
6	75	69	66
7	104	149	unstable

formation behaves similarly to the disturbed behavior, where errors between vehicles quickly go to zero along the string. However, at 130% of the maximum delay, there are small spacing errors excited between the trailing vehicles, and the errors grow along the string. The maximum magnitude of the spacing errors between vehicles 3 through 10 never exceeds the maximum error between vehicles 1 and 2. This behavior is unexpected, but it is not evident when the delay is decreased to the maximum calculated delay.

From the simulation results presented here, it can be seen that there is a connection between disturbance behavior and the effects of delays on the system. String-stable cooperative control forms exhibit similar behavior with delays as when disturbances are introduced. Simulation results show that the spacing errors for communication structure 5, which is a string-unstable control form for the gains $k = 1$ and $\beta = 1$, increase along the string before going to zero. Therefore, the frequency-response analysis of different communication structures can be used to predict the

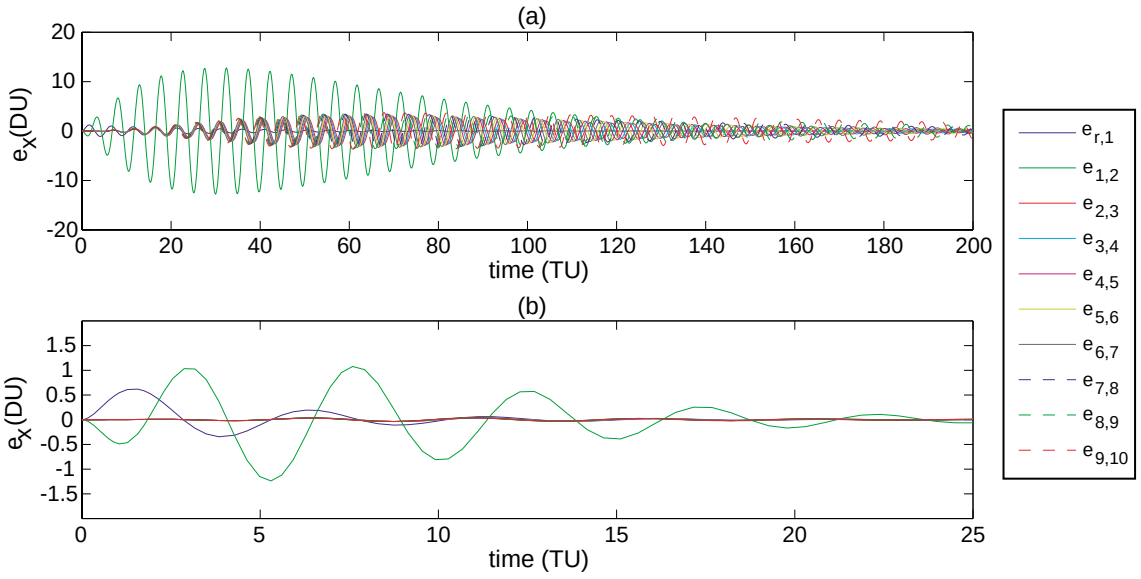

Fig. 46.: Spacing errors for 130% (a) and 100% (b) of the maximum allowable delay for communication structure 4.

behavior of the multivehicle systems to delays in the feedback states.

E. Discussion of Delay-Dependent Stability Analysis

The delay-dependent stability analysis for the system in Equation (7.17) assumed delays in the kinematics in order to write the equations of motion in this first-order form. A modal-coordinate transformation decouples the equations of motion, which permits the stability results for a first-order, scalar DDE to be applied to the $2n$ decoupled equations. Simulation results confirm that this approach correctly determines the stability bound for the delay when the kinematics have induced delays; however, the assumption of delays in the kinematics is not physically based. Whereas it was originally thought that including delays in the kinematics would yield a conservative optimal bound, this was not the case as shown by the simulation results.

The developments here show the contribution that delays in the kinematics have on the stability of a single-DOF system.

Consider a single-DOF system with no delays in the states.

$$\begin{aligned} \dot{x}_1(t) &= x_2(t) \\ \dot{x}_2(t) &= -kx_1(t) - cx_2(t) \end{aligned} \tag{7.25}$$

Stability of this system can be evaluated for the equation: $\ddot{x}_1(t) + c\dot{x}_1(t) + kx_1(t) = 0$, and the system is stable for $c, k > 0$. If delays are included in the feedback states, Equation (7.25) has the following form.

$$\begin{aligned} \dot{y}_1(t) &= y_2(t) \\ \dot{y}_2(t) &= -ky_1(t-\tau) - cy_2(t-\tau) \end{aligned} \tag{7.26}$$

The second-order equation describing the delayed-feedback system becomes $\ddot{y}_1(t) + c\dot{y}_1(t-\tau) + ky_1(t-\tau) = 0$. In this case, stability is not as easily determined for a given delay. As was shown in Section C.1, this second-order form does not have a set of delay-independent gains. In addition, the analysis shown for the first-order, scalar DDE does not easily follow for this particular second-order form. Lastly, assume that the system in Equation (7.26) has delay in the kinematics.

$$\begin{aligned} \dot{z}_1(t) &= z_2(t-\tau) \\ \dot{z}_2(t) &= -kz_1(t-\tau) - cz_2(t-\tau) \end{aligned} \tag{7.27}$$

The trajectories for each of the three systems in Equations (7.25)-(7.27) are different due to the presence of the delays. The second-order equation for the system in Equation (7.27) is $\ddot{z}_1(t) = \dot{z}_2(t-\tau)$, where $\dot{z}_2(t-\tau)$ is approximated by a Taylor series.

$$\dot{z}_2(t-\tau) = \dot{z}_2(t) - \frac{d\dot{z}_2(t)}{dt}|_{\tau=0}\tau + \text{HOT} \tag{7.28}$$

Therefore, $\tau\dddot{z}_1(t) + \ddot{z}_1(t) + c\dot{z}_1(t-\tau) + kz_1(t-\tau) = 0$. Here, it can be seen that the

approximated kinematic delay increases the order of the system [69].

The transcendental characteristic equations for the systems in Equations (7.26) and (7.27) are shown respectively below.

$$s^2 + cse^{-s\tau} + ke^{-s\tau} = 0 \tag{7.29}$$

$$\tau s^3 + s^2 + cse^{-s\tau} + ke^{-s\tau} = 0 \tag{7.30}$$

If no delays are assumed in the feedback, $e^{-s\tau} = 0$, and the effect of delay in the kinematics alone can be investigated. Routh-Hurwitz analysis of Equation (7.29) reveals the asymptotic stability conditions $c, k > 0$; however, analysis of Equation (7.30) reveals that $c, k > 0$ and $c/k > \tau$. This shows that there is an additional stability condition imposed on the system when delays in the kinematics are assumed.

Whereas the theory presented to determine the maximum allowable time delay does not provide the delay for the physical system in which there are no delays in the kinematics, the approach still provides an estimate of the optimal bound. Simulation results show that the delayed-kinematics assumption imposes another stability bound near the calculated bound. However, the calculated optimal bound may be useful in gain selection for stability. In addition, the approach to quantify stability bounds has reduced the computational analysis to essentially solving an eigenvalue problem in order to diagonalize, or decouple, the closed-loop equations of motion. This approach is contrasted with the analytical rigor of finding a Lyapunov-Krasovskiĭ function for each control law or the computational challenges in implementing some of the previously discussed work in Section A.

F. Chapter Summary

In this chapter, the effect of delays on the stability of cooperative multivehicle systems was investigated. Feedback delays in the cooperative control laws can be caused by delays in measurement or communication, and these delays impact stability and performance. The structural form of the cooperative control laws was exploited here to evaluate the delay-independent stability for the decoupled, modal-coordinate form. It was shown that there is no choice of control gains that will ensure stability for all values of the delay. To find the delay-dependent stability bound, a straightforward method was presented to determine the maximum allowable time delay for an n-DOF system using well-known results from the literature on DDEs. This approach assumes delays on the kinematics in order to write the equations of motion in a desired first-order form; however, simulation results show that this is not a conservative assumption. The approach does still provide an estimate of the bound. Simulation results showed that the feedback delays induce similar behavior to the behavior that occurs when the multivehicle system is disturbed.

CHAPTER VIII

NON-INERTIAL AND TIME-BASED SPACING METHODS

The theoretical developments presented in the preceding chapters have all dealt with the design and stability analysis of cooperative control laws based on inertial reference frames. These control laws have been designed to drive spacing errors in the x and y directions between individual vehicles to zero using a desired communication structure. In the preceding theoretical development, it was assumed that the desired distances between vehicles in the x and y directions are constant. In contrast, the development of rigid-body-like formation control laws would assume constant distances between vehicles in some non-inertial frame aligned with the orientation of the desired rigid formation. This rigid-body nature can be achieved using a control law designed in the inertial frame by determining the desired distances between vehicles as a function of time. Therefore, it must be known how the distances between vehicles change in an inertial frame in order to maintain the desired formation in a non-inertial frame. For some design applications, it may be difficult to determine the desired distances between vehicles as a function of time, which motivates the development of spacing control laws in non-inertial reference frames or using different spacing parameters, such as time. In this chapter, three different spacing control forms are investigated that do not assume constant distances in an inertial reference frame.

The development of cooperative control laws for two applications, in particular, is investigated: 1.) spacing along an arbitrary path, and 2.) time-based spacing to an endpoint. These applications are motivated by ongoing research in next-generation air traffic systems. Aircraft are often routed along a common path and air-traffic controllers are responsible for maintaining separations between neighboring aircraft. In the future, aircraft may be equipped to autonomously space along a known flight

path relative to another aircraft. Time-based spacing is a concept being investigated for the separation of aircraft in terminal areas [70]. In the control-law developed here, vehicles determine the time-to-go to a desired endpoint, and this parameter is used to maintain a constant time difference between vehicles at the endpoint. There are several advantages to time-based spacing over distance-based spacing. The time-based spacing approach works well for spacing vehicles along accelerating or decelerating trajectories, where desired distances between vehicles may not be constant. In addition, vehicles on dissimilar trajectories can be spaced at the same endpoint. Another application of time-based spacing is cooperative timing or time-on-target, where vehicles arrive at a desired location in a coordinated manner for imaging or surveillance purposes [71].

The general control approach applied here is to find the desired position along a trajectory relative to the immediately preceding vehicle. The desired position has an associated velocity and acceleration at that point on the trajectory, and each vehicle tracks a desired position, velocity, and acceleration that is determined relative to its lead vehicle. Therefore, to implement this approach, each vehicle must know its reference trajectory.

The chapter is organized as follows. Vehicle spacing with non-constant distances in the inertial frame is presented in Section A. These developments serve to motivate the spacing control forms presented in Sections B and C. In Section B, a control law for spacing vehicles along an arbitrary path is derived. The arbitrary path is parameterized by the arclength parameter, and spacing errors are defined using the arclength and perpendicular distance to the path. The time-based spacing control law is developed in Section C, and simulation results illustrate the implementation of this spacing approach for vehicles on dissimilar trajectories. Internal stability of these control forms is presented in Section D. String stability is also discussed, and

qualitative results are presented based upon simulation results.

A. Spacing with Non-Constant Distances

Consider the general control form presented Equation (3.6). If the first vehicle tracks a circular reference trajectory, constant distances in the x and y directions will yield overlapping trajectories as shown in Figure 47. Here, the desired distance between vehicles is 1 DU in the x and y directions, and the initial positions of the vehicles are denoted by the asterisks. The spacing errors go to zero in the x and y directions as expected.

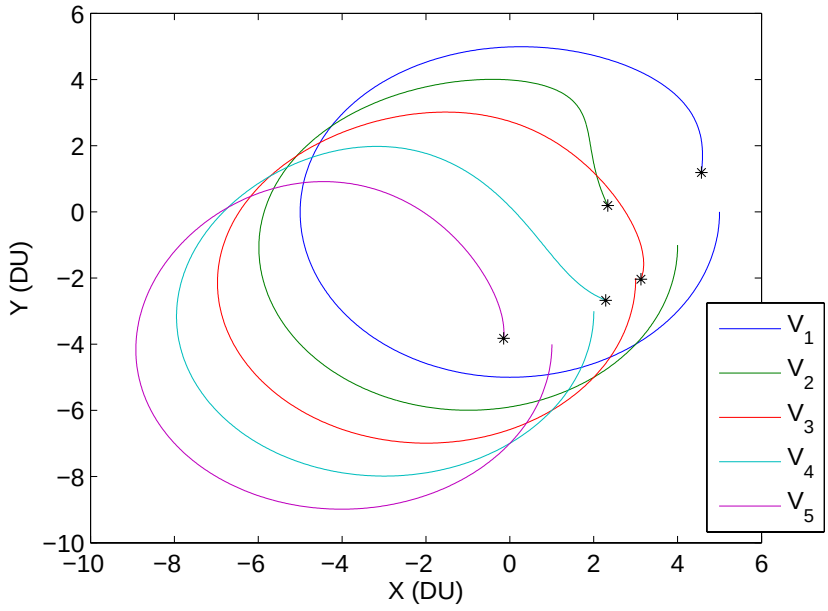

Fig. 47.: Vehicle positions for a circular reference trajectory and constant distances in an inertial frame.

If a rigid-body-like formation is desired wherein the trajectories do not cross for a circular reference trajectory, the control laws can still be designed in the inertial

frame. However, the desired distances between vehicles are not constant, and the first and second derivatives of the distances must be included in the control laws. For example, given a C^2 reference trajectory $\{x_r(t), y_r(t)\}$, a rigid-body orientation can be defined as the orientation of the reference trajectory.

$$\psi = \tan^{-1}\left(\frac{\dot{y}_r}{\dot{x}_r}\right) \tag{8.1}$$

Constant distances between vehicles can be defined in a virtual body-fixed reference frame, where the $\hat{\boldsymbol{b}}_1$ direction is aligned with the heading of the reference trajectory: $\boldsymbol{d} = l\hat{\boldsymbol{b}}_1 + m\hat{\boldsymbol{b}}_2$. These distances and their derivatives can be coordinatized in the inertial frame.

$$\begin{aligned}
d &= (l\cos\psi - m\sin\psi)\,\hat{\boldsymbol{n}}_1 + (l\sin\psi + m\cos\psi)\,\hat{\boldsymbol{n}}_2 \\
\dot{d} &= \left(l\dot{\psi}\sin\psi - m\dot{\psi}\cos\psi\right)\hat{\boldsymbol{n}}_1 + \left(l\dot{\psi}\cos\psi - m\dot{\psi}\sin\psi\right)\hat{\boldsymbol{n}}_2 \\
\ddot{d} &= \left(-l\ddot{\psi}\sin\psi - l\dot{\psi}^2\cos\psi - m\ddot{\psi}\cos\psi + m\dot{\psi}^2\sin\psi\right)\hat{\boldsymbol{n}}_1 + \\
&\qquad + \left(l\ddot{\psi}\cos\psi - l\dot{\psi}^2\sin\psi - m\ddot{\psi}\sin\psi - m\dot{\psi}^2\cos\psi\right)\hat{\boldsymbol{n}}_2
\end{aligned} \tag{8.2}$$

To yield homogeneous error dynamics, the control input to the ith vehicle also includes the second derivatives of the desired distances for the first through ith vehicles. Therefore, the control inputs are the sum of the nominal control inputs shown in Equation (3.6), $\bar{u}$, and the second derivatives of the distances.

$$\begin{aligned}
u_1 &= \bar{u}_1 - \ddot{d}_1 \\
u_2 &= \bar{u}_2 - \left(\ddot{d}_1 + \ddot{d}_2\right) \\
&\vdots \\
u_i &= \bar{u}_i - \left(\ddot{d}_1 + \ddot{d}_2 + ... + \ddot{d}_i\right)
\end{aligned} \tag{8.3}$$

To implement a spacing-control law with non-zero $\ddot{d}$ terms, each vehicle must have

knowledge of the reference trajectory and the desired spacing between all of the preceding vehicles in the formation. This statement can be generalized to all of the communication structures investigated previously.

Figure 48 shows the rigid-body-like motion that results when the desired distances between vehicles are constant in a non-inertial frame. The spacing errors again go to zero, and the vehicles converge to the desired formation from the initial errors in the formation.

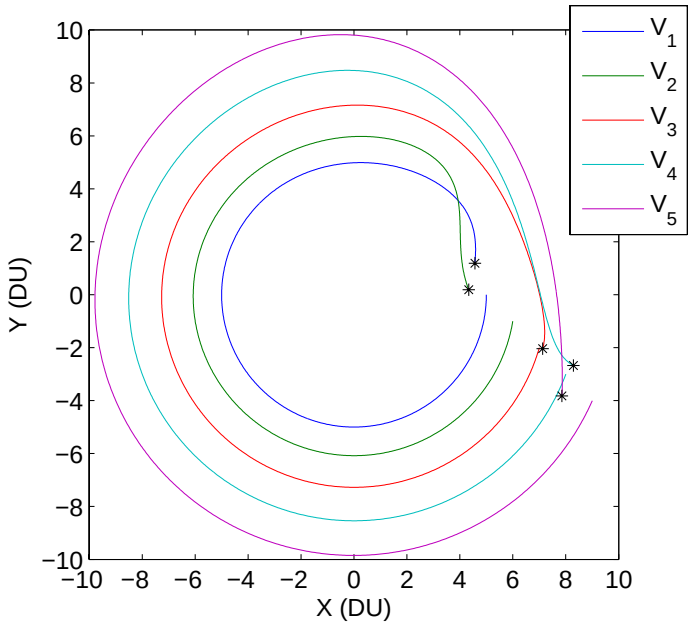

Fig. 48.: Vehicle positions for a circular reference trajectory and changing distances to achieve rigid-body-like motion.

B. Spacing Along an Arbitrary Path

The results presented in the previous section show that vehicles can be spaced along a reference trajectory to achieve constant distances in a non-inertial reference frame.

The implementation of that approach requires that distances between vehicles be written as a function of time, and in addition, the distances between all preceding vehicles in the formation must be known in order to drive spacing errors to zero. In this section, the control laws to space vehicles along an arbitrary path are investigated. Here, the path is parameterized in terms of arclength, or distance along the path, and the arclength parameter is the spacing variable that motivates the control-law design. This approach still requires that all vehicles have knowledge of the reference trajectory; however, the control law design does not require that distances between vehicles be determined as functions of time. Additionally, the theory presented here does not require that vehicles know the $\ddot{d}$ terms for all preceding vehicles.

1. Definition of the Path Reference Frame

Curves in n-dimensional space can be described using geometric properties, such as arclength and curvature. Given a C^1, or smooth, curve in n-dimensions and parameterized in time, the arclength and curvature can be determined. The arclength of a curve is an intrinsic parameter, which depends only on how the curve bends and not on how quickly the curve is traced in time [72].

Given a vector of inertial positions, $\boldsymbol{r}(t)$, and velocities, $\dot{\boldsymbol{r}}(t)$, the length of the curve can be determined by integrating the speed along the path for a given time interval.

$$L\left(\boldsymbol{r}(t_0, t_f)\right) = \int_{t_0}^{t_f} ||\dot{\boldsymbol{r}}(t)||\, dt \tag{8.4}$$

Similarly, the arclength is an intermediate point on the path, $s(t)$. This integral can be used to parameterize the path as a function of arclength rather than time.

$$s(t) = \int_{t_0}^{t} ||\dot{\boldsymbol{r}}(\tau)||\, d\tau \tag{8.5}$$

To parameterize the curve as a function of arclength, Equation (8.5) must be an invertible function. Equation (8.5) will yield a theoretically invertible expression if the speed along the curve is never equal to zero. Given $\dot{\boldsymbol{r}}(t) \neq 0$, the speed along the curve is always positive, and the arclength $s(t)$ is strictly increasing. Thus, time is written as a function of arclength, and the path is described using the arclength parameter. Challenges arise in determining time as a function of arclength when Equation (8.5) does not yield a closed-form solution.

These concepts can be illustrated using a 2-dimensional path. A path-fixed coordinate frame follows the path as shown in Figure 49, where the $\hat{\boldsymbol{b}}_1$ vector is tangent to the path, or aligned with the velocity vector, and the $\hat{\boldsymbol{b}}_2$ vector is perpendicular to the path in the plane. Each reference frame is attached the curve at a given arclength, where $0 < s_A < s_B < s_C$.

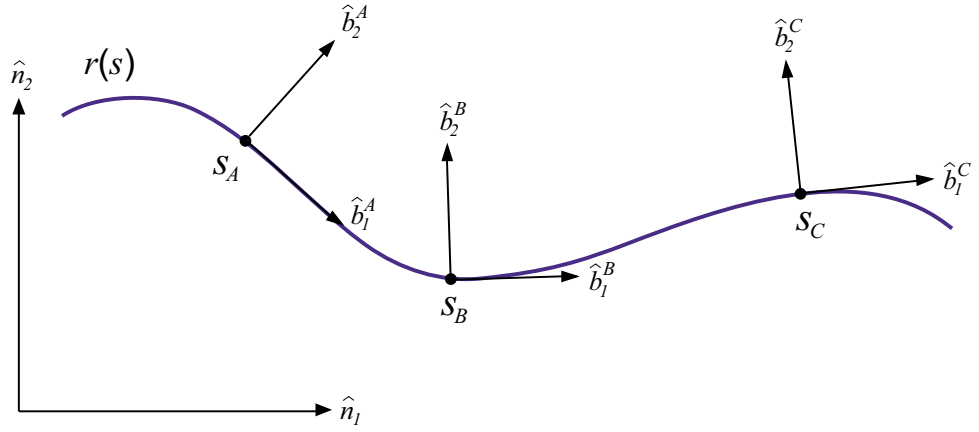

Fig. 49.: Path-fixed reference frames at different arclength positions.

The velocity and acceleration of a vehicle along the path is coordinatized in the

path frame.

$$\dot{\boldsymbol{r}}(t) = v\hat{\boldsymbol{b}}_1 \tag{8.6}$$

$$\ddot{\boldsymbol{r}}(t) = \dot{v}\hat{\boldsymbol{b}}_1 + v\dot{\psi}\hat{\boldsymbol{b}}_2 \tag{8.7}$$

Here, $\dot{\psi}$ is the angular turn rate of the path-fixed frame relative to the inertial axis, and ψ is the angle of the path-fixed frame with respect to the horizontal inertial axis. Acceleration components in the $\hat{\boldsymbol{b}}_1$ and $\hat{\boldsymbol{b}}_2$ directions indicate that a multivehicle system could be spaced along the path and perpendicular to the path, which motivates the definition of along-path and perpendicular-to-path spacing errors.

2. Spacing-Error Definitions

Given a trajectory parameterized by arclength, $\{x_r(s), y_r(s)\}$, vehicles can be spaced along and perpendicular to the trajectory. Figure 50 illustrates the spacing of a vehicle string along a reference path. Each vehicle's (x, y) position is projected onto the reference trajectory to determine the along-path arclength, s_i, and the perpendicular distance, p_i, from the trajectory.

The along-path errors are written as a function of arclength between two adjacent vehicles.

$$\begin{aligned} e_1^s &= s_r - s_1 - d_1^s \\ e_i^s &= s_{i-1} - s_i - d_i^s; \quad i = 2, ..., n \end{aligned} \tag{8.8}$$

Here, d_i^s is a constant arclength relative the preceding vehicle. The perpendicular-to-path errors are similarly defined, where d_i^p is a constant perpendicular distance

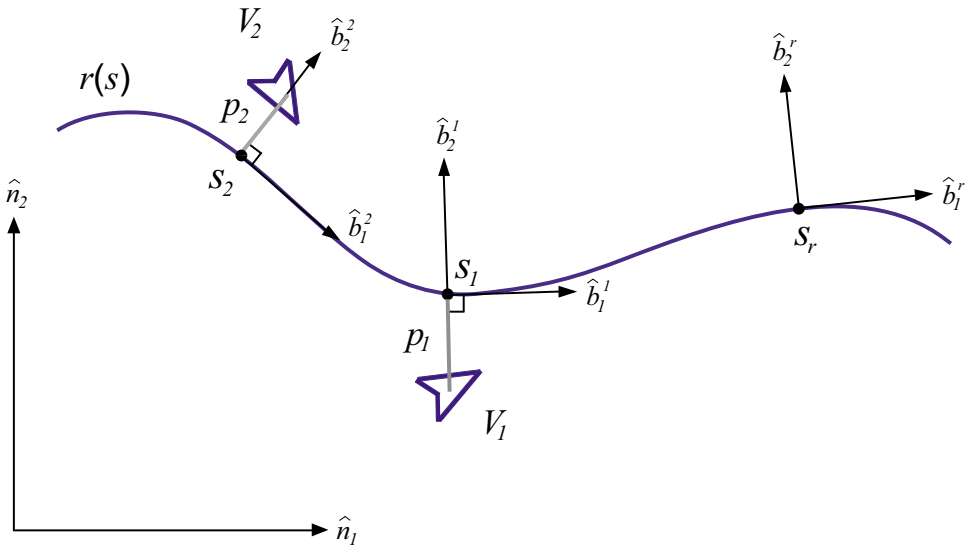

Fig. 50.: Projection of vehicle positions onto the reference trajectory.

relative to the preceding vehicle.

$$e_1^p = p_r - p_1 - d_1^p$$
$$e_i^p = p_{i-1} - p_i - d_i^p; \quad i = 2, ..., n \tag{8.9}$$

The desired arclength and perpendicular distance for the ith vehicle relative to its lead vehicle are denoted as s_i^* and p_i^*, respectively.

$$s_i^* = s_{i-1} - d_i^s; \qquad p_i^* = p_{i-1} - d_i^p \tag{8.10}$$

These values are found from Equations (8.8) and (8.9) when the spacing errors are equal to zero.

3. Spacing Control Law

The along-path position at the desired arclength can be determined from the reference trajectory that is parameterized by arclength: $\{x_r(s_i^*), y_r(s_i^*)\}$. The velocity and acceleration at the along-path position are also determined from the reference trajectory. From the velocity at the along-path position, the orientation of the reference frame at the desired arclength, ψ_i, is determined.

$$\psi_i = \tan^{-1}\left(\frac{\dot{y}_r(s_i^*)}{\dot{x}_r(s_i^*)}\right) \tag{8.11}$$

The desired perpendicular distance, p_i^*, is used to generate a reference position, velocity, and acceleration in the x and y directions.

$$\begin{array}{l|l} x_{i,ref} = x_r(s_i^*) - p_i^*\sin\psi_i & y_{i,ref} = y_r(s_i^*) + p_i^*\cos\psi_i \\ \dot{x}_{i,ref} = \dot{x}_r(s_i^*) - \dot{\psi}_i p_i^*\cos\psi_i & \dot{y}_{i,ref} = \dot{y}_r(s_i^*) - \dot{\psi}_i p_i^*\sin\psi_i \\ \ddot{x}_{i,ref} = \ddot{x}_r(s_i^*) - \ddot{\psi}_i p_i^*\cos\psi_i + \dot{\psi}_i^2 p_i^*\sin\psi_i & \ddot{y}_{i,ref} = \ddot{y}_r(s_i^*) - \ddot{\psi}_i p_i^*\sin\psi_i - \dot{\psi}_i^2 p_i^*\cos\psi_i \end{array} \tag{8.12}$$

Each vehicle tracks the reference position, velocity, and acceleration that are functions of the desired arclength and perpendicular distance.

$$\begin{aligned} u_i &= k_i(x_{i,ref} - x_i) + c_i(\dot{x}_{i,ref} - \dot{x}_i) + \ddot{x}_{i,ref} \\ w_i &= k_i(y_{i,ref} - y_i) + c_i(\dot{y}_{i,ref} - \dot{y}_i) + \ddot{y}_{i,ref} \end{aligned} \tag{8.13}$$

Note that the control laws above do not require spacing information from any of the other vehicles in the formation, which is a significant advantage over designing control laws in an inertial frame. However, each vehicle must have knowledge of a common reference trajectory to implement this spacing scheme.

4. Simulation Results

Simulation results are shown for spacing along a constant-velocity circular path. The circular reference trajectory has radius, R, and angular rate, Ω.

$$\begin{array}{l|l} x_r(t) = R\cos(\Omega t) & y_r(t) = R\sin(\Omega t) \\ \dot{x}_r(t) = -R\Omega\sin(\Omega t) & \dot{y}_r(t) = R\Omega\cos(\Omega t) \\ \ddot{x}_r(t) = -R\Omega^2\cos(\Omega t) & \ddot{y}_r(t) = -R\Omega^2\sin(\Omega t) \end{array} \tag{8.14}$$

Equation (8.5) is used to find the arclength as a function of time, and for the constant-velocity circular path, this relationship can be inverted: $t = s/(R\Omega)$. Therefore, the reference trajectory can be reparameterized as a function of arclength.

$$\begin{array}{l|l} x_r(s) = R\cos\left(s/R\right) & y_r(s) = R\sin\left(s/R\right) \\ \dot{x}_r(s) = -R\Omega\sin\left(s/R\right) & \dot{y}_r(s) = R\Omega\cos\left(s/R\right) \\ \ddot{x}_r(s) = -R\Omega^2\cos\left(s/R\right) & \ddot{y}_r(s) = -R\Omega^2\sin\left(s/R\right) \end{array} \tag{8.15}$$

The arclength and perpendicular position of each vehicle with respect to the reference trajectory are found by projecting the position of each vehicle onto the reference trajectory using nonlinear least squares [73]. The measurement vector is the position of the ith vehicle: $\tilde{\boldsymbol{y}} = [x_i, y_i]^T$, and the nonlinear function is $\boldsymbol{f}(\hat{s}) = [R\cos(\hat{s}/R), R\sin(\hat{s}/R)]^T$. The iterative nonlinear least squares algorithm finds the arclength along the reference trajectory that is perpendicular to the vehicle position.

Figure 51 shows the vehicle positions in the $x - y$ plane. The simulation results are shown for a five-vehicle formation, where the desired spacing between adjacent vehicles is 1 DU along the path and 1 DU perpendicular to the path. In Figure 52, the along-path and perpendicular-to-path spacing errors are shown to converge to zero.

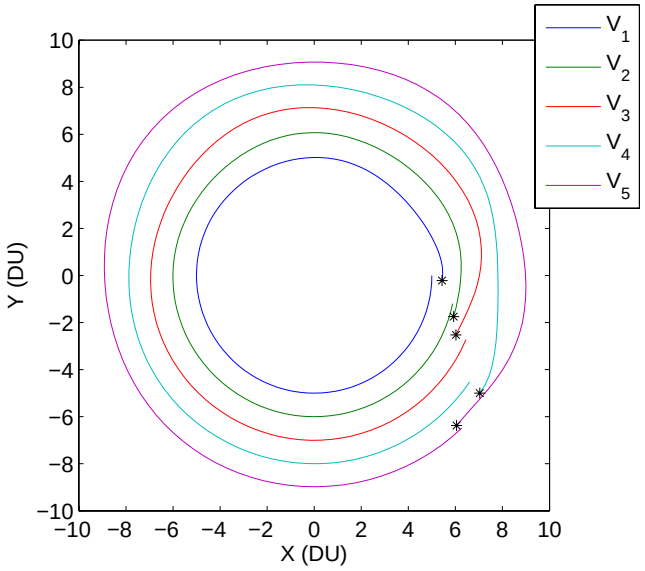

Fig. 51.: Vehicle positions resulting from the control law using arclength as a spacing parameter.

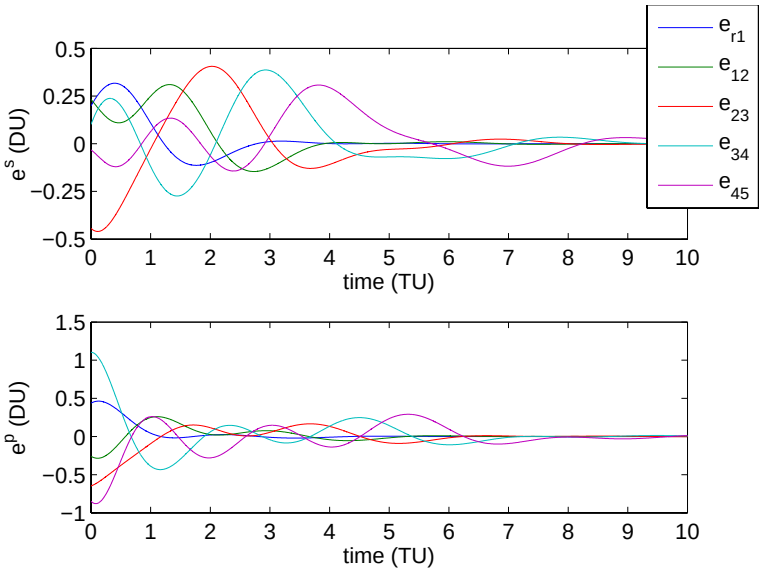

Fig. 52.: Spacing errors in arclength and perpendicular position.

C. Time-Based Spacing

In time-based spacing concepts, spacing control laws can be implemented to maintain constant-time spacing between vehicles regardless of how distances change between adjacent vehicles. Swaroop et al. investigated a constant-time headway spacing control law, where the desired distance between vehicles is related to the velocity of the immediately preceding vehicle [15].

The time-based spacing control law investigated here spaces vehicles along a trajectory in order to achieve a constant-time spacing at a desired endpoint. The spacing control law uses a time-to-go parameter, which is the calculated time that it will take for a vehicle at its current position to reach the endpoint. The time-to-go spacing error is defined analogously to the spacing errors in previous developments.

A time-based spacing scheme relative to a final position allows vehicles to be spaced along dissimilar trajectories. This concept is illustrated in Figure 53, where the trajectories for each vehicle are shown in red, and the time-to-go parameter is denoted by τ.

1. Time-to-go Spacing Errors and Spacing Control Law

The time-to-go error is defined as the error between the time-to-go parameters for two adjacent vehicles, where the desired time-based spacing at the endpoint between two vehicles is $\Delta\tau_i$.

$$\begin{aligned} \epsilon_1 &= \tau_r - \tau_1 + \Delta\tau_1 \\ \epsilon_i &= \tau_{i-1} - \tau_i + \Delta\tau_i; \quad i = 2, ..., n \end{aligned} \tag{8.16}$$

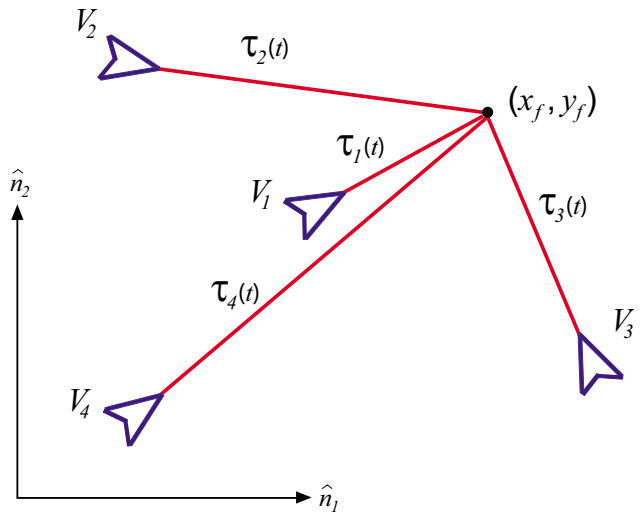

Fig. 53.: Vehicles on different trajectories using time-based spacing at a desired endpoint.

The desired time-to-go for the ith vehicle is defined similar to the definition of the desired arclength and perpendicular distance in Equation (8.10).

$$\tau_i^* = \tau_{i-1} + \Delta\tau_i \tag{8.17}$$

The desired time-to-go is used to determine the desired position, velocity, and acceleration of the ith vehicle along its own reference trajectory, $\{x_r^i(\tau_i^*), y_r^i(\tau_i^*)\}$. An underlying assumption of this development is that the reference trajectory for each vehicle can be parameterized as a function of time-to-go.

The spacing errors of the ith vehicle are defined relative to the desired position, velocity, and acceleration, which are functions of τ_i^*.

$$e_i = x_r^i(\tau_i^*) - x_i; \quad \dot{e}_i = \dot{x}_r^i(\tau_i^*) - \dot{x}_i; \quad \ddot{e}_i = \ddot{x}_r^i(\tau_i^*) - u_i \tag{8.18}$$

The control input to the ith vehicle is a function of the spacing errors.

$$u_i = c_i \dot{e}_i + k_i e_i + \ddot{x}_r^i \left(\tau_i^*\right) \tag{8.19}$$

2. Simulation Results

The time-based spacing concept was simulated for reference trajectories with constant acceleration, which allows the time-to-go to be found analytically. The reference trajectory in the x direction has the following assumed form with initial conditions $x(t_0)$ and $\dot{x}(t_0)$.

$$x_r(t) = \frac{1}{2} a_x \left(t - t_0\right)^2 + \dot{x}(t_0)\left(t - t_0\right) + x(t_0) \tag{8.20}$$

The reference trajectory can also be written as a function of the final time, t_f.

$$x_r(t_f) = x_f = \frac{1}{2} a_x \left(t_f - t\right)^2 + \dot{x}(t)\left(t_f - t\right) + x(t) \tag{8.21}$$

Here, x_f is the desired end position, and $\dot{x}(t)$ and $x(t)$ are the velocity and position of the vehicle at the current time t. The velocity, $\dot{x}(t)$, can be written in terms of the desired velocity at the endpoint, $\dot{x}_f$.

$$\dot{x}(t) = \dot{x}_f - a_x \left(t_f - t\right) \tag{8.22}$$

Substituting Equation (8.22) into Equation (8.21) yields a second-order polynomial that is a function of the time-to-go, $\tau_x \equiv t_f - t$, from which the time-to-go is easily found.

$$\tau_x = \frac{\dot{x}_f \pm \sqrt{\dot{x}_f^2 - 2a_x \left(x_f - x(t)\right)}}{a_x} \tag{8.23}$$

Here, the time-to-go is denoted by τ_x to indicate that this is the time to reach the endpoint in the x direction. The development is identical in the y direction. Due to the decoupled nature of the control and trajectory design, the time-to-go of each

vehicle is computed in both the x and y directions. In this particular implementation, the time-to-go can be different in the x and y directions, and these separate values are used to determine the decoupled control inputs in the x and y directions. The two values will be equal when the vehicle is on its reference trajectory as shown in Figure 54.

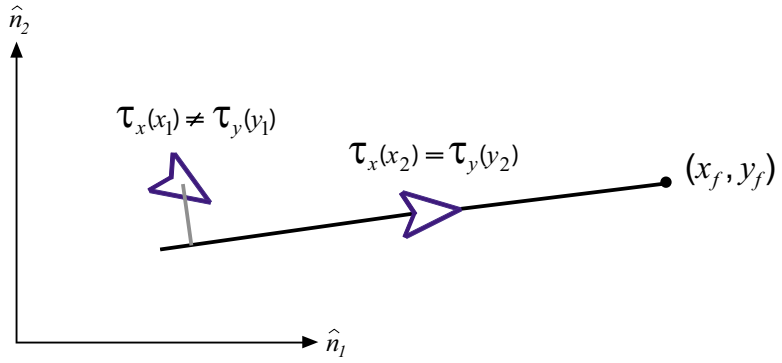

Fig. 54.: The time-to-go determined separately in the x and y directions.

Simulation results show that the time-based spacing control law is able to achieve a constant-time spacing at the desired endpoint. Figure 55 shows the vehicle positions in the $x-y$ plane. Different trajectories are planned to space the vehicles 0.5 TU apart at the endpoint $(x_f, y_f) = (20, 20)$. The planned starting points of the trajectories are shown by the black circles, and the initial conditions of the vehicles are randomly perturbed. The first vehicle tracks a reference time-to-go, τ_r, to cross the final position at 10 TU. The time-to-go errors, ϵ, in the x and y directions are shown in Figure 56. The errors in the time-to-go converge to zero indicating that the desired spacing is achieved at the endpoint.

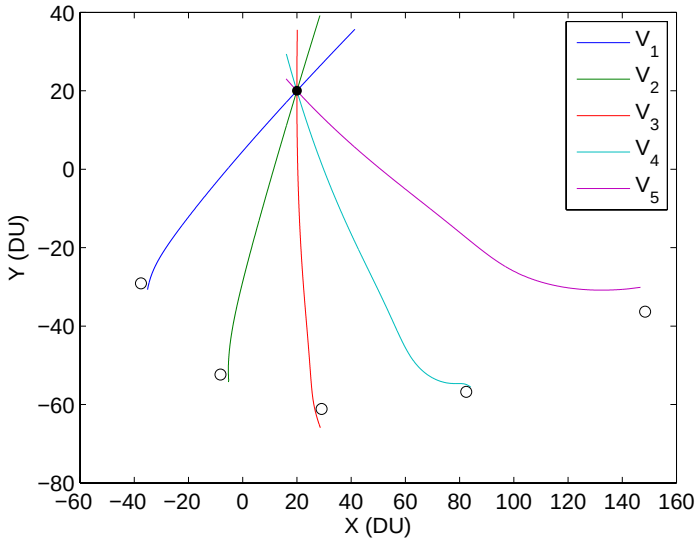

Fig. 55.: Vehicle positions en route to the desired endpoint: $(x_f, y_f) = (20, 20)$.

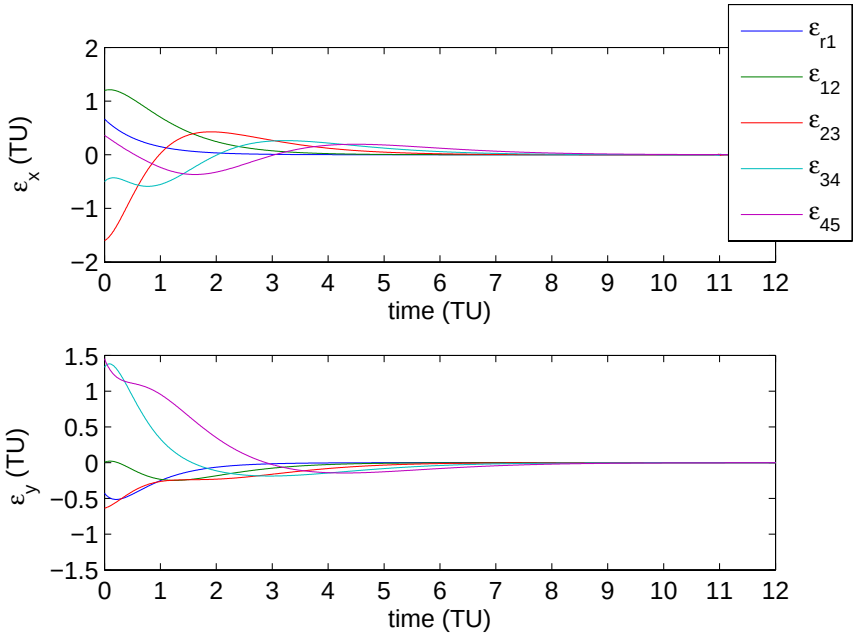

Fig. 56.: Time-to-go errors in the x and y directions.

D. Stability Analysis

For the two spacing-control schemes presented in the previous sections, state information from the immediately preceding vehicle is used to determine a reference position, velocity, and acceleration for the ith vehicle along its own path. The reference position, velocity, and acceleration are implicit, nonlinear functions of the immediately preceding vehicle's states. Proving the internal stability of the multivehicle system for this control design differs from the theoretical results presented in earlier chapters; the system cannot be written in a matrix form from which the eigenvalues are used to determine internal stability.

The internal stability of the vehicle formation is demonstrated in a cascade form, where spacing errors are shown to go to zero sequentially along the string. Spacing errors for either spacing along an arbitrary path or time-based spacing have the same general form.

$$e_1 = \chi_r - \chi_1 - d_1; \quad e_2 = \chi_1 - \chi_2 - d_2; \quad \ldots \quad e_n = \chi_{n-1} - \chi_n - d_n \tag{8.24}$$

Here, χ represents a spacing parameter such as the arclength, s, perpendicular position, p, or the time-to-go, τ. From each e_i term, the parameter χ_i can be written as a function of χ_{i-1} and the spacing error. The ideal spacing parameter, χ_i^*, is found when the spacing error is set equal to zero. By making the appropriate substitutions, it shown that the ideal spacing parameter for the nth vehicle, χ_n^*, is a function of the

spacing errors of all preceding vehicles.

$$\begin{aligned}
&\chi_1 = \chi_r - d_1 - e_1; && \chi_1^* = \chi_r - d_1 \\
&\chi_2 = \chi_1 - d_2 - e_2; && \chi_2^* = \chi_1 - d_2 = \chi_r - e_1 - (d_1 + d_2) \\
&\quad \vdots && \quad \vdots \\
&\chi_n = \chi_{n-1} - d_n - e_n; && \chi_n^* = \chi_r - \sum_{j=1}^{n-1} e_j - \sum_{j=1}^{n} d_j
\end{aligned} \tag{8.25}$$

When the spacing error of the first vehicle goes to zero, the ideal spacing parameter of the second vehicle is no longer a function of e_1 and the second vehicle will converge to its desired spacing. Therefore, the nth vehicle converges to its desired spacing when the spacing errors of the $n-1$ preceding vehicles are zero.

The string stability of these control forms is harder to evaluate because the reference trajectory being tracked is an implicit, nonlinear function of the preceding vehicle's states. Swaroop et al. investigated string stability for a time-based spacing control law [15]. In that paper, the error propagation transfer function for a constant-time headway spacing control law was shown to be string stable. Simulation results demonstrated the string-stable nature of the control law, where the spacing errors between vehicles decreased along the string when the first vehicle was subjected to a step-change in velocity. A similar frequency-domain analysis is not apparent for the control laws investigated in this chapter due to the nonlinear reference trajectory determined by the preceding vehicle.

To investigate the string stability of the control schemes presented here, simulations were run with the velocity of the first vehicle perturbed from the reference velocity. The other vehicles in the formation were started with perfect initial conditions and relative spacing. Figure 57 shows the spacing errors for the path-spacing control law with a circular reference trajectory. The perpendicular spacing errors

increase along the string, which indicates that this control form is string unstable. This result is expected as it assumes a singly-connected leader-follower communication structure (communication structure 5), which was shown to be string unstable in Chapter VI.

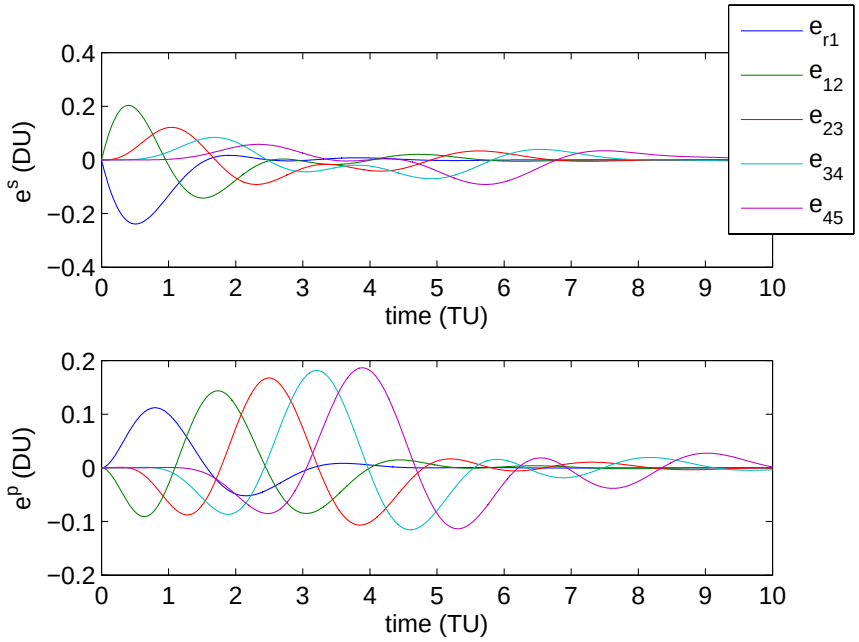

Fig. 57.: Along-path and perpendicular-to-path spacing errors when the velocity of the first vehicle is perturbed.

Figure 58 shows the spacing errors for the time-based spacing control law. Again, the velocity of the first vehicle is perturbed from its reference velocity. The time-to-go spacing errors decrease along the string indicating string stability. Although the control form evaluated here is different from the constant-time-headway control law developed by Swaroop et al., the time-based spacing control law appears to be string stable as well.

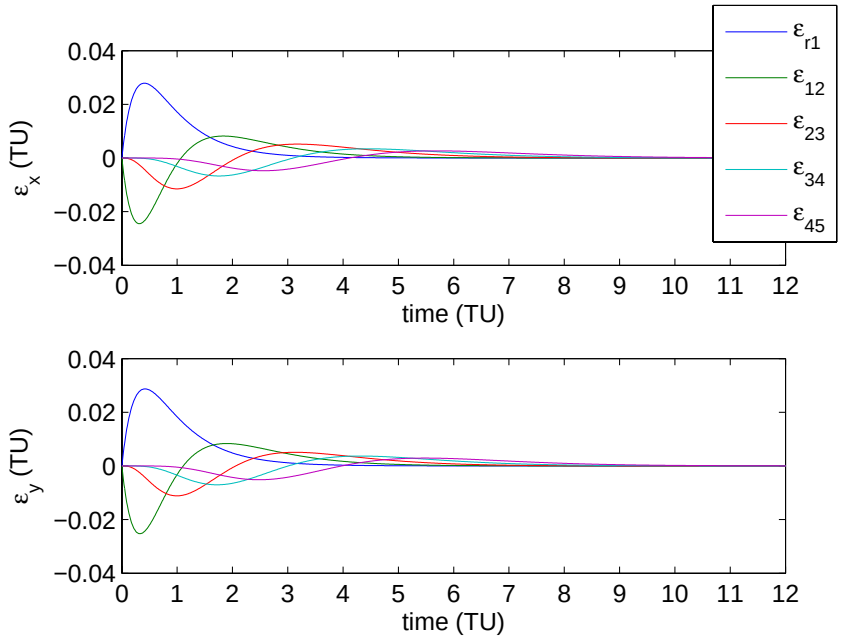

Fig. 58.: Time-to-go spacing errors when the velocity of the first vehicle is perturbed.

E. Chapter Summary

Motivated by spacing control laws in an inertial reference frame with non-constant distances, two cooperative spacing control forms were investigated. For spacing along an arbitrary path, spacing errors were defined using arclength and perpendicular distance parameters. A major advantage of this control form is the reduced information required in implementation versus the implementation of control laws designed in an inertial reference frame. In the time-based spacing scheme, spacing errors were defined between the time-to-go parameters relative to a desired endpoint for adjacent vehicles. Both control schemes employed the same control form where the ith vehicle tracks a reference position, velocity, and acceleration along a trajectory determined by the states of the $(i-1)$th vehicle. The reference trajectory is an implicit, nonlinear

function of the $(i-1)$th vehicle's states.

Internal stability of the formation was shown using a cascade framework; however, string stability is more difficult to analyze for this control form. Whereas qualitative analysis from simulation results indicates that the control law for spacing along an arbitrary trajectory is not string stable because spacing errors grow along the string, simulation results for the time-based spacing indicate that this control law is string stable. Further analysis of these control forms should be investigated in future work.

CHAPTER IX

SUMMARY

This dissertation has investigated the design and stability analysis of decentralized, cooperative control laws for multivehicle systems. The main impacts of this work include:

- the development of a unifying framework for designing decentralized, cooperative control laws for multivehicle systems, where vehicle models can be represented as decoupled, double integrators;
- the analogy of decentralized, cooperative control laws to structural systems, which motivates a mechanics-based approach to analyze the disturbance rejection of different communication structures;
- the development of an approach to find the maximum allowable time delays in a cooperative multivehicle system; and
- an investigation of spacing control laws designed using non-inertial spacing parameters.

The research throughout this dissertation was based upon a nonlinear, kinematic vehicle model that represents planar motion for a wide-variety of vehicle types. The vehicle model was derived and the differential-flatness properties of the model were presented in Chapter II. The differentially-flat vehicle model was shown to have an exact linear representation, which allowed control laws to be designed using double-integrator models decoupled in the x and y directions.

The development of decentralized, cooperative control laws was presented in Chapter III, and this development provided a unifying approach to design control

laws using an assumed communication structure. Control inputs were chosen to yield internal stability of the formation, such that spacing errors between vehicles in the formation go to zero. A general control form was presented, where each vehicle tracks both its immediately preceding vehicle and a reference trajectory. Simulation results showed that vehicle formations converged to the desired formation from errant initial conditions. Additionally, some of the challenges associated with the linear representation of the nonlinear vehicle model were presented in Chapter III.

Two stability notions were investigated in this research: internal stability and string stability. The definition and concept of string stability were presented in Chapter IV. The chapter also included some mathematical preliminaries and results from the literature to show how string stability is determined. The cooperative control form developed in Chapter III was shown to be string stable when lead-vehicle and reference-trajectory tracking were combined.

The theory presented in Chapter V showed that closed-loop equations of motion for the cooperative multivehicle systems are analogous to structural systems. The structurally-analogous equations of motion were written with stiffness and damping matrices, where the form of these matrices was determined by the communication structure. This structural analogy is extended to communication structures that do not have a physical representation, and this special case is discussed. Mathematical preliminaries for the structural form were also presented including modal-coordinate transformations, eigenvalue and eigenvector sensitivities, and proportional damping.

The theory in Chapter VI built upon the structural analogy presented in Chapter V. Two structural-analysis tools were presented in the context of the multivehicle application: modal cost and frequency-response functions. These analysis tools were used to evaluate the disturbance response of the multivehicle systems. The modal-cost tool was used to evaluate the disturbability of different communication structures.

The frequency-response functions were used to evaluate the response of the multivehicle systems to harmonic excitation, and the steady-state errors between vehicles were described using the frequency response. The behavior of the steady-state errors was shown to reveal the string stability of the different control forms; therefore, the frequency-response analysis is a straightforward method to investigate string stability for a general communication structure. One drawback to the structural-analysis tools is the diagonalizability of the stiffness matrix to decouple the system. Simulation results were used to compare different communication structures, and results indicate that a connection to the first vehicle in the formation leads to string-stable control laws with bounded control inputs. Additionally, the frequency-response analysis tool was used to design control gains for desired system performance.

In Chapter VII, the effects of state feedback delays on multivehicle system stability were investigated. The delayed system was modeled using delay differential equations (DDEs). Background was presented on DDEs, and two stability concepts were discussed: delay-independent and delay-dependent stability. Analysis of the delayed closed-loop equations of motions showed that the control gains cannot be designed for stability independent of the delay size. A method to determine the maximum allowable delay for the system was presented, which exploited the structural form of the closed-loop equations of motion for the multivehicle system. Simulation results indicated some challenges in the determination of the stability bounds. Results also showed that the behavior of the system with delays is similar to the behavior induced by disturbances to the system.

In the previous chapters, control laws had been designed and stability was analyzed in an inertial reference frame. However, this control design has flaws in the case that desired distances between vehicles are not constant. Control-law design for spacing in a non-inertial reference frame was investigated in Chapter VIII. Spacing

control laws were developed to space vehicles along an arbitrary path. The resulting control law revealed some advantages over spacing control laws in the inertial frame for non-constant distances between vehicles. A time-based spacing concept was also investigated to achieve constant-time spacing between vehicles at a desired endpoint. The internal stability of these control laws was presented, and a qualitative string-stability analysis was discussed. The control law for spacing along an arbitrary path was qualitatively shown to be string unstable; however, analysis of the time-based spacing control law indicated that that control form is string stable.

REFERENCES

[1] S. Butenko, R. Murphey, and P. Pardalos, Eds., *Recent Developments in Cooperative Control and Optimization*. Boston, Massachusetts: Kluwer Academic Publishers, 2004.

[2] D. D. Siljak, *Decentralized Control of Complex Systems*. New York: Academic, 1991, chapter 9.

[3] J. T. Feddema, C. Lewis, and D. A. Schoenwald, "Decentralized control of cooperative robotic vehicles: Theory and application," *IEEE Transactions on Robotics and Automation*, vol. 18, no. 5, pp. 852–864, 2002.

[4] R. D. Robinett III and J. E. Hurtado, "Stability and control of collective systems," *Journal of Intelligent Robotic Systems*, vol. 39, no. 1, pp. 43–55, 2004.

[5] J. E. Hurtado, R. D. Robinett III, C. R. Dohrmann, and S. Y. Goldsmith, "Decentralized control for a swarm of vehicles performing source localization," *Journal of Intelligent and Robotic Systems*, vol. 41, pp. 1–18, 2004.

[6] D. M. Stipanović, G. İnalhan, R. Teo, and C. J. Tomlin, "Decentralized overlapping control of a formation of unmanned aerial vehicles," *Automatica*, vol. 40, pp. 1285–1296, 2004.

[7] M. Ikeda, D. D. Siljak, and D. E. White, "Decentralized control with overlapping information sets," *Journal of Optimization Theory and Applications*, vol. 34, no. 2, pp. 279–310, 1981.

[8] A. İftar and U. Özgüner, "Contractible controller design and optimal control with state and input inclusion," *Automatica*, vol. 29, no. 3, pp. 593–597, 1990.

[9] R. Caicedo, J. Valasek, and J. Junkins, "Preliminary results of vehicle formation control using dynamic inversion," in *AIAA Aerospace Sciences Meeting and Exhibit*, Reno, NV, January 2004.

[10] R. Olfati-Saber and R. Murray, "Distributed cooperative control of multiple vehicle formations using structural potential functions," in *In 15th IFAC World Congress*, Barcelona, Spain, 2002.

[11] J. A. Fax and R. M. Murray, "Information flow and cooperative control of vehicle formations," *IEEE Transactions on Automatic Control*, vol. 49, no. 9, pp. 1465–1476, 2004.

[12] A. Gattami and R. M. Murray, "A frequency domain condition for stability of interconnected mimo systems," in *Proceedings of the American Control Conference*, 2004, pp. 3723–3728.

[13] D. Swaroop and J. K. Hedrick, "String stability of interconnected systems," *IEEE Transactions on Automatic Control*, vol. 41, no. 3, pp. 349–357, 1996.

[14] ——, "Constant spacing strategies for platooning in automated highway systems," *Journal of Dynamic Systems, Measurement, and Control*, vol. 121, no. 3, pp. 462–470, 1999.

[15] D. Swaroop and K. R. Rajagopal, "A review of constant time headway policy for automatic vehicle following," in *Proceedings of the 2001 IEEE Intelligent Transportation Systems Conference*, Oakland, CA, 2001.

[16] D. Swaroop, "A note about the stability of a string of lti systems," *Transactions of the ASME*, vol. 124, pp. 472–475, 2002.

[17] P. Seiler, A. Pant, and K. Hedrick, "Disturbance propagation in vehicle strings," *IEEE Transactions on Automatic Control*, vol. 49, no. 10, pp. 1835–1841, 2004.

[18] G. Lohr, R. Oseguera-Lohr, T. S. Abbott, and W. Capron, "Flight evaluation of a time-based airborne inter-arrival spacing tool," in *Proceedings of the 5th USA/Europe ATM R&D Seminar*, Budapest, Hungary, 2003.

[19] K. Krishnamurthy, B. Barmore, F. Bussink, L. Weitz, and L. Dahlene, "Fast-time evaluations of an airborne merging and spacing concept for terminal arrival operations," in *Proceedings of the AIAA Guidance, Navigation, and Control Conference*, San Francisco, California, 2005.

[20] B. Barmore, "Airborne precision spacing: A trajectory-based approach to improve terminal area operations," in *Proceedings of the 25th Digital Avionics and Systems Conference*, Portland, Oregon, 2006.

[21] L. A. Weitz, J. E. Hurtado, and A. J. Sinclair, "Decentralized cooperative-control design for multivehicle formations," *Journal of Guidance, Control, and Dynamics*, vol. 31, no. 4, pp. 970–979, 2008.

[22] R. D. Driver, *Ordinary and Delay Differential Equations.* New York: Springer-Verlag, 1977, chapter 5.

[23] L. Dugard and E. I. Verriest, *Stability and Control of Time-Delay Systems.* London, Great Britain: Springer-Verlag, 1998, chapter 1.

[24] T. Mori, "Criteria for asymptotic stability of linear time-delay systems," *IEEE Transactions on Automatic Control*, vol. 30, no. 2, pp. 158–161, 1985.

[25] T. Mori and H. Kokame, "Stability of $\dot{x}(t) = ax(t) + bx(t-\tau)$," *IEEE Transactions on Automatic Control*, vol. 34, no. 4, pp. 460–462, 1989.

[26] J.-P. Richard, "Time-delay systems: An overview of some recent advances and open problems," *Automatica*, vol. 39, pp. 1667–1694, 2003.

[27] L. A. Weitz and J. E. Hurtado, "Investigating time-delay effects for multivehicle formation control," *AIAA Journal of Aerospace Computing, Information, and Communication*, vol. 5, pp. 321–336, 2008.

[28] L. Meirovitch, *Methods of Analytical Dynamics*. New York: McGraw-Hill, 1970, chapter 2, Fundamentals of Analytical Mechanics.

[29] J. L. Junkins and Y. Kim, *Introduction to Dynamics and Control of Flexible Structures*. Washington, DC: American Institute of Aeronautics and Astronautics, 1993, chapter 3.

[30] R. M. Murray, M. Rathinam, and W. Sluis, "Differential flatness of mechanical control systems: A catalog of prototype systems," in *Proceedings of the 1995 ASME International Mechanical Engineering Congress and Expo*, San Francisco, CA, 1995.

[31] M. V. Nieuwstadt, M. Rathinam, and R. Murray, "Differential flatness and absolute equivalence," in *Proceedings of the 33rd Conference on Decision and Control*, Lake Buena Vista, FL, 1994.

[32] S. T. Pledgie, Y. Hao, A. M. Ferreira, S. K. Agrawal, and R. Murphey, "Groups of unmanned vehicles: Differential flatness, trajectory planning, and control," in *Proceedings of the 2002 IEEE International Conference on Robotics & Automation*, Washington, DC, 2002.

[33] C. Altafini, "General n-trailer, differential flatness and equivalence," in *Proceedings of the 38th Conference on Decision & Control*, Phoenix, AZ, 1999.

[34] N. Lećhevin and C. A. Rabbath, "Sampled-data control of a class of nonlinear flat systems with application to unicycle trajectory tracking," *Transactions of the ASME*, vol. 128, pp. 722–728, 2006.

[35] C.-T. Chen, *Linear System Theory and Design.* New York: Oxford University Press, 1999, chapter 8, Section 4.

[36] H. Berghuis and H. Nijmeijer, "Global regulation of robots using only position measurements," *Systems and Control Letters*, vol. 21, no. 4, pp. 289–293, 1993.

[37] K. Subbarao and M. R. Akella, "Differentiator-free nonlinear proportional-integral controllers for rigid-body attitude stabilization," *Journal of Guidance, Control, and Dynamics*, vol. 27, no. 6, pp. 1092–1096, 2004.

[38] R. Azor, I. Y. Bar-Itzhack, and R. R. Harman, "Satellite angular rate estimation from vector measurements," *Journal of Guidance, Control, and Dynamics*, vol. 21, no. 3, pp. 450–457, 1998.

[39] M. R. Akella, "Rigid body attitude tracking without angular velocity feedback," *Systems and Control Letters*, vol. 42, no. 4, pp. 321–326, 2001.

[40] M. Tandale, R. Bowers, and J. Valasek, "Trajectory tracking controller for vision-based probe and drogue autonomous aerial refueling," *Journal of Guidance, Control, and Dynamics*, vol. 29, no. 4, pp. 846–857, 2006.

[41] J. Doebbler, T. Spaeth, J. Valasek, M. J. Monda, and H. Schaub, "Boom and receptacle autonomous air refueling using visual snake optical sensor," *Journal of Guidance, Control, and Dynamics*, vol. 30, no. 6, pp. 1753–1770, 2007.

[42] J. K. Hedrick, D. McMahon, V. Narendran, and D. Swaroop, "Longitudinal vehicle controller design for ivhs systems," in *Proceedings of the American Control*

Conference, Boston, MA, 1991.

[43] S. K. Yadlapalli, S. Darbha, and K. R. Rajagopal, "Information flow and its relation to stability of the motion of vehicles in a rigid formation," *IEEE Transactions on Automatic Control*, vol. 51, no. 8, pp. 1315–1319, 2006.

[44] P. Barooah and J. P. Hespanha, "Error amplification and disturbance propagation in vehicle strings with decentralized linear control," in *Proceedings of the 44th IEEE Conference on Decision and Control, and the European Control Conference*, Seville, Spain, 2005.

[45] J. E. Hurtado, *A Kinematics and Kinetics Primer*. Hurtado - Lulu.com, 2008.

[46] J. P. Keener, *Principles of Applied Mathematics: Transformation and Approximation*. Cambridge, MA: Westview Press, 2000.

[47] R. E. Skelton, "Modal cost analysis for linear matrix-second-order systems," *Journal of Dynamic System, Measurement, and Control*, vol. 102, no. 3, pp. 151–158, 1980.

[48] R. E. Skelton, R. Singh, and J. Ramakrishnan, "Component model reduction by component cost analysis," in *Proceedings of the AIAA Guidance, Navigation, and Control Conference*, Minneapolis, MN, 1988.

[49] J. E. Hurtado, Z. Rahman, and J. L. Junkins, "Vibration suppression for a planar flexible grid: Analysis and experiments," in *Proceedings of the 33rd AIAA Structures, Structural Dynamics and Materials Conference*, Dallas, TX, 1992.

[50] J. E. Hurtado, "Experiments on vibration suppression of a flexible planar grid," Master's thesis, Texas A&M University, College Station, Texas, 1991.

[51] R. R. Craig and A. J. Kurdila, *Fundamentals of Structural Dynamics*. Hoboken, NJ: John Wiley & Sons, Inc., 2006.

[52] Z. Jin and R. M. Murrary, "Stability and performance analysis with double-graph model of vehicle formations," in *Proceedings of the American Control Conference*, 2003, pp. 2223–2228.

[53] K. Subbarao and P. Muralidhar, "Cooperative control of uavs in dynamic pursuit subject to communication delays," in *Proceedings of the AIAA Guidance, Navigation, and Control Conference*, San Francisco, CA, August 2005.

[54] D. Dionne and C. A. Rabbath, "Real-time decentralized pursuer-evader assignment for cooperating ucavs using the dtc algorithm," in *Proceedings of the AIAA Guidance, Navigation, and Control Conference*, Hilton Head, SC, 2007.

[55] V. B. Kolmanovskii and V. R. Nosov, *Stability of Functional Differential Equations*. Orlando, FL: Academic Press, Inc., 1986, chapter 3.2.

[56] S.-I. Niculescu, "Stability and hyperbolicity of linear systems with delayed state: a matrix-pencil approach," *Institute for Mathematics and its Applications: Journal of Mathematical Control & Information*, vol. 15, pp. 331–347, 1998.

[57] N. Chopra and M. W. Spong, "Synchronization of networked passive systems with time delays and application to bilateral teleoperation," in *Proceedings of the Society of Instrumentation and Control Engineering of Japan Annual Conference*, Okayama, Japan, August 2005.

[58] ——, "Passivity-based control of multi-agent systems," in *Advances in Robot Control: From Everyday Physics to Human-Like Movements, Sadao Kawamura*

and Mikhail Svinin, Editors. Berlin, Germany: Spring-Verlag, 2006, pp. 107–134.

[59] T. Kalmàr-Nagy, "A new look at the stability analysis of delay differential equations," in *Proceedings of the ASME International Design Engineering Technical Conferences and the Computers and Information in Engineering Conferences*, Long Beach, CA, 2005.

[60] R. Sipahi and N. Olgac, "Degenerate cases in using the direct method," *ASME Journal of Dynamic Systems, Measurement, and Control*, vol. 125, pp. 194–201, 2003.

[61] ——, "A novel stability study on multiple time-delay stability (mtds) using the root clustering paradigm," in *Proceedings of the 2004 American Control Conference*, Boston, MA, 2004.

[62] ——, "Complete stability robustness of third-order lti multiple time-delay systems," *Automatica*, vol. 41, pp. 1413–1422, 2005.

[63] F. M. Asl and A. G. Ulsoy, "Analytical solution of a system of homogeneous delay differential equations via the lambert function," in *Proceedings of the American Control Conference*, Chicago, IL, 2004, pp. 2496–2500.

[64] ——, "Analysis of a system of linear delay differential equations," *American Society of Mechanical Engineers Journal of Dynamic Systems, Measurement, and Control*, vol. 125, pp. 215–223, 2003.

[65] S. Yi and A. G. Ulsoy, "Solution of a system of linear delay differential equations using the matrix lambert function," in *Proceedings of the American Control Conference*, Minneapolis, MN, 2006.

[66] J. Hale, *Theory of Function Differential Equations.* New York: Springer-Verlag, 1977, chapter 5, Appendix: Stability of Characteristic Equations.

[67] H. Smith, "Mat 598 applied delay differential equations," in *Lecture Notes: Arizona State University*, 2004, pp. 45–50, http://math.la.ase.edu/%7Ehalsmith/FDE.pdf.

[68] B. Lehman and E. Verriest, "Stability of second order differential delay equations with constant coefficients," in *Proceedings of the IEEE American Controls Conference, Vol. 2*, 1992, pp. 1959–1960.

[69] R. Bellman, *Perturbation Techniques in Mathematics, Engineering & Physics*, New York, 1972.

[70] T. S. Abbott, "Speed control law for precision terminal area in-trail self spacing," NASA Langley Research Center, Hampton, VA, Tech. Rep., July 2002, NASA/TM-2002-211742.

[71] D. R. Nelson, T. W. McLain, and R. W. Beard, "Experiments in cooperative timing for miniature air vehicles," *AIAA Journal of Aerospace Computing, Information, and Communication*, vol. 4, pp. 956–967, 2007.

[72] S. J. Colley, *Vector Calculus.* Upper Saddle River, NJ: Prentice-Hall, Inc., 2002.

[73] J. L. Crassidis and J. L. Junkins, *Optimal Estimation of Dynamic Systems.* Boca Raton, FL: Chapman & Hall/CRC Applied Mathematics and Nonlinear Science Series, 2004.

[74] P. Martin, R. M. Murray, and P. Rouchon, "Flat systems," in *Proceedings of the 4th European Control Conference*, 1997, pp. 211–264.

[75] E. Hoffman, D. Ivanescu, C. Shaw, and K. Zeghal, "Analysis of constant time delay airborne spacing concepts between aircraft of mixed types in varying wind conditions," in *Proceedings of the 5th USA/Europe Air Traffic Management R&D Seminar*, Budapest, Hungary, 2003.

[76] J. Roskam, *Airplane Flight Dynamics and Automatic Flight Controls*. Lawrence, KS: Design, Analysis, and Research Corporation, 2001.

[77] J. E. Hurtado, *Kinematic and Kinetic Principles*. Hurtado - Lulu.com, 2007.

[78] R. Mukherjee and D. Chen, "Asymptotic stability theorem for autonomous systems," *Journal of Guidance, Control, and Dynamics*, vol. 16, no. 5, pp. 961–963, 1993.

[79] A. E. Bryson and Y.-C. Ho, *Applied Optimal Control: Optimization, Estimation, and Control*. New York: Taylor & Francis, 1975.

[80] F. L. Lewis and V. L. Syrmos, *Optimal Control*. New York: John Wiley & Sons, Inc., 1995.

[81] R. F. Stengel, *Optimal Control and Estimation*. Mineola, NY: Dover Publications, Inc., 1994.

APPENDIX A

DIFFERENTIAL FLATNESS

Differentially-flat systems have properties that can be exploited to aid in the control of nonlinear systems. Flat systems are particularly suited for trajectory generation and tracking, and thus the trajectory-planning problem is eased for nonlinear systems that are differentially flat. Exploiting the differential-flatness properties for trajectory generation can be contrasted with more traditional linearization approaches, where the linearization may only be valid for a small operating region. In this appendix, differential-flatness is defined and some examples of flat systems are presented.

A. Definition of Differential Flatness

Given a system with states $\boldsymbol{x} \in R^n$ and inputs $\boldsymbol{u} \in R^m$, the system is flat if there are flat outputs $\boldsymbol{y} \in R^m$ (the number of flat outputs is equal to the number of inputs) such that $\boldsymbol{x}$ and $\boldsymbol{u}$ can be written as functions of the flat outputs and their higher derivatives [74].

$$\boldsymbol{y} = \boldsymbol{h}\left(\boldsymbol{x}, \boldsymbol{u}, \dot{\boldsymbol{u}}, ..., \boldsymbol{u}^{(r)}\right) \quad \Rightarrow \quad \begin{aligned} \boldsymbol{x} &= \boldsymbol{f}\left(\boldsymbol{y}, \dot{\boldsymbol{y}}, ..., \boldsymbol{y}^{(q)}\right) \\ \boldsymbol{u} &= \boldsymbol{g}\left(\boldsymbol{y}, \dot{\boldsymbol{y}}, ..., \boldsymbol{y}^{(q)}\right) \end{aligned} \tag{A.1}$$

The states and controls, and thus, the behavior of the system, can be expressed algebraically using the flat outputs and their higher derivatives. This property allows trajectories to be planned in the output space, and the appropriate control inputs can be determined using the mapping [30].

Differential flatness is a geometric property of the system and is independent of the coordinate choice. Martin et al. describe the equivalence of systems, where "two systems are 'equivalent' if there is an invertible transformation exchanging their

trajectories" [74]. An *endogenous transformation* gives a one-to-one transformation between the trajectories of the two systems. Flat systems that describe the dynamics $\dot{\boldsymbol{x}} = \boldsymbol{f}(\boldsymbol{x}, \boldsymbol{u})$ are equivalent to the trivial system that describes a system made up of a chain of integrators. In other words, there is an endogeneous transformation between the trajectories of $\dot{\boldsymbol{x}} = \boldsymbol{f}(\boldsymbol{x}, \boldsymbol{u})$ and the trajectories of the trivial system. For example, consider the chain of integrators.

$$\begin{aligned} \dot{x}_1 &= x_2 \\ \dot{x}_2 &= x_3 \\ &\vdots \\ \dot{x}_{n-1} &= x_n \\ \dot{x}_n &= u \end{aligned}$$

This system is differentially flat with flat output $y = x_1$, where the states $x_2, ..., x_n$ can be written as functions of x_1 and higher derivatives of x_1.

B. Examples of Flat Systems

Currently there is no approach to determine whether a given system is differentially flat. Similarly to Lyapunov-stability analysis, failure to find flat outputs does not mean that the system is not differentially flat. The ruled-manifold criterion provides a necessary conditions for flatness as described by Martin et al. [74]. There are several general systems that are known to be flat including systems linearizable by static feedback, single-input systems, affine systems of co-dimension 1 (the number of controls is one less than the number of states), and affine systems with 2 inputs and 4 states.

All controllable linear systems are differentially flat. Any controllable linear

system can be written in the controllable canonical form from which the flat output can be chosen as the first state. For single-input, single-output systems, the flat output is unique. In multi-input, multi-output systems, the controllable canonical form is not unique, and therefore, the flat outputs are not unique.

APPENDIX B

THREE-DIMENSIONAL VEHICLE MODEL

A. Equations of Motion

Commonly used aircraft equations of motion are based upon a three-dimensional point-mass model [75]. The equations of motion are written as six first-order differential equations, where the states are the inertial position of the aircraft, x, y, and z, the commanded velocity, V, the heading angle, ψ, and the flight path angle, γ.

Figure 59 shows the forces on the aircraft and the velocity vector from three different views. The view in (a) is in the vertical plane and shows a side view of the aircraft. The second view in (b) is also in the vertical plane and shows the front of the aircraft, and the third view in (c) shows the aircraft in the horizontal plane.

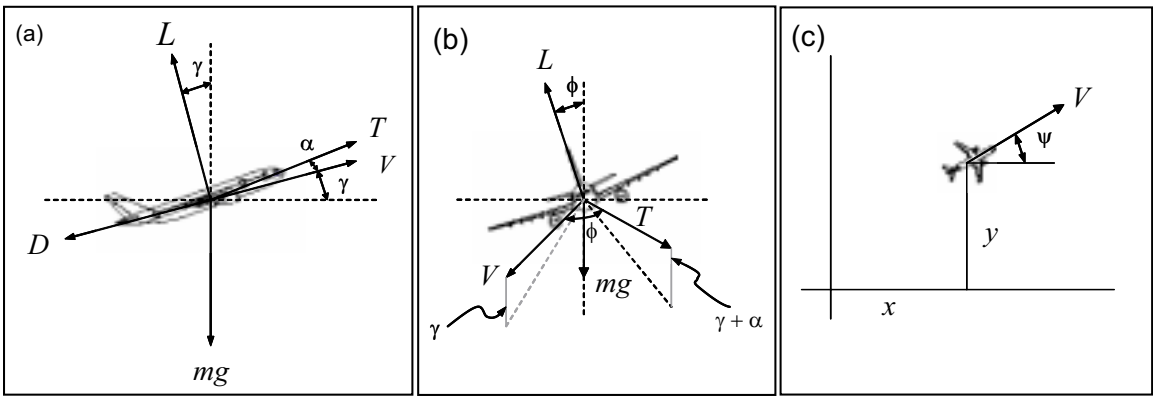

Fig. 59.: Aircraft views of the side (a) and front (b) of the aircraft in the vertical plane and the top of the aircraft (c) in the horizontal plane.

The equations of motion are expressed in the stability axis system, where the $\hat{\boldsymbol{b}}_1$ axis is aligned with the velocity vector [76]. More specifically, the stability axis is

found through two successive simple rotations through the heading angle ψ and the flight-path angle γ as shown in Figure 60. The $\hat{\boldsymbol{b}}_1$ and $\hat{\boldsymbol{b}}_2$ axes create a "horizontal" plane, and the $\hat{\boldsymbol{b}}_1$ and $\hat{\boldsymbol{b}}_3$ axes create a "vertical" plane. The thrust vector, $\boldsymbol{T}$, is rotated from the $\hat{\boldsymbol{b}}_1$ axis by the angle of attack α in the "vertical" plane and by the roll angle, ϕ, in the "horizontal" plane. The lift vector, $\boldsymbol{L}$, is rotated from the $\hat{\boldsymbol{b}}_3$ axis by ϕ. The aerodynamic drag, $\boldsymbol{D}$, acts opposite to the direction of velocity, and the weight of the aircraft acts downward.

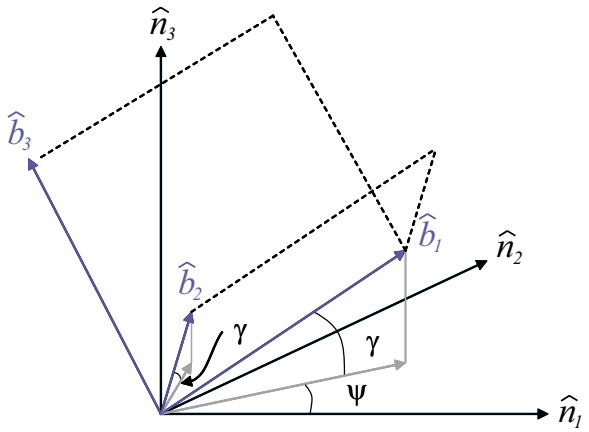

Fig. 60.: Stability-axis reference frame rotated from the inertial frame through the angles γ and ϕ.

The three kinematic equations are shown below, where the velocity vector is written in the inertial coordinates.

$$\dot{x} = V \cos\gamma \cos\psi \tag{B.1}$$

$$\dot{y} = V \cos\gamma \sin\psi \tag{B.2}$$

$$\dot{z} = V \sin\gamma \tag{B.3}$$

The other three first-order equations are found from Newton's second law, $\dot{\boldsymbol{p}} = \boldsymbol{F}$,

where $\boldsymbol{p}$ is the translational momentum vector.

$$\boldsymbol{p} = mV\hat{\boldsymbol{b}}_1 \tag{B.4}$$

The time rate of change of the translational momentum vector, $\dot{\boldsymbol{p}}$, is found using the transport theorem [77].

$$\begin{aligned}\dot{\boldsymbol{p}} &= m\dot{V}\hat{\boldsymbol{b}}_1 + \dot{\psi}\hat{\boldsymbol{p}} \times mV\hat{\boldsymbol{b}}_1 - \dot{\gamma}\hat{\boldsymbol{s}} \times mV\hat{\boldsymbol{b}}_1 \\ &= m\dot{V}\hat{\boldsymbol{b}}_1 + mV\dot{\psi}\hat{\boldsymbol{b}}_2 + mV\dot{\gamma}\hat{\boldsymbol{b}}_3\end{aligned} \tag{B.5}$$

Therefore, from equation (B.5), the following equations are derived.

$$m\dot{V} = \boldsymbol{F} \cdot \hat{\boldsymbol{b}}_1 = T\cos\alpha - D - mg\sin\gamma \tag{B.6}$$

$$mV\dot{\psi} = \boldsymbol{F} \cdot \hat{\boldsymbol{b}}_2 = T\cos\alpha\sin\phi + L\sin\phi \tag{B.7}$$

$$mV\dot{\gamma} = \boldsymbol{F} \cdot \hat{\boldsymbol{b}}_3 = T\sin\alpha + L\cos\phi - mg\cos\gamma \tag{B.8}$$

Aircraft motion can be simulated in three dimensions using the six first-order differential equations in Equations (B.1)-(B.3) and (B.6)-(B.8), where the states are x, y, z, V, ψ, and γ and the control inputs are T, α, and ϕ.

B. Differential-Flatness Relationships

The aircraft equations of motion are differentially flat with flat outputs x, y, and z. The states V, ψ and γ can be written as functions of the first derivatives of the flat outputs.

$$V = \sqrt{\dot{x}^2 + \dot{y}^2 + \dot{z}^2}; \quad \gamma = \sin^{-1}\left(\frac{\dot{z}}{\sqrt{\dot{x}^2 + \dot{y}^2 + \dot{z}^2}}\right); \quad \psi = \tan^{-1}\left(\frac{\dot{y}}{\dot{x}}\right) \tag{B.9}$$

The control inputs, T, α, and ϕ can be written as functions of V, ψ, γ, and their first derivatives.

$$T = \sqrt{\left(m\dot{V} + D + mg\sin\gamma\right)^2 + \left(mV\dot{\gamma} - L\cos\phi + mg\cos\gamma\right)^2} \tag{B.10}$$

$$\alpha = \cos^{-1}\left(\frac{m\dot{V} + D + mg\sin\gamma}{T}\right) \tag{B.11}$$

$$\phi = \sin^{-1}\left(\frac{mV\dot{\gamma}}{m\dot{V} + D + mg\sin\gamma + L}\right) \tag{B.12}$$

The derivatives of V, ψ, and γ are functions of the first and second derivatives of the flat outputs.

$$\dot{V} = \frac{\dot{x}\ddot{x} + \dot{y}\ddot{y} + \dot{z}\ddot{z}}{V}; \quad \dot{\psi} = \frac{\dot{x}\ddot{y} - \dot{y}\ddot{x}}{\dot{x}^2 + \dot{y}^2} \quad \dot{\gamma} = \frac{V\ddot{z} - \dot{z}\dot{V}}{V^2\sqrt{1 - \left(\frac{\dot{z}}{V}\right)^2}} \tag{B.13}$$

The second derivatives of the flat outputs are the highest derivatives in the control inputs, and new control inputs can be defined as $(\ddot{x}, \ddot{y}, \ddot{z}) = (u_x, u_y, u_z)$. As was shown in the planar case, the equations of motion can be decoupled in x, y, and z directions. A linear transformation relates the controls in the double-integrator form to $\dot{V}$, $\dot{\psi}$, and $\dot{\gamma}$, and the aircraft controls are found using Equations (B.10)-(B.12).

$$\begin{bmatrix} \dot{V} \\ \dot{\psi} \\ \dot{\gamma} \end{bmatrix} = \begin{bmatrix} \frac{\dot{x}}{V} & \frac{\dot{y}}{V} & \frac{\dot{z}}{V} \\ -\frac{\dot{y}}{C_1} & -\frac{\dot{x}}{C_1} & 0 \\ -\frac{\dot{x}\dot{z}}{C_2} & -\frac{\dot{y}\dot{z}}{C_2} & \frac{V\left(V - \dot{z}^2\right)}{C_2} \end{bmatrix} \begin{bmatrix} u_x \\ u_y \\ u_z \end{bmatrix}; \quad C_1 = \dot{x}^2 + \dot{y}^2; \quad C_2 = V^3\sqrt{1 - \left(\frac{\dot{z}}{V}\right)^2}$$

APPENDIX C

PROOF OF ASYMPTOTIC STABILITY FOR RATE-FREE CONTROL

Mukherjee, Chen, and Junkins have explored asymptotic stability for autonomous systems using higher derivatives of the Lyapunov function [29, 78]. The theorem presented in the references states that a sufficient condition for asymptotic stability when $V > 0$ and $\dot{V} \leq 0$ for all states in the region Ω is that the derivatives of V are equal to zero on Z up to some even order, where Z is the set of points where $\dot{V}$ is equal to zero, and the first non-zero derivative of V is of odd order and negative definite for all points on Z. The objective is to prove that $\dot{V}$ is negative definite and $\dot{V} = 0$ for all of the equilibrium points.

The linear equations of motion for the rate-free system are restated below (the vehicle index, i, has been dropped for notational simplicity).

$$\dot{\beta} = -\tau\beta + k\epsilon; \quad \ddot{\epsilon} = \ddot{x}_r - u \tag{C.1}$$

An equilibrium solution of Equation (C.1) is given by $\epsilon = 0$, $\dot{\epsilon} = 0$, and $\beta = 0$. For the Lyapunov function $V = \frac{\gamma}{2}\epsilon^2 + \frac{1}{2}\dot{\epsilon}^2 + \frac{1}{2}(-\tau\beta + k\epsilon)^2$ with $u = (\gamma + k^2)\epsilon - \tau k\beta + \ddot{x}_r$, the time derivative of V was found to be negative semi-definite.

$$\dot{V} = -\tau(-\tau\beta + k\epsilon)^2 \leq 0 \tag{C.2}$$

The set Z is defined where $\dot{V} = 0$.

$$Z = \{\epsilon \in \Re, \dot{\epsilon} \in \Re, (-\tau\beta + k\epsilon) = 0\} \tag{C.3}$$

The second derivative of V is zero when evaluated on Z, whereas the third derivative

is a quadratic function of $\dot{\epsilon}$.

$$\begin{aligned} V^{(3)}|_Z &= -2\tau(-\tau\beta + k\epsilon)(-\tau\ddot{\beta} + k\ddot{\epsilon})|_Z - 2\tau(\tau\dot{\beta} + k\dot{\epsilon})^2|_Z \\ &= 0 - 2\tau\left[\tau(-\tau\beta + k\epsilon) + k\dot{\epsilon}\right]^2|_Z \\ &= -2\tau k^2\dot{\epsilon}^2 \leq 0 \end{aligned} \tag{C.4}$$

Here it can be seen that $V^{(3)} < 0$ for all $\dot{\epsilon} \neq 0$, but this expression still does not reveal anything about ϵ. A new set is defined, $Z_{\text{new}} = \{\epsilon \in \Re, \dot{\epsilon} = 0, (-\tau\beta + k\epsilon) = 0\}$, such that the third derivative is equal to zero, and higher derivatives of V are taken. The fourth derivative of V is equal to zero when evaluated on Z_{new}, whereas the fifth derivative is a quadratic function of ϵ.

$$\begin{aligned} V|^{(5)}_{Z_{\text{new}}} &= -4\tau k^2\left[\ddot{\epsilon}^2 + \dot{\epsilon}\epsilon^{(3)}\right]|_{Z_{\text{new}}} \\ &= -4\tau k^2(\ddot{x}_r - u)^2|_{Z_{\text{new}}} \\ &= -4\tau k^2[\ddot{x}_r - (\gamma + k^2)\epsilon + \tau k\beta - \ddot{x}_r]^2|_{Z_{\text{new}}} \\ &= -4\tau k^2[-(\gamma + k^2)\epsilon + k(k\epsilon)]^2|_{Z_{\text{new}}} \\ &= -4\tau k^2(-\gamma\epsilon)^2 < 0, \quad \forall \ \epsilon \neq 0 \end{aligned} \tag{C.5}$$

From Equation (C.5), which is an odd, non-zero derivative of V, we can conclude that $\dot{V} = 0$ only at the equilibrium points: ϵ, $\dot{\epsilon}$, and $\beta = 0$. Therefore, $\dot{V}$ is negative definite, which implies that ϵ, $\dot{\epsilon}$, and β asymptotically approach their equilibrium points.

APPENDIX D

OPTIMAL NON-ZERO-SET-POINT CONTROLLER

The well-known Linear Quadratic Regulator (LQR) is used to determine the optimal full-state feedback gain, K, that minimizes the quadratic cost function in order to drive system states to zero [79, 80].

$$J = \frac{1}{2}\int_{t_0}^{\infty} \left(\boldsymbol{x}^T Q \boldsymbol{x} + \boldsymbol{u}^T R \boldsymbol{u}\right) dt;$$

$$\text{Given: } \dot{\boldsymbol{x}} = A\boldsymbol{x} + B\boldsymbol{u}; \quad \boldsymbol{x}(0) = \boldsymbol{x_0} \tag{D.1}$$

The control law is $\boldsymbol{u}(t) = -K\boldsymbol{x}(t)$, where $K = -R^{-1}B^T S$ is the solution to the differential Riccati equation.

$$\dot{S}(t) = -S(t)A - A^T S(t) - Q + S(t)BR^{-1}B^T S(t), \quad S(\infty) = S_\infty \tag{D.2}$$

To drive the system to a new non-zero steady state, the problem objective can be restated as driving the outputs $\boldsymbol{y}$ to some value $\boldsymbol{y}^*$ as $t \to \infty$ [81]. The output equation is assumed to have the form: $\boldsymbol{y} = H\boldsymbol{x} + D\boldsymbol{u}$. If $\boldsymbol{y}^*$ is constant, the trim states and inputs are $\boldsymbol{x} = \boldsymbol{x}^*$ and $\boldsymbol{u} = \boldsymbol{u}^*$, respectively. Because $\boldsymbol{x}^*$ and $\boldsymbol{u}^*$ are trim states, the following relationships hold.

$$\dot{\boldsymbol{x}}^* = A\boldsymbol{x}^* + B\boldsymbol{u}^* \equiv 0 \tag{D.3}$$

$$\boldsymbol{y}^* = H\boldsymbol{x}^* + D\boldsymbol{u}^* \tag{D.4}$$

The trim states and controls can be determined by solving the matrix equation.

$$\left[\begin{array}{c:c} A & B \\ \hdashline H & D \end{array}\right] \left[\begin{array}{c} \boldsymbol{x}^* \\ \hdashline \boldsymbol{u}^* \end{array}\right] = \left[\begin{array}{c} 0 \\ \hdashline \boldsymbol{y}^* \end{array}\right] \tag{D.5}$$

Here, $A \in R^{n\times n}$, $B \in R^{n\times m}$, $H \in R^{p\times n}$, and $D \in R^{p\times m}$, where n is the number of states, m is the number of control inputs, and p is the number of outputs. The matrix containing A, B, H, and D, is the Quad-Partition Matrix, which must be square ($p = m$) and non-singular to determine unique trim states and controls that satisfy $\boldsymbol{y} = \boldsymbol{y}^*$.

A control is determined to drive the system states to the trim states using LQR. Firstly, the errors with respect to the trim states and controls are defined.

$$\tilde{\boldsymbol{x}} = \boldsymbol{x} - \boldsymbol{x}^* \tag{D.6}$$

$$\tilde{\boldsymbol{u}} = \boldsymbol{u} - \boldsymbol{u}^* \tag{D.7}$$

The system equations for $\tilde{\boldsymbol{x}}$ follow.

$$\dot{\tilde{\boldsymbol{x}}} = \dot{\boldsymbol{x}} - \dot{\boldsymbol{x}}^* = A\boldsymbol{x} + B\boldsymbol{u} - (A\boldsymbol{x}^* + B\boldsymbol{u}^*) = A\tilde{\boldsymbol{x}} + B\tilde{\boldsymbol{u}} \tag{D.8}$$

Now, $\tilde{\boldsymbol{u}}$ is determined to minimize the cost function, J, given the system dynamics.

$$\begin{aligned} J &= \frac{1}{2}\int_{t_0}^{\infty} \left(\tilde{\boldsymbol{x}}^T Q \tilde{\boldsymbol{x}} + \tilde{\boldsymbol{u}}^T R \tilde{\boldsymbol{u}}\right) dt; \\ \text{Given: } \dot{\tilde{\boldsymbol{x}}} &= A\tilde{\boldsymbol{x}} + B\tilde{\boldsymbol{u}}; \quad \tilde{\boldsymbol{x}}(0) = \boldsymbol{x_0} - \boldsymbol{x}^* \end{aligned} \tag{D.9}$$

The solution to the LQR problem in Equation (D.9) has the form: $\tilde{\boldsymbol{u}} = -K\tilde{\boldsymbol{x}}$, and the transformation to the original state and control variables has the following form.

$$\begin{aligned} \boldsymbol{u} &= \boldsymbol{u}^* - K(\boldsymbol{x} - \boldsymbol{x}^*) \\ &= (\boldsymbol{u}^* + K\boldsymbol{x}^*) - K\boldsymbol{x} \end{aligned} \tag{D.10}$$

The parenthetical term in Equation (D.10) is the term related to the non-zero set point, and the remaining term comes from the traditional LQR solution.

APPENDIX E

STIFFNESS AND FORCING MATRICES FOR COMMUNICATION STRUCTURES

The stiffness and forcing matrices are listed for the seven defined communication structures in Figure 22. The D matrix acts on the vector $\boldsymbol{u}_r = [x_r(t)\ \dot{x}_r(t)\ d_{r1}\ d_{12}\ d_{13}\ d_{23}]^T$. Here, we assume that the formation has a constant velocity.

1. Fully Connected:

$$K = \begin{bmatrix} k_r + k_{12} + k_{13} & -k_{12} & -k_{13} \\ -k_{12} & k_{12} + k_{23} & -k_{23} \\ -k_{13} & -k_{23} & k_{13} + k_{23} \end{bmatrix}; \quad D = \begin{bmatrix} k_r & c_r & -k_r & k_{12} & k_{13} & 0 \\ 0 & 0 & 0 & -k_{12} & 0 & k_{23} \\ 0 & 0 & 0 & 0 & -k_{13} & -k_{23} \end{bmatrix}$$

2. Singly Connected to Platoon Lead with Bidirectional Communication between Trailing Vehicles:

$$K = \begin{bmatrix} k_r + k_{12} & -k_{12} & 0 \\ -k_{12} & k_{12} + k_{23} & -k_{23} \\ -k_{13} & -k_{23} & k_{13} + k_{23} \end{bmatrix}; \quad D = \begin{bmatrix} k_r & c_r & -k_r & k_{12} & 0 & 0 \\ 0 & 0 & 0 & -k_{12} & 0 & k_{23} \\ 0 & 0 & 0 & 0 & -k_{13} & -k_{23} \end{bmatrix}$$

3. Bidirectional Connection to Platoon Lead

$$K = \begin{bmatrix} k_r + k_{12} + k_{13} & -k_{12} & -k_{13} \\ -k_{12} & k_{12} & 0 \\ -k_{13} & 0 & k_{13} \end{bmatrix}; \quad D = \begin{bmatrix} k_r & c_r & -k_r & k_{12} & k_{13} & 0 \\ 0 & 0 & 0 & -k_{12} & 0 & 0 \\ 0 & 0 & 0 & 0 & -k_{13} & 0 \end{bmatrix}$$

4. Singly Connected to Platoon Lead

$$K = \begin{bmatrix} k_r & 0 & 0 \\ -k_{12} & k_{12} & 0 \\ -k_{13} & 0 & k_{13} \end{bmatrix}; \quad D = \begin{bmatrix} k_r & c_r & -k_r & 0 & 0 & 0 \\ 0 & 0 & 0 & -k_{12} & 0 & 0 \\ 0 & 0 & 0 & 0 & -k_{13} & 0 \end{bmatrix}$$

5. Singly-Connected Leader-Follower

$$K = \begin{bmatrix} k_r & 0 & 0 \\ -k_{12} & k_{12} & 0 \\ 0 & -k_{23} & k_{23} \end{bmatrix}; \quad D = \begin{bmatrix} k_r & c_r & -k_r & 0 & 0 & 0 \\ 0 & 0 & 0 & -k_{12} & 0 & 0 \\ 0 & 0 & 0 & 0 & 0 & -k_{23} \end{bmatrix}$$

6. Bidirectional Leader-Follower

$$K = \begin{bmatrix} k_r + k_{12} & -k_{12} & 0 \\ -k_{12} & k_{12} + k_{23} & -k_{23} \\ 0 & -k_{23} & k_{23} \end{bmatrix}; \quad D = \begin{bmatrix} k_r & c_r & -k_r & k_{12} & 0 & 0 \\ 0 & 0 & 0 & -k_{12} & 0 & k_{23} \\ 0 & 0 & 0 & 0 & 0 & -k_{23} \end{bmatrix}$$

7. Circular Connection

$$K = \begin{bmatrix} k_r + k_{13} & 0 & -k_{13} \\ -k_{12} & k_{12} & 0 \\ 0 & -k_{23} & k_{23} \end{bmatrix}; \quad D = \begin{bmatrix} k_r & c_r & -k_r & 0 & k_{13} & 0 \\ 0 & 0 & 0 & -k_{12} & 0 & 0 \\ 0 & 0 & 0 & 0 & 0 & -k_{23} \end{bmatrix}$$

VITA

Lesley Anne Weitz is the daughter of William and Debra Weitz of North Tonawanda, New York. Lesley graduated from the University at Buffalo with a Bachelor of Science degree in mechanical engineering in 2002. After working at Moog Inc. in East Aurora, NY, she entered the aerospace engineering department at Texas A&M University under the supervision of Dr. John E. Hurtado in 2003. She received a Master of Science in aerospace engineering in August 2005 and completed her doctoral degree, also in aerospace engineering, in May 2009.

Lesley has been awarded the National Science Foundation Graduate Research Fellowship, the Zonta International Amelia Earhart Fellowship, the Tau Beta Pi Fellowship, the Texas Space Grant Consortium Fellowship, the Lindbergh Grant, the AIAA Guidance, Navigation, and Control Graduate Award, and a NASA Graduate Student Research Fellowship. Lesley has accepted a position in the Center for Advanced Aviation Systems Development (CAASD) at The MITRE Corporation in McLean, Virginia.

Contact Address: Dr. John E. Hurtado; 3141 TAMU; College Station, TX 77843-3141